CALCIUM SIGNALING PLAYERS OF *TOXOPLASMA GONDII*

by

KARLA MARIE MáRQUEZ NOGUERAS

(Under the Direction of Silvia NJ Moreno)

ABSTRACT

Toxoplasma gondii is an Apicomplexan parasite that infects one third of the world's population. The disease caused by this obligate intracellular parasite, toxoplasmosis, is clinically relevant for immunocompromised patients and for the unborn fetus. The pathogenicity of the parasite derived from its lytic cycle where it invades, replicates and egresses out of a host cell. Calcium signaling is part of the signaling pathways that regulates the expression and activation of proteins that are essential for the pathogenicity of *T. gondii.* Calcium increase in the cytosol resulting from influx or release from intracellular stores, will trigger a signaling cascade that can activate a variety of effectors that will activate vital cellular functions like the ones that are part of the parasite pathogenic cycle. The majority of the molecules that form part of this signaling pathway remain uncharacterized. In this work we identified and characterized the first Ca^{2+} channel in *T. gondii*. Additionally, we characterize a organellar Ca^{2+}-binding protein which senses changes of luminal organellar Ca^{2+}. Lastly, we provide evidence of additional roles of previously characterized Ca^{2+}-binding proteins in regulating Ca^{2+} channels.

Apicomplexa belong to an early branch in the eukaryotic evolutionary tree and the discovery of new signaling molecules will generate important information about the origins of complex signaling networks in eukaryotes. In addition, new molecules may provide for potential targets for future chemotherapy.

INDEX WORDS: Toxoplasma gondii, TRP Channel, Ca^{2+} channels, Calcium-binding proteins, Calcium signaling, Calcium homeostasis.

THE CALCIUM SIGNALING PATHWAY OF *TOXOPLASMA GONDII*

by

KARLA MARIE MáRQUEZ NOGUERAS

B.A., UNIVERSIDAD DE PUERTO RICO, MAYAGüEZ, PUERTO RICO, 2012

M.S., UNIVERSIDAD DE PUERTO RICO, MAYAGüEZ, PUERTO RICO, 2014

A Dissertation Submitted to the Graduate Faculty of The University of Georgia in Partial Fulfillment of the Requirements for the Degree

DOCTOR OF PHILOSOPHY

ATHENS, GEORGIA

2020

CALCIUM SIGNALING PLAYERS OF *TOXOPLASMA GONDII*

by

KARLA M. MáRQUEZ NOGUERAS

Major Professor: Silvia NJ Moreno
Committee: Vasant Muralidharan
Jorge Escalante-Semerena
Harry Dailey

Electronic Version Approved:

Ron Walcott
Dean of the Graduate School
The University of Georgia
December 2020

DEDICATION

To my family, for letting me achieve all my dreams, you are the inspiration behind all my goals and dreams. To my family who has inspired me to fight hard for my dreams. Mom, Dad, Mickey, Zuania and Edison all my hard work is for you guys.

ACKNOWLEDGEMENTS

I would like to thank all the people that made this work a possibility.

I would like to acknowledge Dr. Silvia Moreno, which has been a great mentor. She has allowed me to grow as a scientist, supporting my ideas while teaching me how to pursue them. Thank you giving me the opportunity to be a part of your team. I'm thankful for the opportunities that you have given me through the years, your guidance, advice and support.

I would like to thank my committee members who have provided guidance and ideas through these last years.

I would like to also thank Dr. Myriam A. Hortua Triana. She has been a second mentor in my life both professionally and personally. I'm thankful for all the help, guidance, advice, laughs and memories that we have created through these last years. Thank you for everything that you have done.

It is important to surround yourself with people who are willing to support and motivate you. Thank you to Jessica, Sophia and Olivia, who through the years have shared many cries, much frustration and lots of happy memories which have made it possible to finish this PhD.

I feel fortunate to have been surrounded by an incredible team of researchers who have motivated me and pushed me to always bring my best as a scientist. Thank you to everyone who has contributed in any way to my development as a scientist.

I would like to say thank you to Dr. Ivana Kuo. A key and turning point in my career was to have the opportunity to learn electrophysiology. Dr. Kuo opened the doors to her lab and took the time to teach me and train me in this technique. She has also provided much needed mentorship and guidance to a big part of my project. I'm grateful for all her advice and motivation.

I would like to end my acknowledgements recognizing the work of my family. 6 years ago, I took the leap and came to the US to obtain my PhD. I feel grateful and privileged that through every adventure I take my family provides their support. Through every step of this PhD they have cheered and motivated me to reach the goal. Thank you for all the sacrifices you made through the years for me to reach this point. Lastly, I wanted to say thank you to my husband, my biggest fan. Through the times when exhaustion hits, or when I don't feel motivated to keep going, he is always there reminding me that I can do this. There is no bigger cheerleader in my life than him. Thank you for everything that you do, I'm happy that you were my person.

TABLE OF CONTENTS

LIST OF TABLES

Page

LIST OF FIGURES

Page

CHAPTER 1

INTRODUCTION

1.1.1 Discovery and medical relevance of Toxoplasma gondii

One third of the world's population is infected with *Toxoplasma gondii* [1]. *T. gondii* is an obligate intracellular parasite that belongs to the Apicomplexan phylum [2]. Other important parasites like *Plasmodium* (causative agent of Malaria) and *Cryptosporidium* (main cause of infant diarrhea) belong to the same phylum [2]. *Toxoplasma* was first described in 1908 by Nicolle and Manceux, who originally believed it was *Leishmania* [3]. The parasite was first isolated from *Ctenodactylus gundis* from which it obtained its name.

Transmission of *Toxoplasma* occurs through the consumption of undercooked meat, food supplies contaminated with feces of infected cats or congenital transmission from mother to fetus [4, 5]. An interesting characteristic of the parasite is its ability to cross biological barriers like the placenta and the blood brain barrier. Currently around a third of the world's population shows seroprevalence of *Toxoplasma* infection [6]. However, infection rates depend on geographical location as infection rate may be as low as 8% or as high as 75% [7-9].

Toxoplasmosis is one of the main food-borne illnesses in the United States [10]. The majority of infected individuals present as asymptomatic or with mild flu-like symptoms. *Toxoplasma* is an opportunistic pathogen in immunocompetent individuals [11-14]. In these patients more serious complications like encephalitis, myocarditis and ocular diseases have been observed. Virulence of the parasite is dependent on the strain as well as health of the patient [15].

There are a variety of diagnostic tests that can be performed to detect previous or current infection with *Toxoplasma*. One of the main tests utilized to determine infection is the detection of IgM and IgG antibodies. During acute infection these antibodies can be produced as fast as 2 weeks post-infection and can persist for months to years [16]. Unlike IgG, IgM antibodies cannot cross the placental barrier which is useful for detection of congenital infection [17]. PCR against *Toxoplasma* specific genes also has been developed and this has been useful for clinical diagnosis of Toxoplasmosis.

1.1.2 Treatment and prevention of *T. gondii*

Treatment of *Toxoplasma* consists of a variety of drugs which targets the acute infection of the parasite. Current treatment for Toxoplasmosis consists on a combination of pyrimethamine with sulfadiazine [18]. The combination of these drugs targets the folic acid metabolism which inhibits replication of *T. gondii* [19]. Unfortunately, this treatment loses efficacy with continuous use and causes toxicity resulting in discontinuation of the drugs [20].

A combination of clindamycin and azithromycin were also documented for the treatment of Toxoplasmosis [21]. Use of clindamycin has shown to cause fewer

toxic effects when in combination with other drugs in comparison to the toxic effect of pyrimethamine combinations with other drugs [21]. Considering that the current treatments only targets the acute infection and have toxic effects, there is an urgent need to discover new therapeutic targets for the treatment of toxoplasmosis is important strategy to lower the transmission rate is the use of preventative measures. It is advisable for pregnant women to avoid changing cat litter boxes since transmission can occur through infected cat feces [22]. The transmission rate due to the consumption of contaminated or undercooked food sources is also high [23]. Adequate sanitation practices and correct food preparation are important practices to reduce transmission [24].

1.1.3 Life cycle of *T. gondii*

Toxoplasma is able to infect a variety of warm-blooded animals [25]. Inside the host the parasite may replicate asexually or sexually. Sexual replication only happens in the small intestine of the definitive host which are felids (Fig. 1). The definitive host will ingest small animals like mice, rats or meat contaminated with oocytes [26]. Oocytes contain sporozoites and upon ingestion they will rupture inside the feline intestine [27]. Sporozoites will differentiate to tachyzoites which are the fast replicating form of the parasite [28]. After several rounds of replication, the parasites will undergo merogony, where they develop into both male and female gametes [29]. Gametes will fuse to form a zygote which will lead to the formation of immature oocysts which are released into the environment with cat feces [30].

In the intermediate host the parasite only undergoes asexual replication (Fig. 1). When oocysts are ingested by the intermediate host they will rupture and differentiate into tachyzoites [28]. Tachyzoites invade any nucleated cell where they replicate by a process called endodyogeny, where two cells are formed within the mother cell [31]. Cells will replicate every 6 to 8 hours and eventually egress and invade proximal cells where they will invade and continue replication. With time and pressure from the immune system the parasite will slow down and differentiate into bradyzoites within tissue cysts [32]. The formation of tissue cysts containing bradyzoites is a characteristic of the chronic stage of the infection. Bradyzoites can persist for the life of the host and usually do not appear to cause disease. However, immunosuppression may cause reactivation of the infection and result cause the symptoms associated with the acute infection [33].

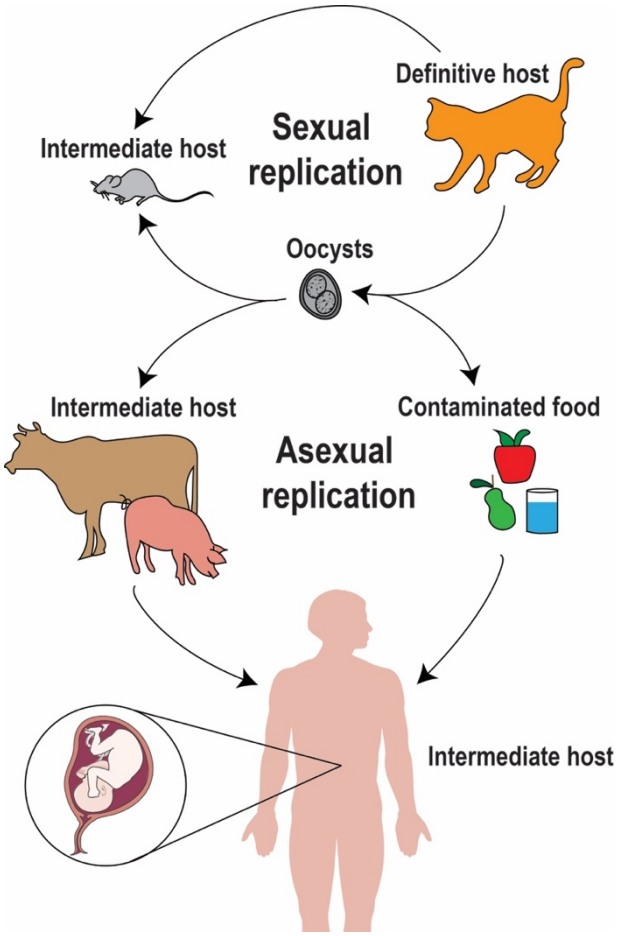

Figure 1.1. Life cycle of *Toxoplasma gondii*. The definitive host of the parasite is the cat, where the parasite can undergo sexual replication. Infected cats shed oocytes into the environment which can be picked up by intermediate hosts. *T. gondii* has the ability to cross the placental barrier infecting the fetus.

1.1.4 Lytic cycle of *T. gondii*

Once the parasite differentiates into tachyzoites it will begin its lytic cycle (Fig. 1.2). The lytic cycle starts when the parasite attaches and invades a host cell. To attach and invade a host cell the parasite extrudes it conoid, a cytoskeletal

structure that forms part of the apical complex. The conoid is connected to tubulin fibers within apical rings and is extruded during the process of invasion, motility and egress [34, 35]. Once the conoid is extruded the parasite will secrete proteins into the invaded cell that will prepare and remodel host cells prior to their invasion by the parasite [36]. The proteins secreted during the invasion are stored in two secretory organelles: micronemes and rhoptries [37]. The rhoptries are club shape organelles that contain proteins that help in the creation of the structure necessary to invade the host cell [38]. Micronemes are organelles that secrete proteins which allows for remodeling of the host cell [39]. While invading, the parasite surrounds itself in a parasitophorous vacuole (PV), which derives from the host membranes and where the parasite replicates. The PV serves as a sieve, where proteins and ions can cross and be utilized by the parasite [40, 41]. Once the parasite successfully invades host cells it will start replicating until an unknown signal triggers the process of egress, where the parasites lyses out of the host cell and glide to find a new cell to invade. The importance of the lytic cycle is the direct relation with the pathogenicity of the parasite. The completion of the lytic cycle ends with the lysis of host cells resulting in destruction of tissue [42].

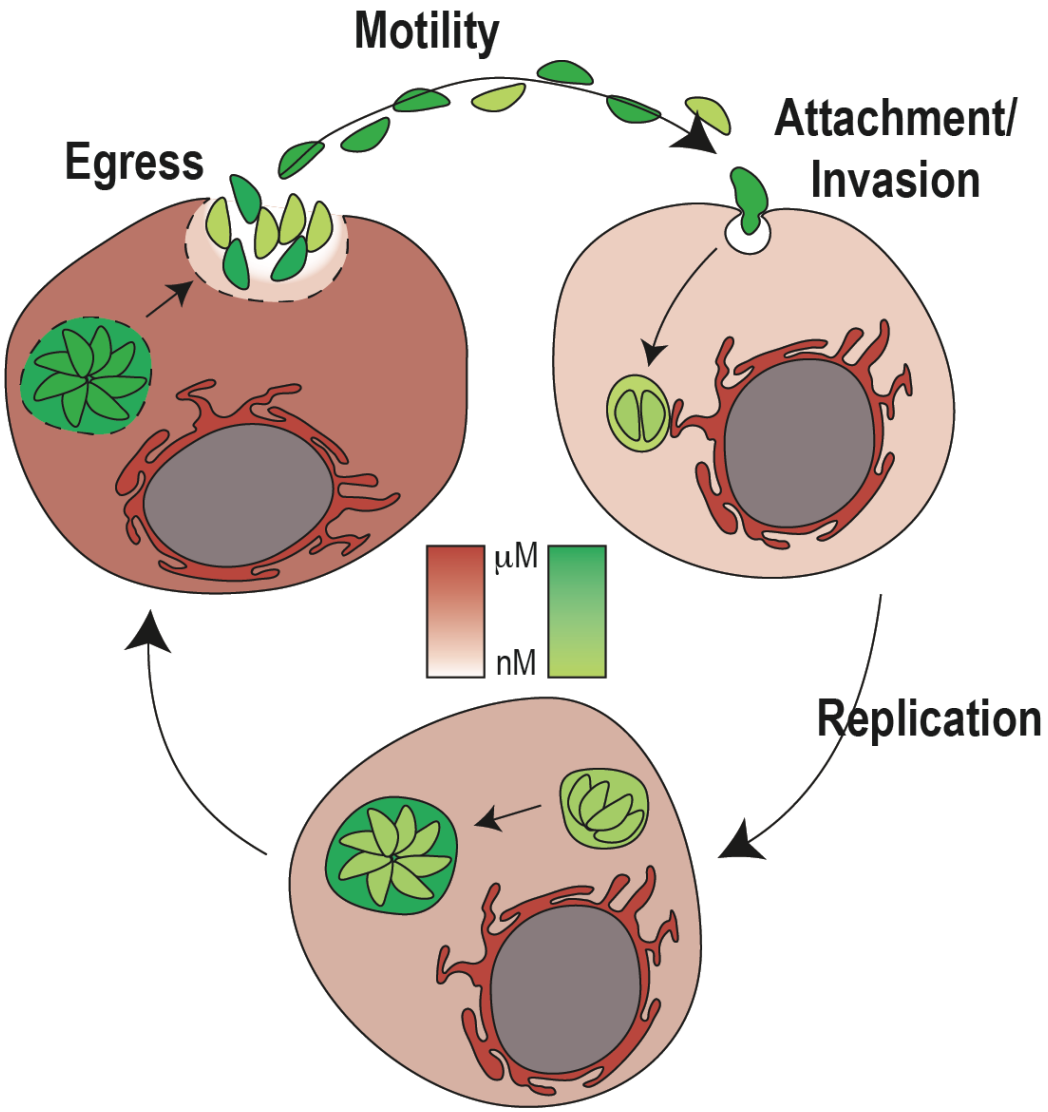

Figure 1.2. Lytic cycle of *T. gondii*. Once Toxoplasma enters its host it will attach and invade the cell. While inside the host the parasite replicates inside the parasitophorous vacuole. Upon a stimulus the parasites egress from the host and moves through the extracellular environment repeating this cycle.

1.1.5 Calcium signaling in *T. gondii*

Calcium ions impact nearly every aspect of cellular life [43]. Cells have evolved to utilize this secondary messenger to regulate and activate signaling

pathways that directly impact cell growth. Cytosolic Ca^{2+} levels are maintained at low levels, since high [Ca^{2+}] can be toxic to the cells. To keep cytosolic Ca^{2+} low cells have developed mechanisms that maintain cytosolic Ca^{2+} and can be utilized later on for signal transduction [44, 45]. Increase of cytosolic Ca^{2+} can occur through the influx from the extracellular environment or the release from the intracellular stores. Organelles are able to contain high [Ca^{2+}] that can activate the signaling molecules in a rapid and efficient manner.

Flux of Ca^{2+} from the extracellular environment in mainly mediated by voltage-gated Ca^{2+} channels. Voltage-gated channels are formed by four subunits where each subunit contains 6 transmembrane domains [46, 47]. Depolarization of the plasma membrane causes a conformational change of the subunits which allows for Ca^{2+} influx to the cell. There are a variety of VGCC's that are expressed in the cells that depend on voltage activation, channel conductance and inactivation [48]. The rapid flow of ions through these channels increase cytosolic Ca^{2+} which is lowered by the combined activity of the plasma membrane Ca^{2+} ATPase (PMCA) and uptake from the intracellular organelles.

The endoplasmic reticulum (ER) is one of the main Ca^{2+} stores present in the cell. Ca^{2+}-ATPases in the membrane of the ER actively pump Ca^{2+} into the store. Luminal Ca^{2+} binding proteins in the ER help sequester the Ca^{2+} which can be utilized to increase cytosolic Ca^{2+}. Release of Ca^{2+} from the ER is mainly mediated by the 1,4,5 triphosphate (IP_3) receptor. External stimulation from the extracellular environment would activate G-coupled receptors which activates the phosphoinositol pathway through phosphoinositide phospholipase C (PI-PLC). PI-

PLC hydrolyzes phosphatidylinositol 4,5 bisphosphate (PIP_2) to produce IP_3 and Diacylglycerol (DAG). IP_3 then bind to the IP_3 Receptor causing release from the ER and increase of cytosolic Ca^{2+}.

Transient Receptor Potential (TRP) channels are another type of channels that allow for Ca^{2+} release from the intracellular organelles. There are 2 groups of TRP channels, with approximately 28 different members [49]. TRP channels are characterized by having six transmembrane domains and by their permeability to cations [50]. TRP channels can be activated by mechanical force, the PI-PLC pathway and Ca^{2+} itself [51]. The activation of these channels will be dependent on the type of TRP channel present in the cell.

Increase of cytosolic Ca^{2+} by depletion of intracellular stores is able to stimulate Ca^{2+} influx through Store Operated Calcium Entry (SOCE). SOCE is mediated by the activation of Orai proteins through the Stromal Interaction Molecule (STIM) localized in the ER. STIM is an ER-Ca^{2+} sensing protein that contains 1 transmembrane domain and an N-terminus EF hand motif. Decreased Ca^{2+} levels in the ER stimulates oligomerization of STIM proteins in the ER membrane which generates junctions between the ER and the plasma membrane. This aggregation leads to the physical interaction with Orai proteins which allows for Ca^{2+} influx. The rapid flux of ions through channels, via influx or release, creates a gradient that allows for the activation of molecules with calcium binding properties.

Regulation and decoding of Ca^{2+} signals in the cells occur mainly through Calcium Binding Proteins (CaBPs). CaBPs are small acidic proteins that contain

specific domains which coordinate the binding of calcium, like EF hand motifs [52]. The EF hand motif was named by the E and F region of parvalbumin (PV), the first molecule described to contain this motif [53]. The structural conformation of these motifs consists of two alpha helixes connected by a loop of 12 acidic amino acids residues that coordinate the binding of Ca^{2+}. These motifs usually are found in pairs which are called EF-hand domains.

Some proteins have evolved motifs that are structurally similar to EF-hand motifs. The amino acid sequences of these EF-hand like motifs defer significantly from the canonical one [54]. However, they are still able to bind Ca^{2+} and to act as key regulators in the Ca^{2+} signaling pathway [55]. The affinity of these proteins for Ca^{2+} depends on the number of EF-hand motifs. Analysis of a variety of proteins showed that binding of Ca^{2+} to one domain may increase or decrease the affinity of the other domains [56, 57]. CaBPs have two structural conformations: and open conformation where calcium is not bound and a closed conformation, which is caused by the binding of calcium [58]. Binding of calcium will collapse the protein, which will activate binding to target proteins.

CaBPs are key in regulating important processes in the cell by activating proteins channels, kinases and other enzymes [59]. As signaling molecules CaBPs can be classified as Ca^{2+} sensor responders or Ca^{2+} sensor relays. Ca^{2+} sensor responders are proteins that contain other domains within the protein in addition to the Ca^{2+} binding domain (e.g. Ca^{2+}-dependent Kinases). Ca^{2+} sensor relays do not contain any other domains within the proteins and must physically interact with its targets to regulate their activities. Most of the CaBPs can be classified into four

main families: the calmodulin (CaM) family, the calcineurin (CN) family, the parvalbumin family and s100 family [60]. The CaM family is the most recognized of the calcium sensor relay proteins and includes proteins like calmodulin, troponin C and the myosin chains [60]. Most apicomplexan genomes encode a single prototypical CaM and a variable number of Calmodulin-like proteins (CMLs).

CML proteins are known to be present in plants and protists, and what distinguishes them from CaM is their low sequence identity to CaM and the presence of EF-hand like motifs [61]. CML proteins can have different subcellular localizations which allows for a wider variety of substrates. In contrast to mammalian CaMs are only reported to be cytosolic [62]. Mammalian CaM have been shown to have high affinity towards Ca^{2+} (K_d ranges from 100 nM to 1 μM) [63]. In comparison, CML proteins are known to have lower Ca^{2+} affinity (mid to high μM levels).

Ca^{2+} signaling plays a role in each step of the *T. gondii* lytic cycle [64-67]. The information available on calcium homeostasis in *Toxoplasma gondii* is surprisingly scant although it has been shown that the ion plays critical roles in its lytic cycle. Increase of cytosolic Ca^{2+} enhances every step of the lytic cycle and therefore virulence of the parasite [68]. Release of Ca^{2+} from the intracellular stores increases cytosolic Ca^{2+} which would stimulate a variety of proteins that signal the parasite for protein secretion, motility and egress. Although Ca^{2+} is important and essential in the regulation of the lytic cycle of the *Toxoplasma*, the molecules that activate and regulate this pathway is highly under characterized [69, 70].

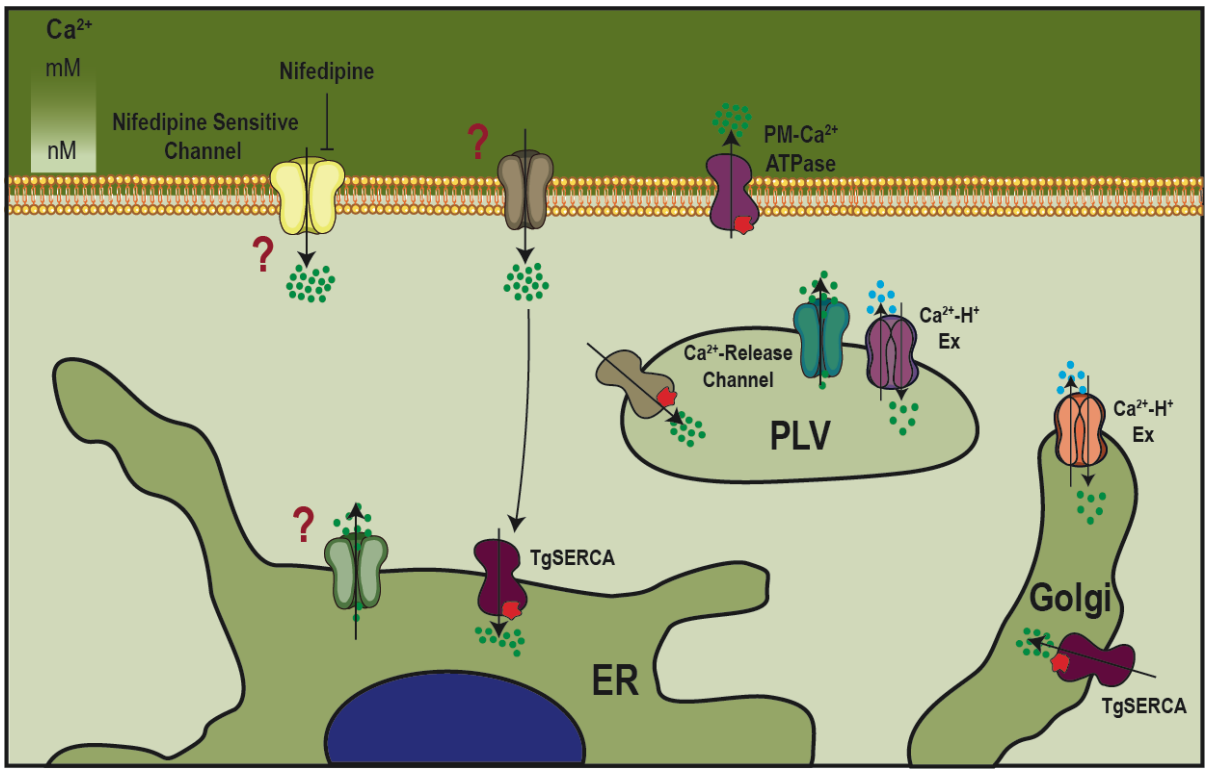

Figure 1.3. Calcium signaling pathway of *T. gondii*. Schematic representation of the molecules described to regulate and maintain Ca^{2+} homeostasis in *T. gondii*.

Intracellular organelles that have been shown to contain calcium, by stimulating release of Ca^{2+} using pharmacological drugs, are the endoplasmic reticulum (ER), acidocalcisomes (AC) and plant-like vacuole (PLV) [71, 72]. Previous work has demonstrated that addition of different extracellular [Ca^{2+}] allows for influx into the cytosol of the parasite. Incubation of the tachyzoites with Nifedipine, an L-type voltage gated Ca^{2+} channel blocker, can significantly decrease Ca^{2+} influx. Ca^{2+} influx also appears to be biphasic, where influx reaches a plateau at low [Ca^{2+}] and stimulated again at high [Ca^{2+}]. This behavior suggests the possibility that two channels mediate Ca^{2+} influx activated by different [Ca^{2+}]. Analysis of the genome of several protist parasite found homologs to voltage-gated

calcium channels (VGCCs) and Transient Receptor Potential (TRP) channels [73]. One of the homologs of TRP Channel identified has been localized to the ER of *Toxoplasma* through the use of high affinity tag. However, none of the identified homologs for TRP Channels or VGCCs have been characterized to mediate Ca^{2+} influx.

In *T. gondii* there are seven CML proteins which have been studied and suggested to play a role in parasite motility and conoid extrusion. Only two of them have been shown to bind Ca^{2+} *in vitro* [74-76]. Essential light chain (ELC1) was localized to the glideosome of tachyzoites [77]. The glideosome is an actomyosin based motor complex that allows for motility and invasion of the parasite. The main components of this complex are actin, myosin (MyoA), a myosin light chain (MLC1) and a CaBP (ELC1). ELC1 binds to MyoA activating the rest of the complex which will signal the parasite for motility. Studies have shown that ELC1 has low affinity (K_d of ~35 μM) for Ca^{2+} [75, 76]. ELC2 is another CML protein that works redundantly in the activation of MyoA [75]. However, the Ca^{2+} affinity of this protein has not been characterized.

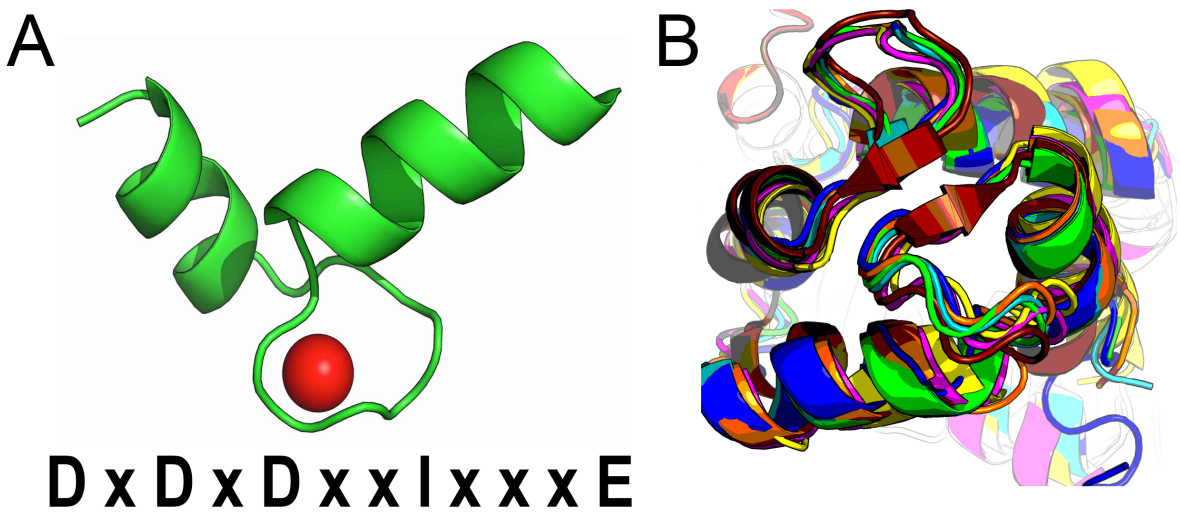

Figure 1.4. Structure of Calcium binding protein in *T. gondii*. A. Structure of an EF-hand motif bound to Ca^{2+}. Amino acid sequence of the calcium binding loop in an EF-hand motif. **B.** Overlay of the conserved predicted structure of the EF-Hand motif of the CaBPs present in *T. gondii*. Structures were predicted by I-Tasser. *Green, TgCaM; Turqoise, HsCaM; Blue, CaM1; Yellow, CaM2; Red, CaM3; Green, ELC1; Magenta, ELC2; Orange, TgCalnuc.*

Recent work localized three of these CML proteins to the conoid of the parasite, CaM1, CaM2 and CaM3 [78]. Deletion of CaM1 and CaM2 causes synthetic lethality in *Toxoplasma*, while CaM3 is essential. Immunoprecipitation of these proteins revealed the shared interaction with Myosin H (MyoH). MyoH is present in the conoidal glideosome which is essential for invasion to a new host cell [34]. The conoidal glideosome differs in that is composed by MyoH and MLC5 and 7. It has been proposed that these proteins work in a redundant manner with MyoH in a similar way that ELC1/ELC2 interact with MyoA. Analysis of the proteome of the conoid showed that these proteins interact with other proteins in

addition to MyoH [79]. We propose that these proteins target a variety of proteins within the Ca^{2+} signaling pathway which, to date, have not been identified. There is a significant gap in our knowledge of the molecules that are part of the Ca^{2+} signaling pathway in *T. gondii*. Understanding this pathway will be critical to the understanding of the biology of *T. gondii*. Uncovering the molecules essential this pathway may provide with new alternatives for chemotherapeutic targets.

1.1.8 DISSERTATION OUTLINE

This thesis will focus on the characterization of important molecules that regulate Ca^{2+}-signaling in *T. gondii* (Fig. 3). The characterization of the molecules that regulate key steps like Ca^{2+} influx and homeostasis have remained uncharacterized. Chapter 2 focuses on the description of the first fully characterized Ca^{2+} channel that mediates one of the mechanisms of Ca^{2+} influx. Previous evidence for the function of Ca^{2+} channels was obtained by examining pharmacological effect of drugs in Ca^{2+} influx. The current study reveals the first identified molecule involved in Ca^{2+} influx in *T. gondii*. We performed an in-depth characterization of the physical properties of the channel using electrophysiological techniques, which provided a new methodology to study Ca^{2+} signaling in the parasite.

Chapter 3 and 4 focuses on the multiple roles of calcium-binding proteins in the activation and regulation of Ca^{2+} signaling. *T. gondii*'s genome has over 66 proteins annotated with Ca^{2+} binding domains, but only a small number have been characterized. Ca^{2+} signals are highly coordinated and require mechanisms that maintain the organellar and cytosolic Ca^{2+}. In these chapter we characterize the

role of a newly identified calcium-binding protein in the maintenance of luminal ER and Golgi Ca^{2+}. Additionally, we characterize the role of another protein within the same pathway that regulates Ca^{2+} release. Chapter 3 focus on the characterization of a previously described CaBP, CaM2, in the regulation of Ca^{2+} channels. The majority of the CaBP proteins have been characterize as redundant activator of myosin light chains. However, since these proteins can target many proteins within the signaling pathway, we present and alternative role for this protein.

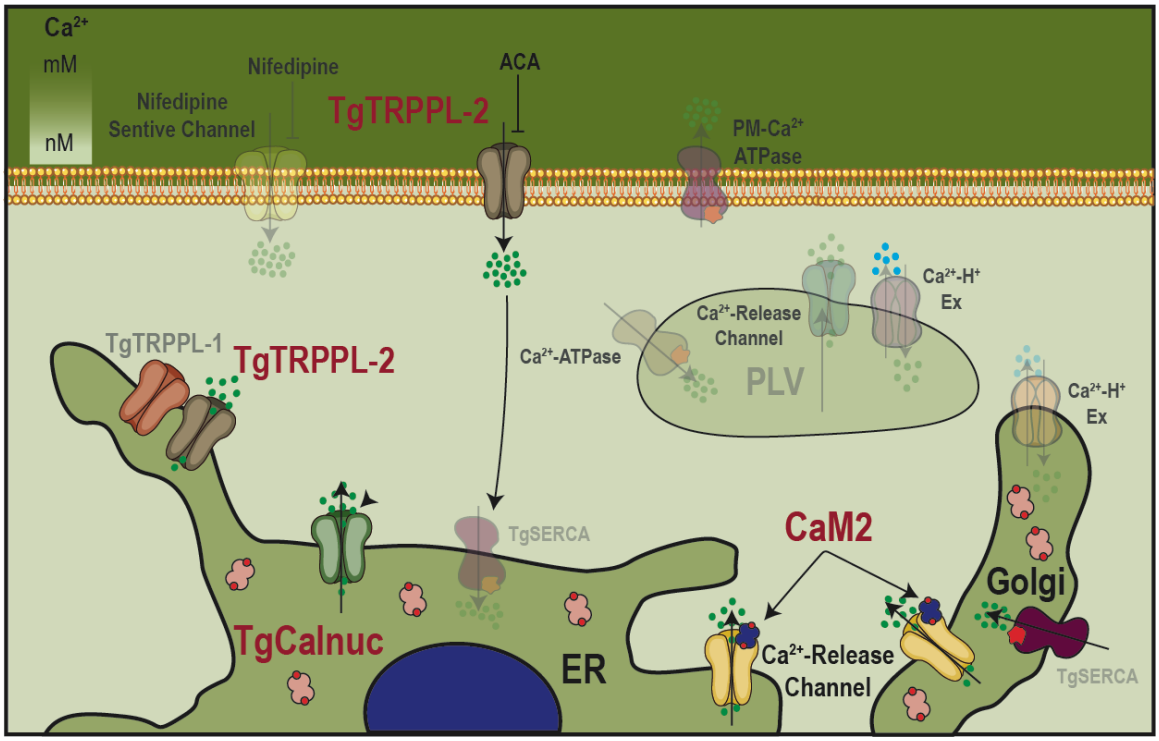

Figure 1.5. New molecules described in the Calcium signaling pathway of *T. gondii*. Schematic representation of the molecules described in this study and their role in the Ca^{2+} signaling pathway of *T. gondii*.

1.1.9 REFERENCES

1. Dubey, J.P., *Toxoplasmosis - a waterborne zoonosis.* Vet Parasitol, 2004. **126**(1-2): p. 57-72.
2. Morrissette, N.S. and L.D. Sibley, *Disruption of microtubules uncouples budding and nuclear division in Toxoplasma gondii.* J Cell Sci, 2002. **115**(Pt 5): p. 1017-25.
3. Nicolle, C. and L.H. Manceaux, *On a leishman body infection (or related organisms) of the gondi. 1908.* Int J Parasitol, 2009. **39**(8): p. 863-4.
4. Hill, D. and J.P. Dubey, *Toxoplasma gondii: transmission, diagnosis and prevention.* Clin Microbiol Infect, 2002. **8**(10): p. 634-40.
5. Tenter, A.M., A.R. Heckeroth, and L.M. Weiss, *Toxoplasma gondii: from animals to humans.* Int J Parasitol, 2000. **30**(12-13): p. 1217-58.
6. Aguirre, A.A., et al., *The One Health Approach to Toxoplasmosis: Epidemiology, Control, and Prevention Strategies.* Ecohealth, 2019. **16**(2): p. 378-390.
7. Montazeri, M., et al., *The global serological prevalence of Toxoplasma gondii in felids during the last five decades (1967-2017): a systematic review and meta-analysis.* Parasit Vectors, 2020. **13**(1): p. 82.
8. Jones, J.L., et al., *Toxoplasma gondii seroprevalence in the United States 2009-2010 and comparison with the past two decades.* Am J Trop Med Hyg, 2014. **90**(6): p. 1135-9.
9. Flegr, J., et al., *Toxoplasmosis--a global threat. Correlation of latent toxoplasmosis with specific disease burden in a set of 88 countries.* PLoS One, 2014. **9**(3): p. e90203.
10. Jones, J.L. and J.P. Dubey, *Foodborne toxoplasmosis.* Clin Infect Dis, 2012. **55**(6): p. 845-51.
11. Luft, B.J., et al., *Toxoplasmic encephalitis in patients with acquired immune deficiency syndrome.* JAMA, 1984. **252**(7): p. 913-7.
12. Luft, B.J. and A. Chua, *Central Nervous System Toxoplasmosis in HIV Pathogenesis, Diagnosis, and Therapy.* Curr Infect Dis Rep, 2000. **2**(4): p. 358-362.
13. Luft, B.J. and J.S. Remington, *Toxoplasmic encephalitis in AIDS.* Clin Infect Dis, 1992. **15**(2): p. 211-22.
14. Sahasrabudhe, N.S., et al., *Pathology of Toxoplasma myocarditis in acquired immunodeficiency syndrome.* Indian J Pathol Microbiol, 2003. **46**(4): p. 649-51.
15. Sibley, L.D. and J.C. Boothroyd, *Virulent strains of Toxoplasma gondii comprise a single clonal lineage.* Nature, 1992. **359**(6390): p. 82-5.
16. Liu, Q., et al., *Diagnosis of toxoplasmosis and typing of Toxoplasma gondii.* Parasit Vectors, 2015. **8**: p. 292.
17. Many, A. and G. Koren, *Toxoplasmosis during pregnancy.* Can Fam Physician, 2006. **52**: p. 29-30, 32.
18. Deng, Y., et al., *Recent progress on anti-Toxoplasma drugs discovery: Design, synthesis and screening.* Eur J Med Chem, 2019. **183**: p. 111711.
19. Lapinskas, P.J. and R.R. Ben-Harari, *Perspective on current and emerging drugs in the treatment of acute and chronic toxoplasmosis.* Postgrad Med, 2019. **131**(8): p. 589-596.

20. Konstantinovic, N., et al., *Treatment of toxoplasmosis: Current options and future perspectives.* Food Waterborne Parasitol, 2019. **15**: p. e00036.
21. Shiojiri, D., et al., *Combination of Clindamycin and Azithromycin as Alternative Treatment for Toxoplasma gondii Encephalitis.* Emerg Infect Dis, 2019. **25**(4): p. 841-843.
22. Bobic, B., I. Villena, and E. Stillwaggon, *Prevention and mitigation of congenital toxoplasmosis. Economic costs and benefits in diverse settings.* Food Waterborne Parasitol, 2019. **16**: p. e00058.
23. Djurkovic-Djakovic, O., et al., *Toxoplasmosis: Overview from a One Health perspective.* Food Waterborne Parasitol, 2019. **15**: p. e00054.
24. Pinto-Ferreira, F., et al., *Patterns of Transmission and Sources of Infection in Outbreaks of Human Toxoplasmosis.* Emerg Infect Dis, 2019. **25**(12): p. 2177-2182.
25. Smith, J.E., *A ubiquitous intracellular parasite: the cellular biology of Toxoplasma gondii.* Int J Parasitol, 1995. **25**(11): p. 1301-9.
26. Frenkel, J.K. and J.P. Dubey, *Toxoplasmosis and its prevention in cats and man.* J Infect Dis, 1972. **126**(6): p. 664-73.
27. Furtado, J.M., et al., *Toxoplasmosis: a global threat.* J Glob Infect Dis, 2011. **3**(3): p. 281-4.
28. Skariah, S., M.K. McIntyre, and D.G. Mordue, *Toxoplasma gondii: determinants of tachyzoite to bradyzoite conversion.* Parasitol Res, 2010. **107**(2): p. 253-60.
29. Ferguson, D.J., et al., *Ultrastructural studies on the sporulation of oocysts of Toxoplasma gondii. I. Development of the zygote and formation of the sporoblasts.* Acta Pathol Microbiol Scand B, 1979. **87B**(3): p. 171-81.
30. Ferguson, D.J., et al., *Ultrastructural studies on the sporulation of oocysts of Toxoplasma gondii. II. Formation of the sporocyst and structure of the sporocyst wall.* Acta Pathol Microbiol Scand B, 1979. **87B**(3): p. 183-90.
31. Gubbels, M.J., et al., *Fussing About Fission: Defining Variety Among Mainstream and Exotic Apicomplexan Cell Division Modes.* Front Cell Infect Microbiol, 2020. **10**: p. 269.
32. Sullivan, W.J., Jr. and V. Jeffers, *Mechanisms of Toxoplasma gondii persistence and latency.* FEMS Microbiol Rev, 2012. **36**(3): p. 717-33.
33. Montoya, J.G. and O. Liesenfeld, *Toxoplasmosis.* Lancet, 2004. **363**(9425): p. 1965-76.
34. Graindorge, A., et al., *The conoid associated motor MyoH is indispensable for Toxoplasma gondii entry and exit from host cells.* PLoS pathogens, 2016. **12**(1): p. e1005388.
35. Dos Santos Pacheco, N., et al., *Evolution, Composition, Assembly, and Function of the Conoid in Apicomplexa.* Trends Parasitol, 2020. **36**(8): p. 688-704.
36. Carruthers, V.B., O.K. Giddings, and L.D. Sibley, *Secretion of micronemal proteins is associated with toxoplasma invasion of host cells.* Cell Microbiol, 1999. **1**(3): p. 225-35.
37. Black, M.W. and J.C. Boothroyd, *Lytic cycle of Toxoplasma gondii.* Microbiol Mol Biol Rev, 2000. **64**(3): p. 607-23.
38. Shen, B. and L.D. Sibley, *The moving junction, a key portal to host cell invasion by apicomplexan parasites.* Curr Opin Microbiol, 2012. **15**(4): p. 449-55.

39. Kemp, L.E., M. Yamamoto, and D. Soldati-Favre, *Subversion of host cellular functions by the apicomplexan parasites.* FEMS Microbiol Rev, 2013. **37**(4): p. 607-31.
40. Joiner, K.A., et al., *Structure and function of the parasitophorous vacuole membrane surrounding Toxoplasma gondii.* Ann N Y Acad Sci, 1994. **730**: p. 1-6.
41. Schwab, J.C., C.J. Beckers, and K.A. Joiner, *The parasitophorous vacuole membrane surrounding intracellular Toxoplasma gondii functions as a molecular sieve.* Proc Natl Acad Sci U S A, 1994. **91**(2): p. 509-13.
42. Blader, I.J., et al., *Lytic Cycle of Toxoplasma gondii: 15 Years Later.* Annu Rev Microbiol, 2015. **69**: p. 463-85.
43. Clapham, D.E., *Calcium signaling.* Cell, 2007. **131**(6): p. 1047-58.
44. Berridge, M.J., M.D. Bootman, and H.L. Roderick, *Calcium signalling: dynamics, homeostasis and remodelling.* Nat Rev Mol Cell Biol, 2003. **4**(7): p. 517-29.
45. Berridge, M.J., P. Lipp, and M.D. Bootman, *The versatility and universality of calcium signalling.* Nat Rev Mol Cell Biol, 2000. **1**(1): p. 11-21.
46. Casamassima, F., et al., *L-type calcium channels and psychiatric disorders: A brief review.* Am J Med Genet B Neuropsychiatr Genet, 2010. **153B**(8): p. 1373-90.
47. Catterall, W.A., *Voltage-gated calcium channels.* Cold Spring Harb Perspect Biol, 2011. **3**(8): p. a003947.
48. Zamponi, G.W., et al., *The Physiology, Pathology, and Pharmacology of Voltage-Gated Calcium Channels and Their Future Therapeutic Potential.* Pharmacol Rev, 2015. **67**(4): p. 821-70.
49. Montell, C., *The TRP superfamily of cation channels.* Sci STKE, 2005. **2005**(272): p. re3.
50. Montell, C., *Physiology, phylogeny, and functions of the TRP superfamily of cation channels.* Sci STKE, 2001. **2001**(90): p. re1.
51. Venkatachalam, K. and C. Montell, *TRP channels.* Annu Rev Biochem, 2007. **76**: p. 387-417.
52. Pepke, S., et al., *A dynamic model of interactions of Ca2+, calmodulin, and catalytic subunits of Ca2+/calmodulin-dependent protein kinase II.* PLoS Comput Biol, 2010. **6**(2): p. e1000675.
53. Elies, J., et al., *An Update to Calcium Binding Proteins.* Adv Exp Med Biol, 2020. **1131**: p. 183-213.
54. Zhou, Y., et al., *Prediction of EF-hand calcium-binding proteins and analysis of bacterial EF-hand proteins.* Proteins, 2006. **65**(3): p. 643-55.
55. Villalobo, A., M. Gonzalez-Munoz, and M.W. Berchtold, *Proteins with calmodulin-like domains: structures and functional roles.* Cell Mol Life Sci, 2019. **76**(12): p. 2299-2328.
56. Weljie, A.M., et al., *Comparative modeling studies of the calmodulin-like domain of calcium-dependent protein kinase from soybean.* Proteins, 2000. **39**(4): p. 343-57.
57. Christodoulou, J., et al., *Evidence for differing roles for each lobe of the calmodulin-like domain in a calcium-dependent protein kinase.* J Biol Chem, 2004. **279**(28): p. 29092-100.

58. Kursula, P., *The many structural faces of calmodulin: a multitasking molecular jackknife.* Amino Acids, 2014. **46**(10): p. 2295-304.
59. Berchtold, M.W. and A. Villalobo, *The many faces of calmodulin in cell proliferation, programmed cell death, autophagy, and cancer.* Biochim Biophys Acta, 2014. **1843**(2): p. 398-435.
60. Yanez, M., J. Gil-Longo, and M. Campos-Toimil, *Calcium binding proteins.* Adv Exp Med Biol, 2012. **740**: p. 461-82.
61. La Verde, V., P. Dominici, and A. Astegno, *Towards Understanding Plant Calcium Signaling through Calmodulin-Like Proteins: A Biochemical and Structural Perspective.* Int J Mol Sci, 2018. **19**(5).
62. Perochon, A., et al., *Calmodulin and calmodulin-like proteins in plant calcium signaling.* Biochimie, 2011. **93**(12): p. 2048-53.
63. Linse, S., A. Helmersson, and S. Forsen, *Calcium binding to calmodulin and its globular domains.* J Biol Chem, 1991. **266**(13): p. 8050-4.
64. Carruthers, V.B., S.N. Moreno, and L.D. Sibley, *Ethanol and acetaldehyde elevate intracellular [Ca2+] and stimulate microneme discharge in Toxoplasma gondii.* Biochem J, 1999. **342 (Pt 2)**: p. 379-86.
65. Borges-Pereira, L., et al., *Calcium Signaling throughout the Toxoplasma gondii Lytic Cycle: A STUDY USING GENETICALLY ENCODED CALCIUM INDICATORS.* J Biol Chem, 2015. **290**(45): p. 26914-26.
66. Mondragon, R. and E. Frixione, *Ca(2+)-dependence of conoid extrusion in Toxoplasma gondii tachyzoites.* The Journal of eukaryotic microbiology, 1996. **43**(2): p. 120-7.
67. LaFavers, K.A., et al., *A novel dense granule protein, GRA41, regulates timing of egress and calcium sensitivity in Toxoplasma gondii.* Cell Microbiol, 2017. **19**(9).
68. Pace, D.A., et al., *Calcium entry in Toxoplasma gondii and its enhancing effect of invasion-linked traits.* J Biol Chem, 2014. **289**(28): p. 19637-47.
69. Lourido, S. and S.N. Moreno, *The calcium signaling toolkit of the Apicomplexan parasites Toxoplasma gondii and Plasmodium spp.* Cell Calcium, 2015. **57**(3): p. 186-93.
70. Hortua Triana, M.A., et al., *Calcium signaling and the lytic cycle of the Apicomplexan parasite Toxoplasma gondii.* Biochim Biophys Acta Mol Cell Res, 2018. **1865**(11 Pt B): p. 1846-1856.
71. Rohloff, P., et al., *Calcium uptake and proton transport by acidocalcisomes of Toxoplasma gondii.* PLoS One, 2011. **6**(4): p. e18390.
72. Miranda, K., et al., *Characterization of a novel organelle in Toxoplasma gondii with similar composition and function to the plant vacuole.* Mol Microbiol, 2010. **76**(6): p. 1358-75.
73. Prole, D.L. and C.W. Taylor, *Identification of intracellular and plasma membrane calcium channel homologues in pathogenic parasites.* PLoS One, 2011. **6**(10): p. e26218.
74. Seeber, F., B. Beuerle, and H.H. Schmidt, *Cloning and functional expression of the calmodulin gene from Toxoplasma gondii.* Mol Biochem Parasitol, 1999. **99**(2): p. 295-9.
75. Williams, M.J., et al., *Two Essential Light Chains Regulate the MyoA Lever Arm To Promote Toxoplasma Gliding Motility.* mBio. **6**(5).

76. Powell, C.J., et al., *Dissecting the molecular assembly of the Toxoplasma gondii MyoA motility complex.* J Biol Chem, 2017. **292**(47): p. 19469-19477.
77. Nebl, T., et al., *Quantitative in vivo analyses reveal calcium-dependent phosphorylation sites and identifies a novel component of the Toxoplasma invasion motor complex.* PLoS Pathog, 2011. **7**(9): p. e1002222.
78. Long, S., et al., *Calmodulin-like proteins localized to the conoid regulate motility and cell invasion by Toxoplasma gondii.* PLoS Pathog, 2017. **13**(5): p. e1006379.
79. Long, S., et al., *A conserved ankyrin repeat-containing protein regulates conoid stability, motility and cell invasion in Toxoplasma gondii.* Nat Commun, 2017. **8**(1): p. 2236.

CHAPTER 2

Calcium signaling by a Transient Receptor Channel is important for *Toxoplasma gondii* growth[1]

[1] Karla M. Márquez-Nogueras, Nathan Chasen, Myriam A. Hortua Triana, Ivana Kuo, Silvia N.J. Moreno. Submitted to *eLife*.

2.1 ABSTRACT

Transient Receptor Potential (TRP) channels participate in calcium (Ca^{2+}) influx and intracellular Ca^{2+} release. TRP channels have not been studied in *Toxoplasma gondii* or any other Apicomplexan parasite. We characterized TgGT1_310560, a protein predicted to possess a TRP domain (TgTRPPL-2) and determined its role in Ca^{2+} signaling in *T. gondii*, the causative agent of toxoplasmosis. TgTRPPL-2 localized to the plasma membrane and the endoplasmic reticulum of *T. gondii*. *ΔTgTRPPL-2* mutant was defective in growth and Ca^{2+} influx. Heterologous expression of TgTRPPL-2 in HEK-3KO cells allowed its functional characterization. Patching of ER-nuclear membranes demonstrated that TgTRPPL-2 is a non-selective cation channel that conducts Ca^{2+}. Pharmacological blockers of TgTRPPL-2 inhibited Ca^{2+} influx and parasite growth. This is the first report of an Apicomplexan channel that conducts Ca^{2+} and initiates the Ca^{2+} signaling cascade that culminates in the stimulation of motility, invasion and egress. TgTRPPL-2 is a potential target for combating Toxoplasmosis.

2.2 INTRODUCTION

Ca^{2+} signaling is universal and forms part of the signaling pathways that activate or modulate a variety of physiological responses like gene transcription, muscle contraction, cell differentiation and proliferation [44]. Ca^{2+} signals can be generated through the opening of ion channels that allow the downward flow of Ca^{2+} from either outside the cell or from intracellular stores like the endoplasmic reticulum [43].

Toxoplasma gondii is an intracellular parasite from the Apicomplexan phylum, that causes toxoplasmosis in humans [42]. Infection with *T. gondii* may lead to severe complications in immunocompromised patients like encephalitis, myocarditis and death [80]. The *T. gondii* tachyzoite engages in a lytic cycle directly responsible for the pathogenicity of the infection as it results in lysis of host cells [37]. The lytic cycle consists of active invasion of host cells, replication inside a parasitophorous vacuole and egress to search for a new host cell to invade. Ca^{2+} signals resulting from Ca^{2+} influx or from intracellular release, trigger a signaling cascade in the parasite that culminates in the stimulation of essential features of its lytic cycle, like motility, invasion, egress and secretion of proteins essential for attachment to the host cell [69, 70].

Previous work from our lab showed the presence of Ca^{2+} influx activity at the plasma membrane of *T. gondii* tachyzoites that was functional in extracellular tachyzoites [68] and intracellular replicating parasite [81]. The application of

voltage operated Ca^{2+} channel blockers such as nifedipine inhibited ~ 80% of Ca^{2+} influx, and the residual Ca^{2+} entry activity suggested the potential existence of more than one channel at the plasma membrane of *T. gondii* [68]. The molecular entity of these channels has remained elusive.

Transient Receptor Potential (TRP) channels are a large family of cation permeable channels grouped into seven subfamilies based on their gene sequence TRP channels can be activated by a multitude of stimuli and are involved in a wide range of cellular functions [83]. Most TRP channels are permeable to Ca^{2+} and all of them are permeable to monovalent cations [83]. Some TRP channels can participate in Ca^{2+} influx as well as Ca^{2+} release from intracellular stores [51, 84]. Mutations in these molecules are associated with a diverse set of diseases, due to their wide distribution in various tissues and their roles in pathological conditions like cancer and renal physiology making these channels important therapeutic targets [85]. The polycystin TRP (TRPP) subfamily of proteins are implicated in Autosomal Dominant Polycystic Kidney Disease (ADPKD) [86].

Predicted protein sequences with TRP domains have been found in most parasitic protozoa, although in lower numbers and types than in other organisms [87]. This could be the result of the evolutionary distance between the species studied, or because of loss of specific functions resulting from evolution of the parasitic lifestyle [87, 88]. A genome analysis of a number of pathogenic protozoan parasites [73] searching for genes with homology to mammalian Ca^{2+} channels identified two *T. gondii* hypothetical genes (TgGT1_247370 and TgGT1_310560)

with homologous regions to the TRPP family [89]. We termed these genes *TgTRPPL-1* and *TgTRPPL-2*. Previous work from our laboratory, localized TgTRPPL-1 to the ER with high resolution tags due to its low level of expression [90].

In this work we characterize TgTRPPL-2 in *T. gondii*, which represents the first TRP cation channel studied in any Apicomplexan parasite. Using reverse genetic approaches, we determine the role of TgTRPPL-2 in the lytic cycle of the parasite. We also characterize the electrophysiological features of TgTRPPL-2 and its role in Ca^{2+} influx and, interestingly, find that pharmacological agents that block the activity of TgTRPPL-2 also inhibited Ca^{2+} influx in the parasite and parasite growth. TgTRPPL-2 emerges as one of the molecular entities involved in initiating Ca^{2+} signals in *T. gondii*.

2.3 EXPERIMENTAL PROCEDURES

Toxoplasma growth

All parasite strains were continuously maintained *in vitro* by serial passage in Dulbecco's modified minimal essential media (DMEM) with 1% FBS, 2.5 µg/ml amphotericin B, 100 µg/ml streptomycin in the human telomerase reverse transcriptase immortalized foreskin fibroblasts (hTERT) [91]. Carboxy-terminus tagging was done in the parental line RHTatiΔku80 (TatiΔku80) [92] a parasite line that contains the tetracyclin-regulated transactivator system that allows conditional expression of genes [93] and also in which the *ku80* gene was deleted increasing efficiency of homologues recombination [94].

Generation of mutants

The smHA-LIC-CAT plasmid was used for in situ C-terminal tagging of TgTRPPL-2-smHA [90]. Carboxy-terminus tagging was done in the parental line RHTatiΔku80 (TatiΔku80) [92] a parasite line that contains the tetracyclin-regulated transactivator system that allows conditional expression of genes [93] and also in which the *ku80* gene was deleted increasing efficiency of homologues recombination [94]. Briefly, a homology region of 974 bp covering the 3' region of the gene of interest excluding the STOP codon was amplified by PCR using *T. gondii* RH genomic DNA as template and cloned into the plasmid. Plasmids correctly built were selected by restriction digest and confirmed by sequencing. The oligonucleotides primers used for PCR and for creating the gene-tagging plasmids and for PCR validations are listed in Table S3 (Primers T1-T3). Prior to transfection all plasmids were linearized within the region of homology. Approximately 20 µg of plasmid DNA was transfected into $1x10^7$ T. gondii strain RHTatiΔKu80 using a Gene Pulser X Cell electroporator (BioRad). Selection for integration of the targeting plasmid was performed with 20µM chloramphenicol, and clones were isolated by limiting dilution. DNA of selected clones were isolated and screened by PCR using primers located upstream of the homology region (forward) and downstream into the plasmids (reverse).

To disrupt the *TgTRPPL-2* (TgGT1_310560) gene a single guide RNA against TgTRPPL-2 was constructed as described [95]. The single guide RNA was mutagenized with the desired sequence in a plasmid that contains the Cas9 using the Q5 Mutagenesis Kit following manufacturer's instructions. The correct mutation was verified by sequencing. The pyrimethamine-resistant DHFR cassette was

amplified by PCR with primers containing 50 bp homology arms of the region upstream and downstream of the start and stop codon of the *TgTRPPL-2* gene. sgTgTRPPL-2 CRISPR plasmid was co-transfected with the DHFR cassette (3:1 respectively) into RH tachyzoites. Selection followed with pyrimethamine for 7 days. Parasites were sub-cloned by limiting dilution and screening for clones was done by PCR. The primers used for the creation of the ΔTgTRPPL-2 are listed in Table S3 (Primer K1-K4).

Quantitative PCR. Total RNA from parental, Δ*TgTRPPL-2* and Δ*TgTRPPL2-trppl2* was extracted and reversed-transcribed into cDNA. The qPCR reaction was done using the iQ^{TM}SYBR Green master mix (BioRad), plus primers, and the reverse-transcribed cDNA (Primers shown in Table S3, Q1-Q2). The qRT-PCR was carried out on a CFX96^{TM} PCR Real-Time detection system (C1000Touch^{TM} Thermal cycler, BioRad). Relative quantification software (CFX Maestro^{TM} software) was used for the analysis and relative expression levels were calculated as the fold change using the formula $2^{\Delta\Delta}$CT {Livak, 1995 #318}. Normalization was done using Actin and Tubulin primers as reference. Experiments were repeated three times with triplicate samples.

***Western blot analysis*.** SDS-polyacrylamide gel electrophoresis (SDS-PAGE) followed established protocols [96]. Lysates were prepared by resuspending a pellet of 1 x 10^8 tachyzoites in 50 µL of Cell Lytic^{M} lysis buffer containing 12.5 U benzonase and 1 X protease cocktail inhibitor (P8340 Sigma). The reaction was stopped with one volume of 2% SDS and 1 mM EDTA. Total lysates were boiled in Laemmli sample buffer (BioRad). Immunoblotting followed established protocols

using mouse anti-HA monoclonal antibody (1:1,000) (Roche). Detection was done using the Odyssey Clx LICOR system using goat anti-mouse IRDye800WC (1:10,000). Loading control for westerns were done with primary mouse-anti-tubulin antibodies at a 1:15,000 dilution and goat anti-mouse IRDDye800WC as secondary (1:10,000).

Immunofluorescence microscopy Extracellular parasites were collected and purified as previously described [97]. Parasites were washed once with buffer A with glucose (BAG, 116 mM NaCl, 5.4 mM KCl, 0.8 mM $MgSO_4$, 5.5 mM glucose and 50 mM HEPES, pH 7.4) and an aliquot with 2 x 10^4 parasites was overlaid on a coverslip previously treated with poly-L-Lysine. Intracellular tachyzoites were grown on hTERT cells on coverslips previously infected with freshly lysed parasites. Both extracellular and intracellular parasites were fixed with 3% paraformaldehyde for 20 min at room temperature (RT), permeabilized with 0.3% Triton X-100, blocked with 3% bovine serum albumin (BSA), and exposed to primary antibodies (Ratα-HA 1:100). The secondary antibodies used were goat-αrat Alexa Fluor 488 (Life Technologies) at a 1:1,000 dilution. For co-localization studies we used α-Sag1 (1:1,000) as membrane marker and α-TgSERCA as ER marker (1:1,000). Slides were examined using an Olympus IX-71 inverted fluorescence microscope with a photometric CoolSNAP HQ charge-coupled device (CCD) camera driven by DeltaVision software (Applied Precision, Seattle, WA).

Immunoprecipitation assays. Freshly lysed tachyzoites expressing TgTRPPL-2-smHA were collected and filtered through an 8 µM membrane (Whatman).

Tachyzoites were washed twice in BAG and resuspended in lysis buffer (50mM Tris-HCl, pH 7.4, 150 mM KCl, 1 mM EDTA, 0.4% NP-40) to a final concentration of 2 x 10^9 total cells. Lysis was allowed to proceed for thirty minutes at 4^{o}C and cells were centrifuged at 15,000 x g for 20 min. Immunoprecipitation of TgTRPPL-2-smHA protein was performed using the Pierce HA Tag/Co-IP Kit (Thermo Fisher Scientific, Waltham, MA) according to manufacturer's instructions. Briefly, HA magnetic beads were washed twice in lysis buffer and mixed with the parasite lysate by vortexing for 1 hour at RT. Beads were collected and the flow-through fraction was saved for further analysis. Beads were washed twice in wash buffer (50mM Tris-HCl, pH 7.4, 150 mM KCl, 1 mM EDTA, 0.1% NP-40) and once in ddH_2O by gentle mixing. The tagged protein was recovered by mixing the beads with 1x Laemmli buffer and heated at 65^{o}C for 10 min. The supernatant was collected and used for PAGE and western blots. The corresponding band was cut and resuspended in water and analyzed using LC-Mass Spectrometry. Samples were sent to the Proteomics and Mass Spectrometry Core Facility at the University of Georgia for analysis.

Growth and Invasion Assays. Plaques growth was done as previously described, with slight modifications {Liu, 2014 #136}. Briefly, 200 egressed tachyzoites were allowed to infect confluent hTERT cells for 7 days. After seven days cells were fixed with ethanol and stained with crystal violet. Plaque sizes were analyzed using FIJI [98]. Invasion assay were performed as previously described, with slight modifications [99]. A subconfluent monolayer of HFF cells were infected with 2x10^7 tachyzoites in the presence of 1.8 mM or 0.5 mM Ca^{2+} and placed for 20 minutes

on ice and subsequently transferred for 5 minutes to a 37°C water bath for parasite invasion. Cells were immediately fixed with 3% paraformaldehyde for 20 minutes. Extracellular parasites (attached) were stained using Rabbit□Sag1 (1:1,000) prior to permeabilization while intracellular parasites (invaded) were stained with Mouse□Sag1 (1:200). Secondary antibodies were goat-□rabbit Alexa Fluor 546 (1:1,000) and goat-□mouse Alexa Fluor 488 (1:1,000). Images were taken with an Olympus IX-71 inverted fluorescence microscope with a Photometric CoolSNAP HQ CCD camera driven by DeltaVision software (Applied Precision, Seattle, WA). Quantification was made of ten-fields of view at a 1000 magnification from three independent biological replicates. Percentage of invaded vs attached was quantified by dividing the amount of parasite invaded or attached by the total parasites quantified in the field of view.

Egress experiments. hTERT cells were infected with $5x10^5$ of RH or □TgTRPPL-2 tachyzoites. 24 h after infection parasitophorous vacuoles were observed by microscopy and washed with Ringer's buffer (155 mM NaCl, 3 mM KCl, 1 mM MgCl2, 3 mM NaH2PO4H2O, 10 mM HEPES, pH 7.3, and 5 mM glucose). Ringer's buffer was used as extracellular buffer in the presence or absence of 1.8 mM Ca^{2+}. Drugs were added in Ringer's buffer 30 seconds after imaging at the following concentrations: saponin (0.02%) or Zaprinast (100 □M). Images were acquired in a time-lapse mode with an acquisition rate of 3 seconds for 12-20 minutes. For statistical analysis, egress time was quantified as the first parasite to egress out of the parasitophorous vacuole. Statistical analysis was done for 3 independent biological replicates and at least 5 PVs per experiment.

Cytosolic calcium measurements. Parasites were loaded with Fura2-AM as described in [100]. Briefly, fresh lysed parasites were washed twice at 1,800 rpm for 10 min at room temperature in buffer A (BAG) (116 mM NaCl, 5.4 mM KCl, 0.8 mM MgSO4, 5.5 mM d-glucose and 50 mM Hepes, pH 7.4). Parasites were resuspended to a final density of $1x10^9$ parasites/mL in loading buffer (Ringer's plus 1.5% sucrose, and 5 μM Fura2-AM). The suspension was incubated for 26 min at 26 °C with mild agitation. Subsequently, the parasites were washed twice with Ringer's buffer to remove extracellular dye. Parasites were resuspended to a final density of $1x10^9$ parasites/mL in Ringer's buffer and kept in ice. Parasites are viable for a few hours under these conditions. For fluorescence measurements, $2x10^7$ parasites/mL were placed in a cuvette with 2.5 mL of Ringer's buffer. The cuvette was placed in a thermostatically controlled Hitachi F-7000 fluorescence spectrophotometer for Ca^{2+} measurements. Excitation was at 340 and 380 nm, and emission at 510 nm. The Fura2-AM fluorescence relationship to intracellular Ca^{2+} concentration ($[101]_i$) was calibrated from the ratio of 340/380 nm fluorescence values after subtraction of the background fluorescence of the cells at 340 and 380 nm as previously described [102]. Changes in $[101]_i$ (ΔF $[Ca^{2+}]$) were measured by subtracting the highest peak of calcium in the first 20 s after addition of calcium or 100 s after the addition of drugs minus the baseline.

Antibody production of TgTRPPL-2. The antigenic region for TgTRPPL-2 chosen for antibody production was identified using the IEDB suite of antigenicity prediction software. The DNA sequence was amplified from RH genomic DNA and cloned into the pET-32 LIC/EK vector (Novagen), which adds an N-terminal

thioredoxin and histidine tag to the expressed protein. Recombinant CP1Ag was expressed and initially purified via a nickel-affinity column (HisPur Thermo Fisher) as previously described [103]. Cleavage of the N-terminal thioredoxin and histidine tag was done by biotinylated thrombin. The antigen was passed again through the nickel column and the purified tag-less antigen was gently eluted using 10 mM imidazole. Antibodies in mice were generated as previously described [104]. Swiss Webster mice (Charles River) were inoculated intraperitoneally with 100 µg of TgTRPPL-2 mixed with complete Freund's adjuvant, followed by two boosts with 50 µg of TgTRPPL-2, with each boost being mixed with incomplete Freund's adjuvant. The final serum was collected by cardiac puncture after CO_2 euthanasia. The animal protocol used was approved by the UGA Institutional Animal Care and Use Committee (IACUC).

Cell transfections and culture of DT40-3KO Cells.

Total RNA of wild type *T. gondii* were extracted and reversed transcribed into cDNA. TgTRPPL-2 whole cDNA was amplified using primers shown in Table S1 (Primers C1-C6). The amplified cDNA was cloned into the Zero Blunt TOPO vector using the cloning kit per manufacturers instruction. Correct insertion was verified by colony PCR using M13F and M13R primers. Restriction digests was performed to remove the insert from the vector using the following restriction enzymes: BamHI and AvrII. The purified *TgTRPPL-2 cDNA* was ligated to linearized pCDNA 3.1 plasmid. Ligation to the vector was confirmed by PCR and sequencing. Purified TRPPL-2-pCDNA was used to co-transfect DT40-3KO cells.

DT40 cells which have the 3 endogenous isoforms of the IP3 Receptor knocked out were a gift from Dr. David Yule [101, 105]. The cells were maintained in Dulbecco's modified minimal essential media (DMEM) with 10% Fetal Bovine Serum 2.5 µg/ml amphotericin B and 100 µg/ml streptomycin. Cells were transiently transfected as previously described [106] with 2.5 μg of TgTRPPL-2, PC2 or RFP DNA targeted to the ER. Each plasmid DNA were diluted in 200 μL of Opti-MEM with 25 μL of Polyethylenimine and incubated for 10 min. The mix was then added to semi confluent DT40-3KO cells in a dropwise manner, and 24 h later the media was changed.

Preparation of Nuclear extracts. 48 hours after transfection, cells were collected and the nucleus extracted as previously described [107]. $2x10^7$ of transiently transfected cells were collected in ice cold PBS. Cells were spun down and washed twice in PBS and resuspended in Nuclei Isolation Solution (150 mM KCl, 250 mM Sucrose, 10 mM Tris-HCl, 1.4 mM B-Mercaptoethanol, 0.2 mM PMSF, pH 7.3). Cells were homogenized with a homogenizer and stored on ice. 100 μL of nuclei were transferred to cover slips previously coated with poly-L-lysine and incubated for 20 minutes before filling the chamber with bath solution.

Patch clamp of Nuclear membranes. Nuclear extract expressing TgTRPPL-2 or the respective control together with gCaMPER [108] were measured. Electrical currents were recorded using Standard Wall Borosilicate Capillaries (Harvard Bioscience, Massachusets) with 10-15 MΩ resistance. Holding potentials were maintained at 0 mV. The internal solution contained: 140 mM KCl or CsCl, 10 mM HEPES, 1.8 mM or 10 mM free Ca^{2+} adjusted with EGTA. Standard Bath Solution

contained the same reagents and concentrations as the pipette solution using 100 nM of free Ca^{2+}. The single-channel conductance was obtained from the current-voltage relationship for each condition tested. Calcium currents were elicited by applying pulses from -80 mV up to 20 mV for 25 seconds. Analysis of amplitude, open probability and channel conductance were done using a 45 kHz filter. Data for recording was collected using the HEKA Electronic Patch Clamp EPC10 (Harvard Bioscience, Massachusetts).

Statistics. Statistical analysis was performed by Student's T-test using GraphPad PRISM version 8.2. All experimental data was analyzed from three biological replicates. Error bars shown represent Standard Error of the Mean (SEM) of the biological replicates analyzed. For the electrophysiological analysis a total of 3 cells per biological replicate (9 total cells) were analyzed. Each cell was depolarized a total of 5 times per experimental conditions.

2.4 Results

2.4.1 TgTRPPL-2 (TgGT1_310560) localizes to the plasma membrane and the Endoplasmic Reticulum

Two genes in the *T. gondii's* genome annotated as hypothetical proteins possess Polycystic Kidney Disease (PKD) domains, which are characteristic of the Subfamily P (polycystin) of TRP channels. Mammalian TRPP channels contain 6 transmembrane domains with a large extracellular loop between the first and second transmembrane domain [49]. We termed these molecules in *T. gondii* TgTRPPL-1 (TgGT1_247370) and TgTRPPL-2 (TgGT1_310560). Using BLAST to

compare the amino acid sequences of the mammalian *PKD2* and *TgTRPPL-2* showed low sequence homology (21.7%), even at the PKD Domains. The *TgGT1_310560* gene predicts the expression of a protein of 2,191 amino acids with an apparent molecular weight of 237 kDa and 14 transmembrane domains. The predicted topology [109] showed a large extracellular loop between the first and second transmembrane domain, which is characteristic of PKD Channels (Fig. 1A, *TgGT1_310560 cartoon*). Because our initial analysis showed low sequence homology, we next analyzed the amino acid sequence using the software HHPred, which searches for homology based on protein sequence and secondary structure [110]. Sequence analysis of TgTRPPL-2 showed high homology to mammalian PKD2, and the top 10 hits are homologous to PKD2 of a variety of organisms (Table S1).

To investigate the localization of TgTRPPL-2, we introduced the high affinity tag smHA [19] at the 3' terminus of the *TgTRPPL-2* locus and isolated TgTRPPL-2-smHA cell clones. Carboxy-terminus tagging was done in the parental line RHTatiΔku80 (*TatiΔku80*) which favors homologous recombination [23]. Correct incorporation of the tag in the TgTRPPL-2-smHA line was validated by PCR (Fig. S1A) and western blot analysis using anti-HA antibodies (Fig. 1B). A band of approximately ~150 kDa was observed in lysates of TgTRPPL-2-smHA tachyzoites, which is nearly 87 kDa smaller (Fig. 1B) than the predicted size of 237 kDa without taking into account the smHA tag (~39 kDa).

Interestingly, a recent release of ToxoDBv.45 presents additional models for the *TgGT1_310560* gene from different *T. gondii* strains. The gene model for

TgVAND_310560 shows two fragments, *TgVAND_310560A,* which predicts a protein with 9 TMD and a size of ~107.97 kDa and *TgVAND_310560B*, which predicts a protein with 6 TMD and a size of ~116.6 kDa. Sequence alignments of the *TgGT1_310560* gene with the gene models for the VAND strain (A and B) shows 98% homology between them (Fig. 1C). The *T. gondii* VAND strain is an isolate from South America and belongs to the hypervirulent Type I group, as the GT1 and RH strains. According to the gene model of the VAND strain, the predicted MW of the TgVAND_310560B protein would be similar to the band size observed in our western blots (116.6 + 39) with a predicted topology of 6 TMD, in closer agreement with typical TRP channels [112, 113].

To further demonstrate that the protein band observed in the western blot analysis corresponded to the tagged TgTRPPL-2 gene, we performed immunoprecipitations with anti-HA of lysates from the TgTRPPL-2-smHA cells. The immunoprecipitated samples were developed in a PAGE gel. The ~150 kDa band was sliced and analyzed by mass spectrometry (Fig. S1B, *red box*)(Table S2). According to the results, approximately ~700 amino acids toward the C-terminus domain were covered by the peptides corresponding to a 66% coverage. Comparison of the coverage with the TgVAND_310560B predicted protein, approximately 66% of the sequence was recovered by the mass spectrometry analysis. This result indicated that the TgGT1_310560 is likely cleaved, a characteristic common with other TRP channels [114].

We next investigated the cellular location of TgTRPPL-2. Immunofluorescence analysis (IFAs) of extracellular and intracellular parasites

showed that TgTRPPL-2-smHA may localize to peripheral vesicles close to the plasma membrane and to the endoplasmic reticulum (ER) (Fig. 1D-E). Some co-localization with the plasma membrane surface antigen (Sag1) and the sarco-endoplasmic reticulum Ca^{2+} ATPase (TgSERCA) (ER marker) was observed (Fig. 1D-E). However, considering the low-level of expression of TgTRPPL-2, it was difficult to draw definitive conclusions about its localization.

We next raised polyclonal antibodies against a fragment peptide of TgTRPPL-2, which is indicated in Fig. 1A (*highlighted in green*). The peptide was expressed in bacteria, purified and used for immunization of mice. Mouse serum was isolated and affinity purified prior to its use for IFAs. The localization at the periphery of extracellular tachyzoites was further confirmed by co-localization with αSAG1 (Fig. 1F). In addition, extracellular tachyzoites showed intracellular staining that co-localized with TgSERCA (Fig. 1F) supporting ER localization. Additionally, IFAs of intracellular tachyzoites showed that TgTRPPL-2 co-localized with αSAG1 and αSERCA (Fig.1G).

In summary, TgTRPPL-2 is expressed in *T. gondii* tachyzoites, it is likely post-translationally cleaved and localizes to the PM and the ER.

2.4.2. TgTRPPL-2 is important for growth, invasion and egress of Toxoplasma gondii

With the aim to investigate the physiological role of TgTRPPL-2 in *T. gondii,* we generated *ΔTgTRPPL-2* mutants using the CRISPR-Cas9 approach to disrupt the transcription of *TgTRPPL-2* by inserting a dihydrofolate reductase-thymidylate synthase (DHFR) cassette in the *TgTRPPL-2* genomic locus (Fig. 2A). Genetic

controls for the insertion were done by PCR, and qPCR showed a significant decrease in the levels of *TgTRPPL-2* transcripts (Fig. 2B).

We next complemented the *ΔTgTRPPL-2* mutants with Cosmid PSBLZ13 [115] that contains the whole genomic locus of the *TgTRPPL-2* gene and generated the cell line *ΔTgTRPPL-2-trppl2.* Controls for the expression of *TgTRPPL-2* was done by qPCR and by IFAs, which further confirmed the identity of the tagged gene, as it was not expressed in the *DTgTRPPL-2* mutants and was present in the complemented line *ΔTgTRPPL-2-trppl2* (Fig. 2B-C). Further validation of the absence of expression of TgTRPP2-L and its complementation is shown in Figs S2A-B with additional IFA images and westerns of the *ΔTgTRPPL-2* and *ΔTgTRPPL-2-trppl2* (Fig S2B).

We next evaluated if the expression of *TgTRPPL-2* would impact *T. gondii* growth by plaque assays, in which the parasite engages in repetitive cycles of invasion, replication, and egress causing host cell lysis and formation of plaques observed as white spots by staining with crystal violet. The *ΔTgTRPPL-2* parasites formed smaller plaques compared to its parental counterpart indicating a growth defect (Fig. 2D). This growth defect was partially restored in the complemented cell line (Fig. 2D). We reasoned that the overexpression of *TgTRPPL-2* in the *ΔTgTRPPL-2-trppl2* mutants likely affect parasite fitness masking the rescue effect.

To determine which step of the lytic cycle was affected we performed invasion and egress assays. For invasion we used the red green assay [99] under two extracellular Ca^{2+} (1.8 and 0.5 mM) conditions. Quantification of invasion in the

presence of 1.8 mM Ca^{2+} showed a lower invasion rate for the *ΔTgTRPPL-2* (Fig. 2.2E). Reducing the extracellular concentration of Ca^{2+} to 0.5 mM resulted in a reduced rate of invasion by the parental cells, which was similar to the invasion rate of the *ΔTgTRPPL-2* mutants. This result demonstrated that TgTRPPL-2 is important for invasion at higher concentrations of extracellular Ca^{2+}.

Egress of intracellular tachyzoites can be triggered by permeabilizing infected host cells with saponin in the presence of a buffer containing 1.8 mM of extracellular Ca^{2+}. Under these conditions egress of the *ΔTgTRPPL-2* mutants was slower than egress of the parental strain (Fig. 2F). Additionally, when egress was stimulated by Zaprinast, which increases cytosolic Ca^{2+}, also resulted in the *ΔTgTRPPL-2* mutants taking longer to egress (Fig. 2G). For both assays tested, the *ΔTgTRPPL-2* mutants took twice the time to egress compared to the parental line.

In summary, disruption of the TgTRPPL-*2* locus negatively impacted two important steps of the *T. gondii* lytic cycle, invasion and egress, which impacted parasite growth.

2.4.3. The role TgTRPPL-2 in Ca^{2+} influx

We previously showed that *T. gondii* tachyzoites allow influx of Ca^{2+} when exposed to 2 mM extracellular Ca^{2+} [97]. To determine the role of TgTRPPL-2 in this pathway, we loaded *ΔTgTRPPL-2* parasites with Fura-2AM to study intracellular Ca^{2+} changes after exposing them to 1.8 mM extracellular Ca^{2+} (Fig. 3A). The resting cytosolic Ca^{2+} concentration of *ΔTgTRPPL-2* mutants was around 75 nM which is similar to the resting concentration of parental cells (~70-100 nM).

Adding 1.8 mM to the extracellular buffer caused an increase in cytosolic Ca^{2+} in both the parental strain and the *ΔTgTRPPL-2* mutants (Fig. 3B). However, Ca^{2+} influx of the *ΔTgTRPPL-2* mutants was significantly lower (Fig. 3C) and it was decreased almost 50%. The *ΔTgTRPPL-2-trppl2* complemented mutants, however, regained the Ca^{2+} influx activity and they even showed higher Ca^{2+} influx than parental cells, consistent with the higher expression of *TgTRPPL-2* shown by qPCR (Fig. 2B). The reduction of Ca^{2+} influx was further confirmed when adding 1 mM extracellular calcium to the *ΔTgTRPPL-2* mutants (Fig. S3A).

When *T. gondii* tachyzoites are suspended in a high Ca^{2+} buffer from the beginning of the experiment there is a slow constitutive influx of Ca^{2+}, that we attribute to leakage through a PM channel (Fig. 3D, *parental black tracing*). Interestingly, this leakage activity was significantly reduced in the *ΔTgTRPPL-2* mutants (Fig. 3D-E, *blue tracing and bar*), supporting a role of TgTRPPL-2 in constitutive Ca^{2+} influx at the PM. Additional evidence is provided by the enhanced Ca^{2+} leakage observed with the *ΔTgTRPPL-2-trppl2* complemented mutants (Fig. 3D-E, *purple tracing and bar*). The high Ca^{2+} leakage and Ca^{2+} influx observed with the *ΔTgTRPPL-2-trppl2* mutants may affect parasite fitness and would explain the partial growth recovery of these mutants.

Ca^{2+} channels may also be modulated by Ca^{2+} itself [116]. We previously showed that a cytosolic [Ca^{2+}] increase may activate Ca^{2+} influx at the PM (Ca^{2+} activated Ca^{2+} entry) [68]. We next investigated if the Ca^{2+} activated Ca^{2+} entry (CACE) activity was due to the functioning of TgTRPPL-2 at the PM. We added thapsigargin (Thap) to tachyzoites in suspension (Fig. 3F), which results in a

cytosolic Ca^{2+} increase due to inhibition of the SERCA-Ca^{2+}-ATPase (SERCA) resulting in uncompensated Ca^{2+} efflux into the cytosol. This elevated cytosolic Ca^{2+} stimulates further Ca^{2+} influx at the PM, which we assessed as an increase in cytosolic Ca^{2+} following addition of high Ca^{2+} to the buffer (Fig 3F, *black tracing*). Note that the $D[Ca^{2+}]_{cyt}$ shown in Fig. 3H, *black column*, is almost 2.5 times higher than the $D[Ca^{2+}]_{cyt}$ observed without previous addition of thap (Fig. 3C, *black column*). This CACE activity was absent in the *ΔTgTRPPL-2* mutants (Fig. 3F, *blue tracing*) but was restored in the *ΔTgTRPPL-2-trppl2* complemented strain (Fig. 3F, *purple tracing*). Quantifications of the rate of Ca^{2+} increase after adding Ca^{2+} and statistical analyses are shown in Fig. 3G-H. Note that the *ΔTgTRPPL-2* mutants showed a reduced response to the addition of thap and also to the addition of Ca^{2+}. Comparing the response to the addition of extracellular Ca^{2+} shown in Fig. 3H, *blue column*, the $\Delta[Ca^{2+}]_{cyt}$ is similar to the one measured directly without previous addition of Thap (compare with the *blue column* in Fig 3C). This result points to a complete absence of the modulatory effect of cytosolic Ca^{2+} on the PM Ca^{2+} influx in the *ΔTgTRPPL-2* mutants which is restored in the *ΔTgTRPPL-2-trppl2* parasites.

We next tested Zaprinast, which increases the levels of cGMP resulting in Ca^{2+} release from an unidentified store [117]. We previously showed the Ca^{2+} release was almost 2.5 times higher in the presence of extracellular Ca^{2+} compared with the absence of extracellular Ca^{2+} [117]. We attributed this increase to stimulation of the PM Ca^{2+} channel by cytosolic Ca^{2+} (CACE). When testing this phenotype with the *ΔTgTRPPL-2* mutants, we observed that the increased response was absent (Fig. 3I-K). Also note that even the release of Ca^{2+} from intracellular stores

by Zaprinast in the presence of low extracellular Ca^{2+} (~50 nM) was significantly decreased in the *ΔTgTRPPL-2* mutants (Fig. S3B-C). The modulatory action of elevated cytosolic Ca^{2+} in Ca^{2} influx was absent in the *ΔTgTRPPL-2* mutants (Fig. 3I-K).

Taken together, these results support a role for TgTRPPL-2 in Ca^{2+} influx at the PM. In addition, TgTRPPL-2 is modulated by cytosolic Ca^{2+} and it is responsible for a constitutive PM Ca^{2+} influx pathway.

2.4.4. TgTRPPL-2 is a cation conducting channel

With the aim of establishing whether TgTRPPL-2 functions as a channel and if it is able to conduct Ca^{2+} we cloned the cDNA of the *TgTRPPL-2* gene into a mammalian expression vector (pCDNA3.1) for expression in human embryonic kidney 293 cells (HEK-3KO) [101]. These HEK cell line is genetically modified and the 3 isoforms of the inositol 1,4,5-trisphosphate receptor (IP_3R) are deleted, to reduce background Ca^{2+} currents [101]. TgTRPPL-2 was mostly expressed at the ER of HEK cells as assessed by co-localization with a red fluorescent protein (RFP) targeted to the ER and compared with the mammalian homolog Polycystin 2 (PC2) (Fig. 4A). Because of this, we isolated nuclear/ER membranes (Fig. 4B) for single channel patch clamp experiments and further characterization of the permeability properties of TgTRPPL-2 (Fig. 4C).

In the presence of 1.8 mM of Ca^{2+} inside the patch pipette and 100 nM of Ca^{2+} in the bath solution (see scheme of Fig. 4B), the membranes isolated from control cells, held at –80 mV, showed very little activity and the conductance remained at less than 1.5 pA (Fig. 4D, *control tracing*). Some channel activity was observed

after artificially depolarizing membranes (–80 to +20 mV) presumably due to opening of potassium channels. In comparison, when analyzing membranes isolated from cells expressing TgTRPPL-2 a significant increase in the open probability and current sizes was observed (Fig. 4D, *TgTRPPL-2 blue tracing*). The current-voltage relationship was linear and significantly different from the one from control cells (Fig. 4E, *blue vs. black line*).

We compared the activity of TgTRPPL-2 with the mammalian PKD Channel PC2 in parallel experiments since PC2 has been well characterized in the literature. Activity of PC2 expressing cells displayed a voltage-dependent behavior, as the current-voltage relationship was not linear, with a conductance of ~73 pS (Fig. 4D-E, *red tracing*). Previous work has demonstrated that PC2 can be voltage dependent. Additionally, depending on the experimental setup, conductance for PC2 can be variable. Comparing our experimental approach to previous work, conductance for PC2 in a high Ca^{2+} solution is similar (~73 pS vs. ~ 97 pS). Although TgTRPPL-2 does not appear to be voltage dependent, conductance of the channel is similar to its mammalian homologue.

Ca^{2+} is able to modulate the activity of channels and TRP-P channels have been shown to be activated by Ca^{2+} as some of them have an EF-hand motif at the C-terminus [116, 118]. To determine whether Ca^{2+} is able to modulate the activity of TgTRPPL-2 we first varied the [Ca^{2+}] inside the pipette (in equilibrium with the ER lumen). When the Ca^{2+} concentration was increased to 10 mM Ca^{2+} there was a significant inhibition of TgTRPPL-2 channel activity. With high Ca^{2+} concentration, the channel displayed voltage-dependent inhibition over the -75 to

-25 mV range and conductance was significantly decreased (Fig. 4F). In the presence of 1.8 mM Ca^{2+} inside the pipette, TgTRPPL-2 had a conductance of ~55 pS, which is significantly higher than the conductance calculated for control membranes. The conductance decreased to ~21 pS when Ca^{2+} was increased to 10 mM.

Although no evidence for a conserved EF-hand motif was found in TgTRPPL-2 we checked for the potential modulation by cytosolic Ca^{2+}. Increasing the concentration of Ca^{2+} in the bath solution from 100 nM to 10 μM (which would simulate changes in cytosolic Ca^{2+}), enhanced channel activity from membranes expressing TgTRPPL-2 (Fig. 4G-H, *blue vs. gold line*). Interestingly, increasing the $[Ca^{2+}]$ only increased the open probability when the membrane was depolarized to -80 mV (Fig. 4I). However, increase of the $[Ca^{2+}]$ of the bath solution, increased the conductance of the channel almost 2.5x, suggesting modulation of the channel by Ca^{2+} itself. In conclusion, these data indicate that TgTRPPL-2 is able to conduct Ca^{2+} currents and is modulated by cytosolic Ca^{2+}.

To distinguish whether TgTRPPL-2 is able to conduct cation currents and to determine if the activity measured could be the result of permeation of potassium, we replaced potassium with the non-permeable ion cesium [119, 120]. In the presence of 1.8 mM Ca^{2+} inside the pipette, in a cesium chloride solution, membranes from TgTRPPL-2 and PC2 expressing cells have a significantly higher activity than control cells (Fig. 5A). The current-voltage relationship is linear through different applied voltages and significantly different from that of control cells in potassium or cesium chloride solution (Fig. 5B). Although channel

conductance is slightly higher in potassium chloride, it is not significantly different than the calculated conductance and open probability obtained in Cesium chloride (Fig. 5B-C). However, when applying voltages higher than -40 mVs, the channel was open for longer times in the presence of cesium chloride vs potassium chloride (Fig. 5D, *green vs. blue line*). These results indicate that TgTRPPL-2 permeates Ca^{2+}, however it can also conduct potassium, since channel conductance is slightly higher in the potassium chloride solution.

We further demonstrate that TgTRPPL-2 is able to conduct Ca^{2+} by following Ca^{2+} changes of TgTRPPL-2-HEK-3KO or RFP-ER-HEK-3KO cells co-transfected with a genetic Ca^{2+} indicator, allowing to measure ER luminal Ca^{2+} changes and current activity simultaneously. Luminal Ca^{2+} changes were followed through one cycle of membrane depolarization from -80 mV to 40 mV (Fig. S4A). The fluorescence of the Ca^{2+} indicator decreased in the TgTRPPL-2 expressing cells with time as voltage was applied. In both potassium as well as cesium chloride solutions at 1.8 mM Ca^{2+} we observed that the fluorescence decrease was significantly larger when the HEK-3KO cells expressed *TgTRPPL-2* (Fig. S4B-C vs. D-E). The slope for the fluorescence decrease appeared higher in the cesium chloride solution than in the potassium solution, although was quite variable (Fig. S4F-G). In summary, the observed decrease in the fluorescence of the Ca^{2+} indicator supports the Ca^{2+} permeation activity of TgTRPPL-2, which agrees with the single channel conductance measurements.

2.4.5. Inhibition of TgTRPPL2 by TRP Channel Inhibitors

Previous results from our laboratory demonstrated Ca^{2+} influx in *T. gondii* and its inhibition by L-type voltage gated Ca^{2+} channel blockers like nifedipine (Fig. 2.6A) [68]. Taking into account that TgTRPPL-2 is a cation permeable channel and localizes to the PM, we next investigated if the residual Ca^{2+} influx activity observed with the *ΔTgTRPPL-2* mutants could be blocked with nifedipine. Interestingly, pre-incubation with nifedipine of the *ΔTgTRPPL-2* parasites showed that the initial cytosolic Ca^{2+} was elevated and it was around ~400 nM (compared to 100 nM of the parental strain under identical conditions) in Ca^{2+}-free buffer (Fig. 6B). Further addition of extracellular Ca^{2+} did not result in Ca^{2+} influx and only a slow steady cytosolic Ca^{2+} increase was observed (Fig. 6B). We attribute the higher cytosolic Ca^{2+} in the presence of nifedipine to leakage of stored Ca^{2+} into the cytosol as the cell is trying to compensate for the complete absence of Ca^{2+} influx. However, the lack of Ca^{2+} influx after adding extracellular Ca^{2+}, with almost 100% inhibition, points to a role for TgTRPPL-2 in Ca^{2+} influx and addition of nifedipine resulted in complete loss of Ca^{2+} influx.

We next tested the effect of anthranilic acid (ACA), a wide spectrum TRP channel inhibitor [121], on Ca^{2+} influx of both parental controls and □*TgTRPPL-2* mutants (Fig. 6C). ACA inhibited Ca^{2+} influx by 40-50% of the parental cell line (Fig. 6C, *black vs. red tracing*). However, preincubation of □TgTRPPL-2 tachyzoites with ACA, did not further reduce Ca^{2+} influx (Fig. 6C, *dark blue vs. light blue tracings*). Sensitivity to both nifedipine and ACA was restored in the complemented cell line (Fig. 6D). These results point to TgTRPPL-2 as a PM

channel that conducts Ca^{2+}, and it is relevant for its influx from the extracellular milieu, and is sensitive to TRP channel inhibitors.

2.4.6. The Role of TRPPL-2 as a Ca^{2+} leak channel at the ER membrane

The dual localization of TgTRPPL-2 at the PM and ER indicates the potential function of the channel at both locations (Fig. 1D). Efflux of Ca^{2+} to the cytosol is observed after inhibiting the TgSERCA with Thap[100]. We tested the effect of ACA in ER Ca^{2+} efflux, and observed that incubation of tachyzoites of the parental strain with ACA, significantly decreased the efflux of Ca^{2+} caused by Thap (Fig. 6 E-F, *black line and bar vs. red line and bar*). The ACA inhibited ER Ca^{2+} efflux rate was comparable to the decreased efflux rate triggered by Thap of the *ΔTgTRPPL-2* mutants (Fig. 6F, *blue bar versus red bar and* Fig. 3D). In addition, Ca^{2+}-activated Ca^{2+} entry, evaluated by adding 1.8 mM of extracellular Ca^{2+} 50 s after stimulating efflux with Thap, was inhibited by ACA (Fig. 6G, *green versus gold line*). Ca^{2+} influx after Thap was reduced to basal Ca^{2+} influx (without pre-addition of Thap) for both parental and *ΔTgTRPPL-2* mutants. Note that Ca^{2+} influx in *ΔTgTRPPL-2* tachyzoites after stimulus by Thap, and Ca^{2+} influx in the parental strain without any stimulus are similar because the modulation of Ca^{2+} influx by cytosolic Ca^{2+} is lost in the *ΔTgTRPPL-2* parasites (Fig. 6H, *black versus blue bars*). In conclusion, ACA inhibited both efflux of Ca^{2+} from the ER as well as Ca^{2+}-induced Ca^{2+} entry. This led us to propose that TgTRPPL-2, in addition to mediate Ca^{2+} influx at the plasma membrane may also mediate Ca^{2+} leakage from the ER, a pathway sensitive to the TRP-channel inhibitor ACA.

To further validate the specificity of ACA for the inhibition of TgTRPPL-2, we tested this inhibitor and a second broad spectrum TRP channel inhibitor, benzamil, against single channel conductance. Channel activity of TgTRPPL-2 was significantly decreased by both ACA and benzamil (Fig. 7A-B). ACA diminished the amplitude of the channel by reducing the probability and time that the channel remained open (Fig. 7C, E). Conductance of the channel was reduced to almost half in the presence of ACA (Fig. 7B), which correlates with the inhibition of Ca^{2+} entry in *T. gondii.* In comparison to ACA, benzamil only reduced the open probability of TgTRPPL-2 but not the length of time the channel was open (Fig. 7D-E)). The conductance of TgTRPPL-2 was reduced to one third of the control in the presence of benzamil (Fig. 7B).

Most interesting, we tested both inhibitors, ACA and benzamil in *in vitro* growth assays (Fig. 7F-G, *top panel and parental bars*) and found that they both inhibited *in vitro T. gondii* growth. We calculated the IC_{50} for ACA at 1.4 ± 0.4 mM. Interestingly, neither ACA nor benzamil affected the growth of the *ΔTgTRPPL-2* mutants (Fig. 7G). Note that these cells already grow at a slower rate, which did not change in the presence of the inhibitors. However, cilnidipine, a voltage-gated Ca^{2+} channel blocker, completely inhibited growth of both parental and *ΔTgTRPPL-2* mutants (Fig. 7G).

In conclusion, TgTRPPL-2 is a cation permeable channel that can be inhibited by broad spectrum TRP channel inhibitors. Inhibition of channel activity affects parasite growth.

2.5 DISCUSSION

In this study we report the presence and functional role of a *T. gondii* channel, TgTRPPL-2, that localizes to the plasma membrane and the endoplasmic reticulum. The corresponding gene *TgGT1_310560*, was annotated as hypothetical but was predicted as a transient receptor potential channel based on a bioinformatic analysis of the *T. gondii* genome comparing it with TRP channel genes of mammalian origin [73]. Here, we established that TgTRPPL-2 is important for both Ca^{2+} influx at the PM and Ca^{2+} efflux from the ER of *T. gondii* tachyzoites. TgTRPPL-2, expressed in HEK-3KO cells, conducted currents in high calcium solutions and was not voltage dependent. Interestingly, Ca^{2+} itself modulated the conductance of TgTRPPL-2. Broad spectrum TRP channel inhibitors like ACA and benzamil, inhibited the activity of TgTRPPL-2, Ca^{2+} influx in the parasite as well as parasite growth.

Silencing of TgTRPPL-2 in the *DTgTRPPL-2* mutants impacted both invasion and egress of *T. gondii*, resulting in a general growth defect. Extracellular tachyzoites, which are surrounded by high Ca^{2+} are able to use Ca^{2+} influx to stimulate invasion of a new host cell and carry on their lytic cycle. The *DTgTRPPL-2* mutants showed a reduction in their host invasion ability suggesting the defect may be due to a reduction in Ca^{2+} influx because of the absence of TgTRPPL-2. Interestingly, the reduction in Ca^{2+} influx (~50%) in the *DTgTRPPL-2* mutants was comparable to the reduction of invasion suggesting that TgTRPPL-2 is involved in the Ca^{2+} influx pathway that stimulates invasion. Delay in the ability of the *DTgTRPPL-2* mutants to egress could be caused by a defective efflux of Ca^{2+} from

the ER, which was significantly lower in the mutants. This was evidence for the function of TgTRPPL2 as a Ca^{2+} channel at the ER membrane.

The impact of silencing TgTRPPL-2 on *T. gondii* growth, was not total and parasites still were able to perform lytic cycle activities at a reduced rate. The main defects of the *DTgTRPPL-2* mutants: invasion, egress, Ca^{2+} influx and ER Ca^{2+} efflux was not complete likely because more than one mechanism or channel is functional at both locations (PM and ER). We hypothesize the presence of another channel at the PM, likely the one responsible for the Ca^{2+} influx activity that is inhibited by nifedipine [68]. It is also possible that a release channel responsive to IP_3 may be involved in release of Ca^{2+} from the ER [122] with TgTRPPL-2 having a role in efflux under conditions of ER Ca^{2+} overload.

Numerous observations in *T. gondii* have demonstrated that intracellular Ca^{2+} oscillations in the parasite precede the activation of distinct steps of the lytic cycle [69, 70]. Influx of both extracellular and intracellular Ca^{2+} pools into the parasite cytosol contribute to the activation of downstream signaling pathways decoded into critical biological steps of the parasite lytic cycle [70, 123]. Ca^{2+} influx at the plasma membrane of *T. gondii* is highly regulated, stimulated by cytosolic Ca^{2+} and is operational in extracellular [68] and intracellular replicating tachyzoites [81]. Our data with the *DTgTRPPL-2* cells identified TgTRPPL-2 as a functional protein at the plasma membrane and the ER and in both locations would allow Ca^{2+} influx into the cytosol. The dual localization of TgTRPPL-2 is in accord with other TRP channels in other cells, which showed a dynamic localization between vesicular organelles and the plasma membrane where they facilitate Ca^{2+} influx [124]. In this

regard, the mammalian ortholog, PC2, localizes to both the plasma membrane and the ER [125].

T. gondii expresses a SERCA-Ca^{2+}-ATPase, a P-type ATPase, that couples ATP hydrolysis to the transport of ions across biological membranes (TgSERCA) and localizes to the ER [126]. TgSERCA is sensitive to thapsigargin (Thap), a sesquiterpene lactone derived from the plant *Thapsia garganica* [127, 128] and previous studies showed that inhibition of TgSERCA by Thap resulted in cytosolic Ca^{2+} efflux through an unknown channel [68, 100]. In mammalian cells, the passive Ca^{2+} efflux from the ER is thought to prevent ER Ca^{2+} overload and helps maintain the steady-state concentration of luminal Ca^{2+} permitting cytosolic Ca^{2+} signaling [43, 129]. Several membrane proteins have been proposed to be involved in the ER Ca^{2+} efflux/leak pathway including TRP channels [130]. Results from this work support a role for TgTRPPL-2 in ER Ca^{2+} leakage in *T. gondii*. Ca^{2+} efflux from the ER observed after adding Thap or Zaprinast was also significantly decreased in the *ΔTgTRPPL-2* mutants. These results support a functional role for TgTRPPL-2 at the membrane of the ER as the constitutive leak channel involved in Ca^{2+} efflux when the store is filled. This could also be the mechanism by which the ER supplies Ca^{2+} to other organelles like the mitochondria or the plant-like vacuole (PLV) a lysosome like compartment [72].

Previous work from our laboratory showed that the Ca^{2+} influx at the plasma membrane did not operate as store operated Ca^{2+} entry (SOCE) which was shown with experiments testing surrogate ions like Mn^{2+} [68]. This result was supported by the lack of components of the SOCE pathway, STIM and ORAI from the *T.*

gondii genome [73]. However, this activity was modulated by cytosolic Ca^{2+} [68] and this modulation was absent in the *ΔTgTRPPL-2* cells supporting a role for TgTRPPL-2 as the channel responsible for Ca^{2+} influx at the PM activated by cytosolic Ca^{2+}. TRP channels have been shown to play a role in Ca^{2+}-activated Ca^{2+} entry [131]. Release of Ca^{2+} from intracellular stores like the ER, is also significantly diminished in the *ΔTgTRPPL-2* mutants, which could affect the stimulation of Ca^{2+} influx. However, when using Zaprinast, which raised cytosolic Ca^{2+} at a much higher level than Thap, the stimulation of Ca^{2+} influx by cytosolic Ca^{2+} was absent. This further supports that TgTRPPL-2 functions at the PM mediating Ca^{2+} influx and is modulated by cytosolic Ca^{2+}.

We showed that TgTRPPL-2 was able to conduct currents with conductance values comparable to the values of mammalian TRP channels [132-134]. Previous work with PC2, showed that Ca^{2+} modulated the activity of PC2 [132, 135-138]. Sustained cytosolic Ca^{2+} increase inhibited PC2 currents [137] while other studies showed that cytosolic Ca^{2+} increase from physiological (100 nM) to μM levels increased the activity of the channel [132, 138]. We observed some of these responses with TgTRPPL-2, as increasing Ca^{2+} inside the pipette (ER luminal) showed a significant decrease in the currents. Comparably, increasing Ca^{2+} concentration in the bath solution (cytosolic) from physiological levels to μM levels showed an increase of 2.5x in the conductance of TgTRPPL-2. Although cytosolic [Ca^{2+}] is unlikely to reach those high μM levels, the potential presence of Ca^{2+} microdomains at the plasma membrane or the ER membrane would result in higher concentrations of Ca^{2+} at the exit of the channel due to slow diffusion of

Ca^{2+} ions [139-141].

Because PKD channels are cation permeable they could also permeate Na^{+} or K^{+}. In the case of TgTRPPL-2 we showed that it can mediate Ca^{2+} transport when no other ions are present in the solution. We did not determine the ionic selectivity of TgTRPPL-2, and we can only propose that TgTRPPL-2 is a cation permeable channel. In cilia, PKD channels have been described to have relatively high conductance [132, 142]. The conductance calculated for TgTRPPL-2 is within range of what has been described for PC2 in other cells (30-157 pS). However, it is important to note that the properties described for any channel will depend on the experimental approaches used.

Anthranilic acid and benzamil are broad spectrum inhibitors that have the ability to inhibit TRP channel activity. ACA is a weak base that inhibits currents mediated by TRP channels. ACA does not block the pore of the channel as most inhibitors but rather reduce the open probability of the channel. In a similar manner, benzamil is also able to inhibit currents mediated by TRP channels by binding to a site that modulates their activity rather than blocking its pore. In our experiments testing ACA and benzamyl we observed that while the inhibitors affected Ca^{2+} influx and growth of the parental cell line, neither affected the already reduced growth and Ca^{2+} influx of the *ΔTgTRPPL-2* mutants. This result combined with the inhibition of TgTRPPL-2 currents impacting both open probability and time that the channel remained open points to TgTRPPL-2 as the target of ACA and benzamyl.

Recent studies on Ca^{2+} signaling in *T. gondii* have expanded our understanding of the link between Ca^{2+} and critical facets of parasite biology (i.e., gliding motility,

microneme secretion, host cell invasion and egress). However, important molecular players have remained enigmatic, like the PM channels responsible for Ca^{2+} influx and the ER channel responsible for the passive leakage into the cytosol. Characterization of TgTRPPL-2 and its function at the ER and PM fills a small gap in our knowledge of Ca^{2+} signaling and homeostasis in *T. gondii* (Fig. 8). This study is the first biophysical characterization of a channel in *T. gondii* (or any Apicomplexan parasite) and TgTRPPL-2 represents the first identified molecule to mediate Ca^{2+} influx into the cytosol of *T. gondii* at the plasma membrane and the ER. In addition, this study identifies TgTRPPL-2 as a potential target for combatting Toxoplasmosis.

2.6 REFERENCES

37. Black, M.W. and J.C. Boothroyd, *Lytic cycle of Toxoplasma gondii.* Microbiol Mol Biol Rev, 2000. **64**(3): p. 607-23.
42. Blader, I.J., et al., *Lytic Cycle of Toxoplasma gondii: 15 Years Later.* Annu Rev Microbiol, 2015. **69**: p. 463-85.
43. Clapham, D.E., *Calcium signaling.* Cell, 2007. **131**(6): p. 1047-58.
44. Berridge, M.J., M.D. Bootman, and H.L. Roderick, *Calcium signalling: dynamics, homeostasis and remodelling.* Nat Rev Mol Cell Biol, 2003. **4**(7): p. 517-29.
49. Montell, C., *The TRP superfamily of cation channels.* Sci STKE, 2005. **2005**(272): p. re3.
51. Venkatachalam, K. and C. Montell, *TRP channels.* Annu Rev Biochem, 2007. **76**: p. 387-417.
68. Pace, D.A., et al., *Calcium entry in Toxoplasma gondii and its enhancing effect of invasion-linked traits.* J Biol Chem, 2014. **289**(28): p. 19637-47.
69. Lourido, S. and S.N. Moreno, *The calcium signaling toolkit of the Apicomplexan parasites Toxoplasma gondii and Plasmodium spp.* Cell Calcium, 2015. **57**(3): p. 186-93.
70. Hortua Triana, M.A., et al., *Calcium signaling and the lytic cycle of the Apicomplexan parasite Toxoplasma gondii.* Biochim Biophys Acta Mol Cell Res, 2018. **1865**(11 Pt B): p. 1846-1856.

72. Miranda, K., et al., *Characterization of a novel organelle in Toxoplasma gondii with similar composition and function to the plant vacuole.* Mol Microbiol, 2010. **76**(6): p. 1358-75.
73. Prole, D.L. and C.W. Taylor, *Identification of intracellular and plasma membrane calcium channel homologues in pathogenic parasites.* PLoS One, 2011. **6**(10): p. e26218.
80. Weiss, L.M. and J.P. Dubey, *Toxoplasmosis: A history of clinical observations.* Int J Parasitol, 2009. **39**(8): p. 895-901.
81. Vella, S.A., et al., *The Role of Potassium and Host Calcium Signaling in Toxoplasma gondii egress.* bioRxiv, 2020: p. 2020.03.06.980508.
82. Nilius, B. and G. Owsianik, *The transient receptor potential family of ion channels.* Genome Biol, 2011. **12**(3): p. 218.
83. Zhou, J., *Polycystins and primary cilia: primers for cell cycle progression.* Annu Rev Physiol, 2009. **71**: p. 83-113.
84. Koulen, P., et al., *Polycystin-2 is an intracellular calcium release channel.* Nat Cell Biol, 2002. **4**(3): p. 191-7.
85. Samanta, A., T.E.T. Hughes, and V.Y. Moiseenkova-Bell, *Transient Receptor Potential (TRP) Channels.* Subcell Biochem, 2018. **87**: p. 141-165.
86. Wang, Z., et al., *The ion channel function of polycystin-1 in the polycystin-1/polycystin-2 complex.* EMBO Rep, 2019. **20**(11): p. e48336.
87. Wolstenholme, A.J., *Ion channels and receptor as targets for the control of parasitic nematodes.* Int J Parasitol Drugs Drug Resist, 2011. **1**(1): p. 2-13.
88. Eckardt, L., et al., *In vivo recording of monophasic action potentials in awake dogs--new applications for experimental electrophysiology.* Basic Res Cardiol, 2001. **96**(2): p. 169-74.
89. Boucher, C. and R. Sandford, *Autosomal dominant polycystic kidney disease (ADPKD, MIM 173900, PKD1 and PKD2 genes, protein products known as polycystin-1 and polycystin-2).* Eur J Hum Genet, 2004. **12**(5): p. 347-54.
90. Hortua triana, M.A., Marquez-Nogueras, K., Chang, L., Stasic, A.J., Li, C., Spiegel, K., Sharma, A., Li, Z.H., Moreno, S.N.J., *Tagging of Weakly Expressed Toxoplasma gondii Calcium-*
Related Genes with High-Affinity Tags. Journal of Eukaryotic Microbiology, 2018. **In press**.
91. Farwell, D.G., et al., *Genetic and epigenetic changes in human epithelial cells immortalized by telomerase.* Am J Pathol, 2000. **156**(5): p. 1537-47.
92. Sheiner, L., et al., *A systematic screen to discover and analyze apicoplast proteins identifies a conserved and essential protein import factor.* PLoS Pathog, 2011. **7**(12): p. e1002392.
93. Meissner, M., et al., *Modulation of myosin A expression by a newly established tetracycline repressor-based inducible system in Toxoplasma gondii.* Nucleic Acids Res, 2001. **29**(22): p. E115.
94. Fox, B.A., et al., *Efficient gene replacements in Toxoplasma gondii strains deficient for nonhomologous end joining.* Eukaryot Cell, 2009. **8**(4): p. 520-9.
95. Shen, B., et al., *Development of CRISPR/Cas9 for Efficient Genome Editing in Toxoplasma gondii.* Methods Mol Biol, 2017. **1498**: p. 79-103.

96. Laemmli, U.K., *Cleavage of structural proteins during the assembly of the head of bacteriophage T4.* Nature, 1970. **227**(5259): p. 680-5.
97. Liu, J., et al., *A vacuolar-H(+) -pyrophosphatase (TgVP1) is required for microneme secretion, host cell invasion, and extracellular survival of Toxoplasma gondii.* Mol Microbiol, 2014. **93**(4): p. 698-712.
98. Schindelin, J., et al., *Fiji: an open-source platform for biological-image analysis.* Nat Methods, 2012. **9**(7): p. 676-82.
99. Kafsack, B.F., C. Beckers, and V.B. Carruthers, *Synchronous invasion of host cells by Toxoplasma gondii.* Mol Biochem Parasitol, 2004. **136**(2): p. 309-11.
100. Moreno, S.N. and L. Zhong, *Acidocalcisomes in Toxoplasma gondii tachyzoites.* Biochem J, 1996. **313 (Pt 2)**: p. 655-9.
101. Alzayady, K.J., et al., *Defining the stoichiometry of inositol 1,4,5-trisphosphate binding required to initiate Ca2+ release.* Sci Signal, 2016. **9**(422): p. ra35.
102. Grynkiewicz, G., M. Poenie, and R.Y. Tsien, *A new generation of Ca2+ indicators with greatly improved fluorescence properties.* J Biol Chem, 1985. **260**(6): p. 3440-50.
103. Chasen, N.M., et al., *A Glycosylphosphatidylinositol-Anchored Carbonic Anhydrase-Related Protein of Toxoplasma gondii Is Important for Rhoptry Biogenesis and Virulence.* mSphere, 2017. **2**(3).
104. Chasen, N.M., et al., *The Vacuolar Zinc Transporter TgZnT Protects Toxoplasma gondii from Zinc Toxicity.* mSphere, 2019. **4**(3).
105. Alzayady, K.J., et al., *Functional inositol 1,4,5-trisphosphate receptors assembled from concatenated homo- and heteromeric subunits.* J Biol Chem, 2013. **288**(41): p. 29772-84.
106. Longo, P.A., et al., *Transient mammalian cell transfection with polyethylenimine (PEI).* Methods Enzymol, 2013. **529**: p. 227-40.
107. Mak, D.O., et al., *Isolating nuclei from cultured cells for patch-clamp electrophysiology of intracellular Ca(2+) channels.* Cold Spring Harb Protoc, 2013. **2013**(9): p. 880-4.
108. Henderson, M.J., et al., *A Low Affinity GCaMP3 Variant (GCaMPer) for Imaging the Endoplasmic Reticulum Calcium Store.* PLoS One, 2015. **10**(10): p. e0139273.
109. Omasits, U., et al., *Protter: interactive protein feature visualization and integration with experimental proteomic data.* Bioinformatics, 2014. **30**(6): p. 884-6.
110. Soding, J., A. Biegert, and A.N. Lupas, *The HHpred interactive server for protein homology detection and structure prediction.* Nucleic Acids Res, 2005. **33**(Web Server issue): p. W244-8.
111. Hortua Triana, M.A., et al., *Tagging of Weakly Expressed Toxoplasma gondii Calcium-Related Genes with High-Affinity Tags.* J Eukaryot Microbiol, 2018. **65**(5): p. 709-721.
112. Shen, P.S., et al., *The Structure of the Polycystic Kidney Disease Channel PKD2 in Lipid Nanodiscs.* Cell, 2016. **167**(3): p. 763-773 e11.
113. Su, Q., et al., *Cryo-EM structure of the polycystic kidney disease-like channel PKD2L1.* Nat Commun, 2018. **9**(1): p. 1192.

114. Merrick, D., et al., *Polycystin-1 cleavage and the regulation of transcriptional pathways.* Pediatr Nephrol, 2014. **29**(4): p. 505-11.
115. Vinayak, S., et al., *Genetic manipulation of the Toxoplasma gondii genome by fosmid recombineering.* mBio, 2014. **5**(6): p. e02021.
116. Petri, E.T., et al., *Structure of the EF-hand domain of polycystin-2 suggests a mechanism for Ca2+-dependent regulation of polycystin-2 channel activity.* Proc Natl Acad Sci U S A, 2010. **107**(20): p. 9176-81.
117. Sidik, S.M., et al., *Using a Genetically Encoded Sensor to Identify Inhibitors of Toxoplasma gondii Ca2+ Signaling.* J Biol Chem, 2016. **291**(18): p. 9566-80.
118. Celic, A., et al., *Domain mapping of the polycystin-2 C-terminal tail using de novo molecular modeling and biophysical analysis.* J Biol Chem, 2008. **283**(42): p. 28305-12.
119. Almog, M. and A. Korngreen, *Characterization of voltage-gated Ca(2+) conductances in layer 5 neocortical pyramidal neurons from rats.* PLoS One, 2009. **4**(4): p. e4841.
120. Wu, L.G., et al., *Calcium channel types with distinct presynaptic localization couple differentially to transmitter release in single calyx-type synapses.* J Neurosci, 1999. **19**(2): p. 726-36.
121. Harteneck, C., H. Frenzel, and R. Kraft, *N-(p-amylcinnamoyl)anthranilic acid (ACA): a phospholipase A(2) inhibitor and TRP channel blocker.* Cardiovasc Drug Rev, 2007. **25**(1): p. 61-75.
122. Lovett, J.L., et al., *Toxoplasma gondii microneme secretion involves intracellular Ca(2+) release from inositol 1,4,5-triphosphate (IP(3))/ryanodine-sensitive stores.* J Biol Chem, 2002. **277**(29): p. 25870-6.
123. Lovett, J.L. and L.D. Sibley, *Intracellular calcium stores in Toxoplasma gondii govern invasion of host cells.* J Cell Sci, 2003. **116**(Pt 14): p. 3009-16.
124. Bezzerides, V.J., et al., *Rapid vesicular translocation and insertion of TRP channels.* Nat Cell Biol, 2004. **6**(8): p. 709-20.
125. Cai, Y., et al., *Identification and characterization of polycystin-2, the PKD2 gene product.* J Biol Chem, 1999. **274**(40): p. 28557-65.
126. Nagamune, K., W.L. Beatty, and L.D. Sibley, *Artemisinin induces calcium-dependent protein secretion in the protozoan parasite Toxoplasma gondii.* Eukaryot Cell, 2007. **6**(11): p. 2147-56.
127. Sagara, Y. and G. Inesi, *Inhibition of the sarcoplasmic reticulum Ca2+ transport ATPase by thapsigargin at subnanomolar concentrations.* J Biol Chem, 1991. **266**(21): p. 13503-6.
128. Thastrup, O., et al., *Thapsigargin, a tumor promoter, discharges intracellular Ca2+ stores by specific inhibition of the endoplasmic reticulum Ca2(+)-ATPase.* Proceedings of the National Academy of Sciences of the United States of America, 1990. **87**(7): p. 2466-70.
129. Guerrero-Hernandez, A., A. Dagnino-Acosta, and A. Verkhratsky, *An intelligent sarco-endoplasmic reticulum Ca2+ store: release and leak channels have differential access to a concealed Ca2+ pool.* Cell Calcium, 2010. **48**(2-3): p. 143-9.
130. Carreras-Sureda, A., P. Pihan, and C. Hetz, *Calcium signaling at the endoplasmic reticulum: fine-tuning stress responses.* Cell Calcium, 2018. **70**: p. 24-31.

131. Ta, C.M., et al., *Structure and function of polycystin channels in primary cilia.* Cell Signal, 2020. **72**: p. 109626.
132. Kleene, S.J. and N.K. Kleene, *The native TRPP2-dependent channel of murine renal primary cilia.* Am J Physiol Renal Physiol, 2017. **312**(1): p. F96-F108.
133. Liu, X., et al., *Polycystin-2 is an essential ion channel subunit in the primary cilium of the renal collecting duct epithelium.* Elife, 2018. **7**.
134. Vien, T.N., et al., *Molecular dysregulation of ciliary polycystin-2 channels caused by variants in the TOP domain.* Proc Natl Acad Sci U S A, 2020. **117**(19): p. 10329-10338.
135. Kuo, I.Y., et al., *The number and location of EF hand motifs dictates the calcium dependence of polycystin-2 function.* FASEB J, 2014. **28**(5): p. 2332-46.
136. Yang, Y., et al., *Oligomerization of the polycystin-2 C-terminal tail and effects on its Ca2+-binding properties.* J Biol Chem, 2015. **290**(16): p. 10544-54.
137. DeCaen, P.G., et al., *Atypical calcium regulation of the PKD2-L1 polycystin ion channel.* Elife, 2016. **5**.
138. Chen, X.Z., et al., *Polycystin-L is a calcium-regulated cation channel permeable to calcium ions.* Nature, 1999. **401**(6751): p. 383-6.
139. Burgoyne, T., S. Patel, and E.R. Eden, *Calcium signaling at ER membrane contact sites.* Biochim Biophys Acta, 2015. **1853**(9): p. 2012-7.
140. Berridge, M.J., *Calcium microdomains: organization and function.* Cell Calcium, 2006. **40**(5-6): p. 405-12.
141. Mulier, M., J. Vriens, and T. Voets, *TRP channel pores and local calcium signals.* Cell Calcium, 2017. **66**: p. 19-24.
142. Liu, X., H.L. Ong, and I. Ambudkar, *TRP Channel Involvement in Salivary Glands-Some Good, Some Bad.* Cells, 2018. **7**(7).

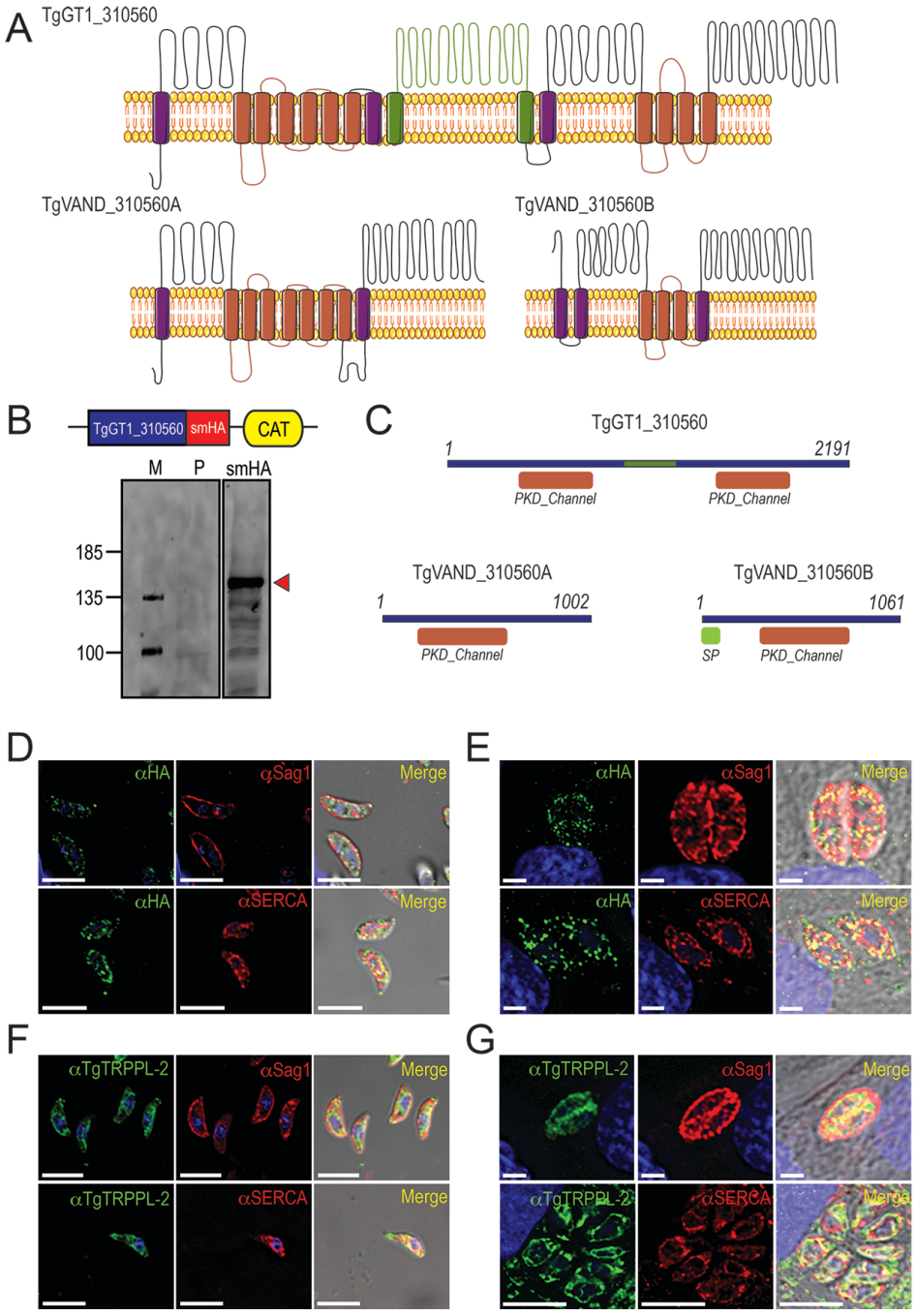

Figure 2.1. TgTRPPL-2 localizes to the plasma membrane (PM) and ER of *T. gondii*. A. Predicted topology for TgTRPPL-2 in GT1 and VAND strains. Model was generated with the Protter application [109]. The PKD Domain is highlighted in orange. The domain used to generate antibodies is highlighted in green. **B.**

Schematic representation of C-terminal tagging of TgTRPPL-2 in TatiΔKu80 parasites and western blots of TgTRPPL-2-smHA membranes using aHA (1:1,000) showing a major band at approximately 150 kDa (*red arrowhead*). **C.** Schematic representation of the InterPro Domain annotation of TgTRPPL-2 in GT1 and VAND strains. **D.** IFAs of extracellular tachyzoites using aHA antibody show vesicular staining close to the PM and intracellular. Co-localization with αSAG1 and αSERCA show partial co-localization with both markers. **E.** IFAs of intracellular tachyzoites with αHA (1:100), αSag1 (1:1,000) and αSERCA (1:1,000) showing co-localization at the PM and ER. **F-G.** IFAs of extracellular and intracellular tachyzoites respectively with αTRPPL-2 (1:1,000) showing labeling of the protein at the periphery, co-localized with αSAG1 (1:1,000) and ER co-localized with αTgSERCA (1:1,000).

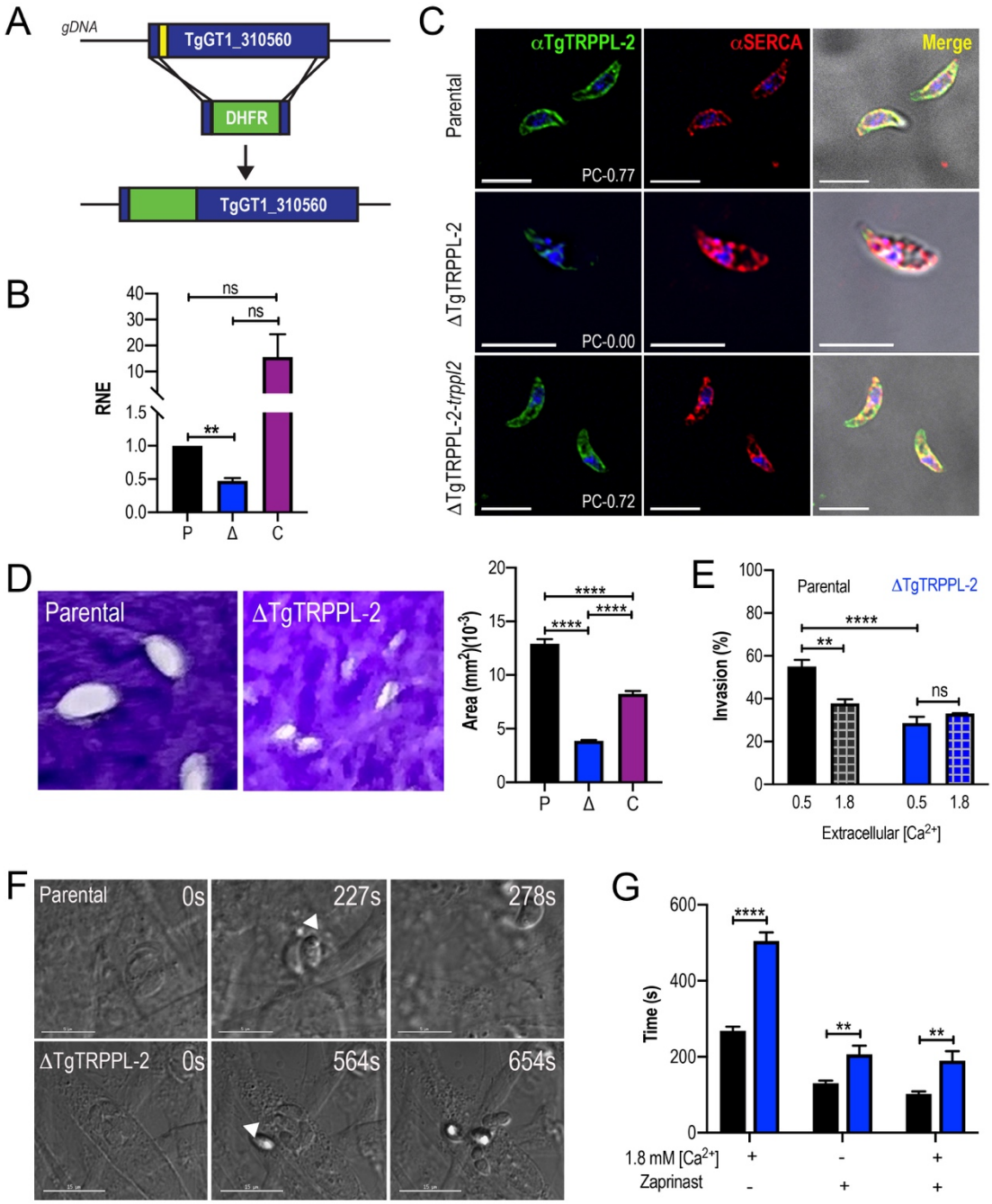

Figure 2.2. TgTRPPL-2 and its role in *T. gondii* growth. Schematic representation of the generation of *ΔTgTRPPL-2* in the *T. gondii* RH strain. **B.** qPCR of total RNA from *ΔTgTRPPL-2, ΔTgTRPPL-2-trppl2* and parental strains using primers upstream and downstream of the insertion site of the DHFR cassette. **C.** IFAs of extracellular parasites showing PM labeling with aTgTRPPL2

(1:1,000) and co-localization with aSERCA (1:1,000). PC, Pearson coefficient. **D**. Plaque assays of parental (P), *ΔTgTRPPL-2* (D) and *ΔTgTRPPL-2-trppl2* (C) cells. Quantification of plaque sizes from three independent biological experiments using student's t-test. ****p< 0.0001. **E.** Red green assays of parental, *ΔTgTRPPL-2* and *ΔTgTRPPL-2-trppl2* cells quantifying invaded and attached intracellular parasites. Assays were done at two concentrations of extracellular Ca^{2+}: 0.5 and 1.8 mM. Asterisk indicate p value for significant difference, ** p< 0.001, **** p< 0.0001. **F.** Time to egress stimulated by saponin/Ca^{2+} at 1.8 mM extracellular Ca^{2+} of both parental or the *ΔTgTRPPL-2 mutants*. **G.** Statistical analysis of average egress time stimulated by saponin or Zaprinast in the presence or absence of extracellular calcium. Analysis was performed from three independent biological replicates using student's t-test. Asterisk indicate p value for significant difference. ** p< 0.003, **** p<0.0001. *Black bars* represent parental strain, *blue bar*s represent DTgTRPPL-2.

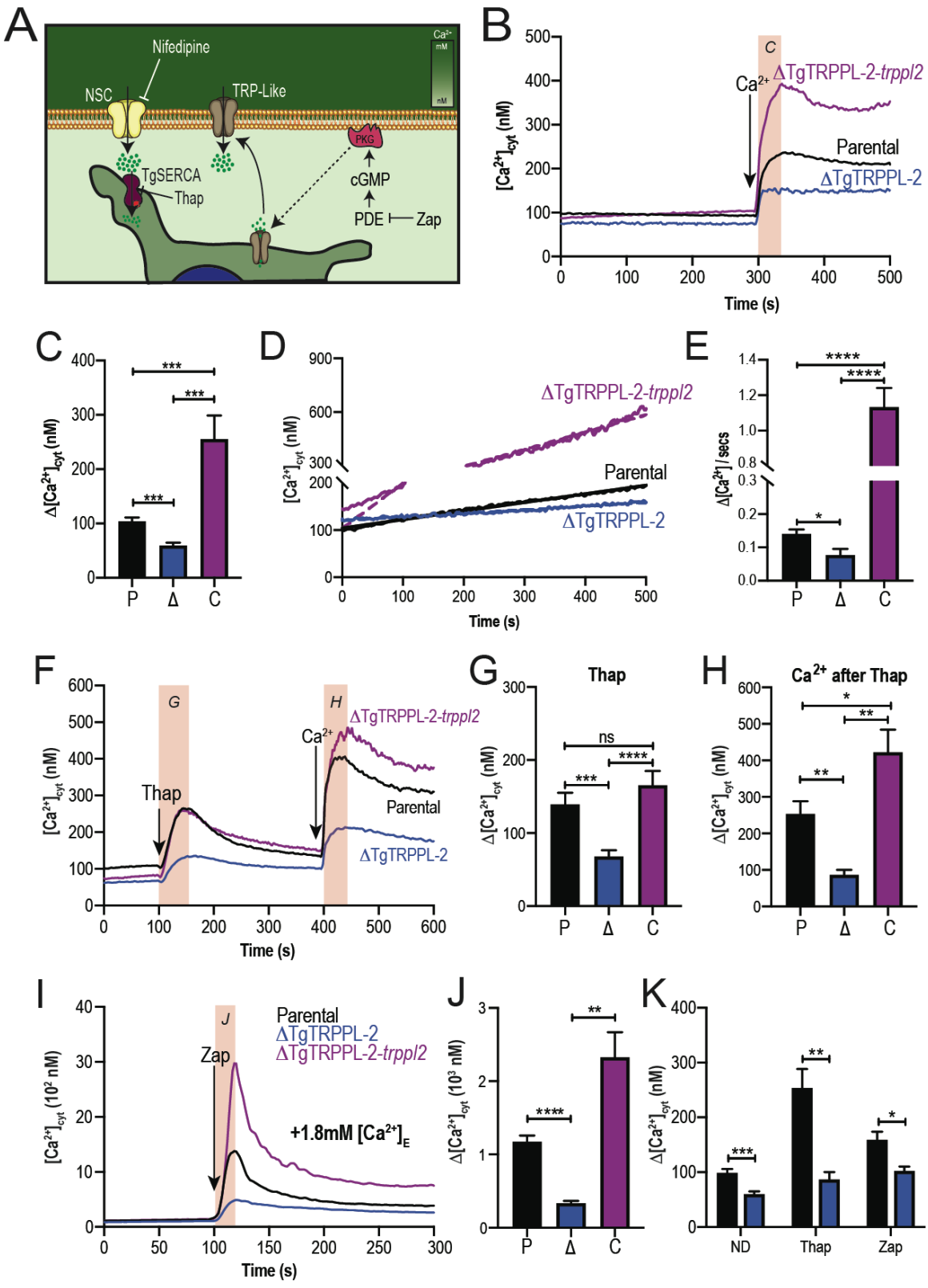
A
Nifedipine
NSC
TRP-Like
Ca2+
mM
nM
PKG
TgSERCA
Thap
cGMP
PDE
Zap
B
C
Ca2+
ΔTgTRPPL-2-trppl2
Parental
ΔTgTRPPL-2
[Ca2+]cyt (nM)
Time (s)
C
Δ[Ca2+]cyt (nM)
P
Δ
C
D
ΔTgTRPPL-2-trppl2
Parental
ΔTgTRPPL-2
[Ca2+]cyt (nM)
Time (s)
E
Δ[Ca2+]/ secs
P
Δ
C
F
G
H
Thap
Ca2+
ΔTgTRPPL-2-trppl2
Parental
ΔTgTRPPL-2
[Ca2+]cyt (nM)
Time (s)
G
Thap
Δ[Ca2+]cyt (nM)
ns
P
Δ
C
H
Ca2+ after Thap
Δ[Ca2+]cyt (nM)
P
Δ
C
I
J
Zap
Parental
ΔTgTRPPL-2
ΔTgTRPPL-2-trppl2
+1.8mM [Ca2+]E
[Ca2+]cyt (102 nM)
Time (s)
J
Δ[Ca2+]cyt (103 nM)
P
Δ
C
K
Δ[Ca2+]cyt (nM)
ND
Thap
Zap

Figure 2.3. The role of TgTRPPL-2 in PM Ca^{2+} influx. A. Scheme showing the mechanism of Ca^{2+} influx and how cytosolic Ca^{2+} may activate the PM channel (Ca^{2+}-activated Calcium Entry). *NSC, Nifedipine-Sensitive Channel; PKG, Protein Kinase G; PDE, phosphodiesterase; Thap, Thapsigargin.* **B.** Cytosolic Ca^{2+} measurements of Fura-2 loaded tachyzoites of the parental (P), *ΔTgTRPPL-2* (D) and *ΔTgTRPPL-2-trppl2* (C) lines. The buffer contains 100 mM EGTA and at 300 sec, 1.8 mM Ca^{2+} was added to the cuvette. *Orange box* indicated the area used for the quantification presented in *C*. **C.** Quantification and statistical analysis of the change in cytosolic Ca^{2+} during the first 20 s after addition of extracellular Ca^{2+}. *** p< 0.0002. **D.** Cytosolic Ca^{2+} increase of parasites pre-incubated with 1.8 mM Ca^{2+}. **E.** Quantification and statistical analysis of the slope from *D*. **** p< 0.0001. **F.** Ca^{2+} efflux after adding Thap (1 μM) followed by Ca^{2+} influx after the addition of 1.8 mM extracellular Ca^{2+}. *Orange box* indicates the area used for the quantification presented in *G* and *H*. **G.** Quantification and statistical analysis of the change in cytosolic Ca^{2+} 50 s after the addition of Thap *(Thap)* and **(H)** 20 s after the addition of 1.8 mM of Ca^{2+} *(Ca^{2+} after Thap)*. *** p< 0.0008, **** p<0.0001. **G.** Calcium-activated Calcium Entry with Zaprinast (100 μM) in the presence of 1.8 mM extracellular Ca^{2+}. **J.** Quantification and statistical analysis of cytosolic Ca^{2+} increase during the first 15 s after adding Zaprinast (100 μM) (*Orange box*, in I). ** p< 0.001, **** p< 0.0001. **K.** Quantification and statistical analysis of Ca^{2+} influx during the 20 s after adding Ca^{2+} without additions (ND) or after adding Thap or Zap. * p< 0.02, ** p< 0.005, *** p< 0.0008. Statistical analysis for all experiments

were done from at least three independent trials using student's t-test. P values are indicated with asterisks for each panel.

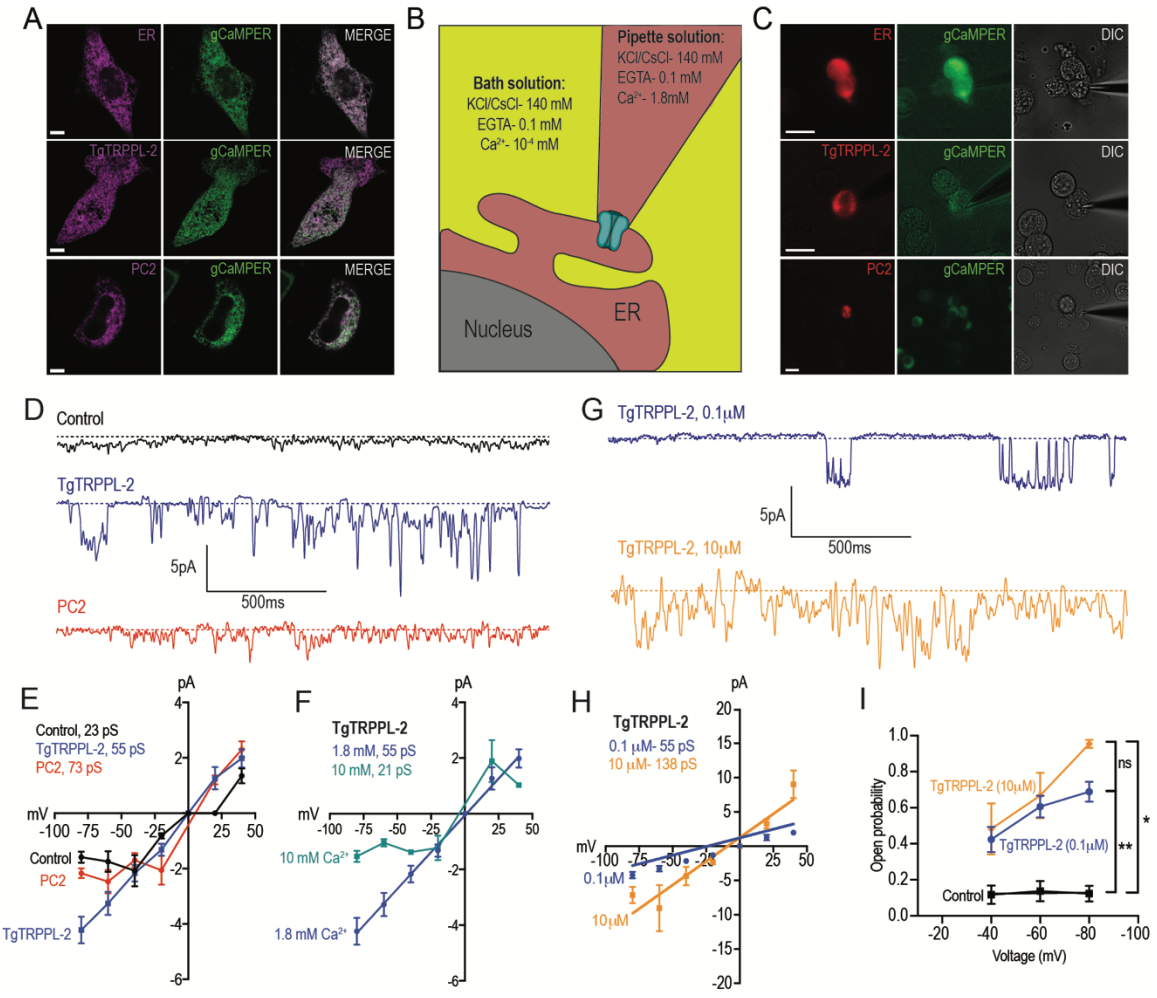

Figure 2.4. Functional studies of TgTRPPL-2 expressed in DT40-3KO cells. **A,** Images of 3KO-DT40 cells expressing an ER-marker, PC2 or TgTRPPL-2 with the genetic calcium indicator gCAMPER. **B.** Schematic representation of nuclear-ER patch clamp arrangements. Ionic composition and concentration for bath and pipette solutions are shown. **C.** Patched nuclear-extract expressing ER-marker, PC2 or TgTRPPL-2 with the genetic calcium indicator gCaMPER. **D.** Representative tracing of currents recorded in the presence of 1.8 mM luminal

Ca^{2+} in 140 mM KCl solution of Control, *TgTRPPL-2* or *PC2* expressing cells. Tracings represent ~2 s from 25 s recording and filtered at 45 kHz. **E.** Current-voltage relationship comparing single-channel conductance shown in *D* of Control, PC2 and TgTRPPL-2 expressing cells. *Inset*, calculated channel conductance for control, TgTRPPL-2 and PC2 from -80 to -40 mVs. **F.** Current-voltage relationship comparing single-channel conductance of TgTRPPL-2 expressing cells at 1.8 and 10 mM [Ca^{2+}] in the pipette solution. *Inset*, calculated channel conductance for the conditions analyzed. **G.** Representative tracing of currents recorded from TgTRPPL-2 expressing cells using different concentration of [Ca^{2+}] in the intracellular or extracellular environment (Solution A vs. Solution B) (Table S4). Tracings represent ~2 s from a 25 s recording and filtered at 45 kHz. **H.** Current-voltage relationship comparing single-channel conductance of TgTRPPL-2 expressing cells at 0.1 and 10 μM [Ca^{2+}] in the bath solution. *Inset*, calculated channel conductance for the different [Ca^{2+}]. **I.** Open probability of control and TgTRPPL-2 expressing cells in the presence of different [Ca^{2+}] in the bath solution in comparison to the Control. Asterisk indicate p value for significant difference. *p< 0.01, **p<0.001.

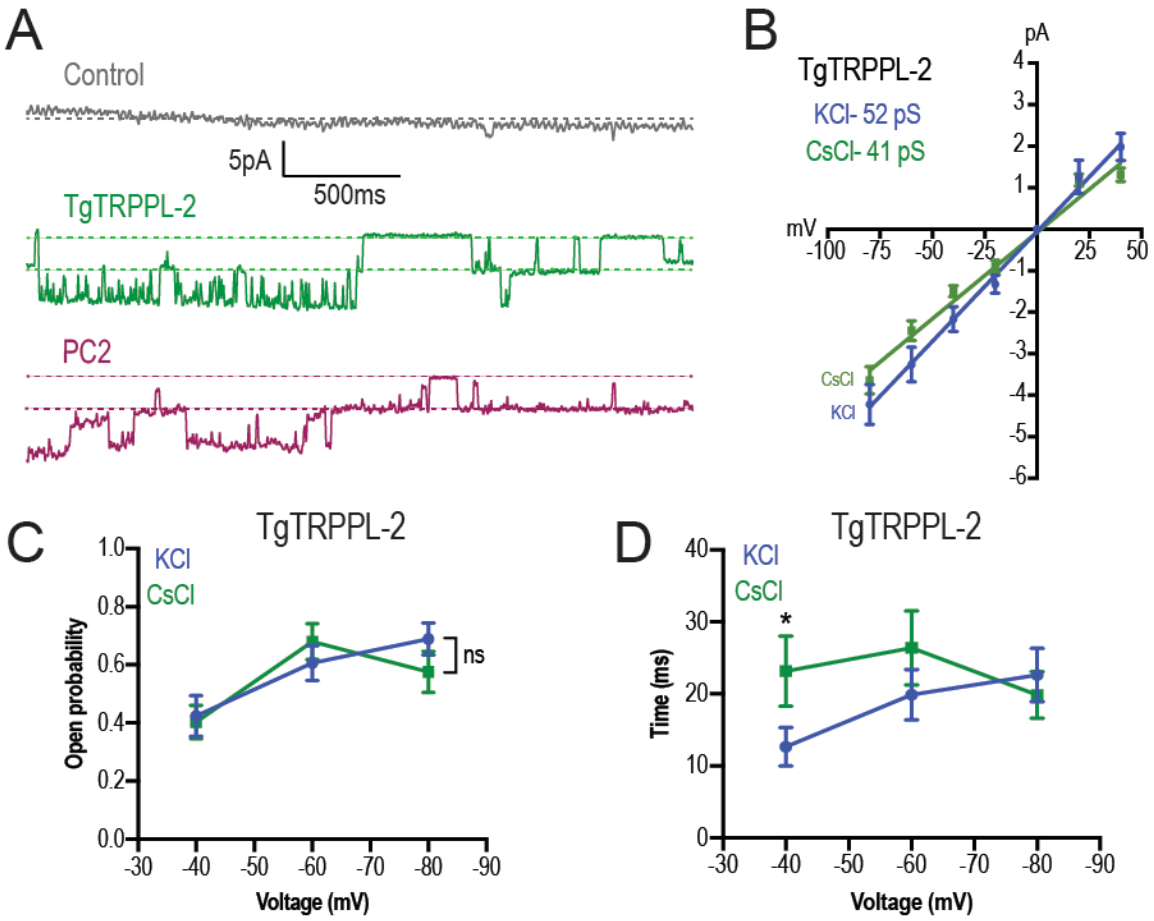

Figure 2.5. TgTRPPL-2 permeates Ca^{2+}. A. Representative tracing of currents recorded at -80 mV in the presence of 1.8 mM Ca^{2+} inside the pipette (Solution D) of nuclear extracts from Control, *TgTRPPL-2* or *PC2* expressing cells. Traces are a representation of 2 seconds of sampling from a total time of 25 seconds. **B.** Current-voltage relationship comparing single-channel conductance of TgTRPPL-2 cells in 1.8 mM of intracellular Ca^{2+} in KCl (*blue*) or CsCl (*green*) buffer. *Inset*, Channel conductance of TgTRPPL-2 in the different conditions analyzed. **C.** Calculated open probability of TgTRPPL-2 expressing cells in the presence of 1.8 mM intracellular Ca^{2+} in a KCl (*blue*) or CsCl (*green*) buffer. **D.** Average time of channel opening of TgTRPPL-2 expressing cells in the presence of 1.8 mM

intracellular Ca^{2+} in a KCl (*blue*) or CsCl (*green*). Asterisk indicate p value for significant difference. * $p < 0.04$.

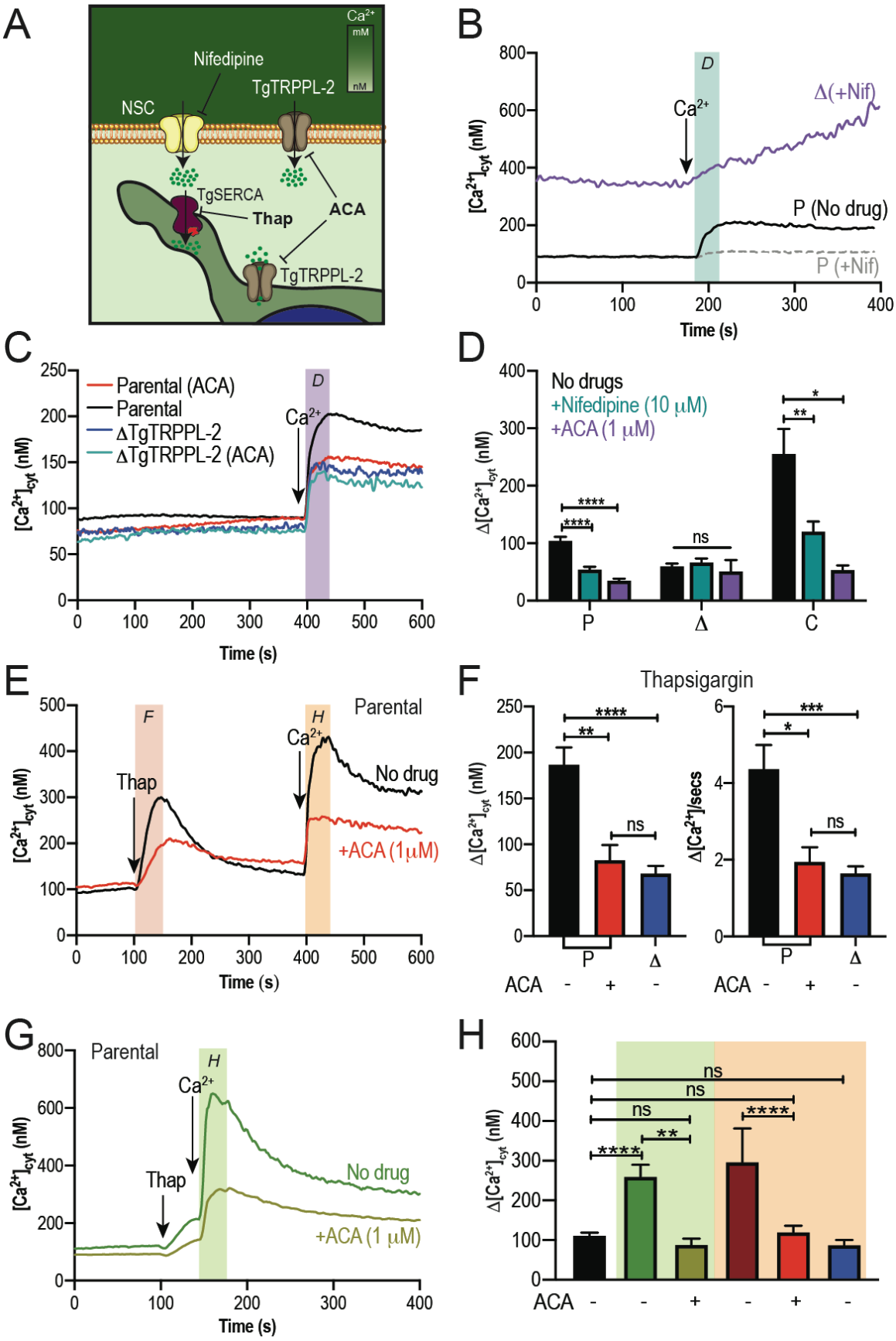
A
Ca2+
mM
nM
Nifedipine
TgTRPPL-2
NSC
TgSERCA
Thap
ACA
TgTRPPL-2
B
D
Ca2+
Δ(+Nif)
P (No drug)
P (+Nif)
[Ca2+]cyt (nM)
Time (s)
C
Parental (ACA)
Parental
ΔTgTRPPL-2
ΔTgTRPPL-2 (ACA)
D
Ca2+
[Ca2+]cyt (nM)
Time (s)
D
No drugs
+Nifedipine (10 μM)
+ACA (1 μM)
Δ[Ca2+]cyt (nM)
****
****
ns
*
**
P
Δ
C
E
F
H
Parental
Thap
Ca2+
No drug
+ACA (1μM)
[Ca2+]cyt (nM)
Time (s)
F
Thapsigargin
Δ[Ca2+]cyt (nM)
Δ[Ca2+]/secs
****
**
ns
***
*
ns
P
Δ
ACA - + -
G
Parental
H
Ca2+
Thap
No drug
+ACA (1 μM)
[Ca2+]cyt (nM)
Time (s)
H
Δ[Ca2+]cyt (nM)
ns
ns
ns
****
**
****
ACA - - + - + -

Figure 2.6. Regulation of TgTRPPL-2 by Ca^{2+} and inhibition by TRP inhibitors. **A.** Scheme showing TgTRPPL-2 acting at the PM and ER. **B**. Cytosolic Ca^{2+} measurements of Fura2 loaded tachyzoites pre-incubated with 10 µM nifedipine. 1.8 mM Ca^{2+} was added where indicated. *Blue box* indicates the area used for the quantification presented in *D*. **C.** Cytosolic Ca^{2+} measurements of suspensions of parental and *⊿TgTRPPL-2* parasites pre-incubated for 3 min with ACA (1 µM). 1.8 mM Ca^{2+} was added where indicated. *Purple box* shows the area used for the quantifications presented in *D*. **D.** Change in cytosolic Ca^{2+} during the first 20 s after addition of Ca^{2+} in the presence of 10 µM of nifedipine or 1 µM ACA. Asterisk indicate p value for significant difference. * p<0.01, ** p<0.003, **** p<0.0001. **E.** Cytosolic Ca^{2+} increase after adding Thap (1 µM) to a suspension of tachyzoites. The red line shows a similar experiment but the cells were pre-incubated with ACA for 3 min. *Pink and orange boxes* show the areas used for the quantifications presented in *F*. **F.** Quantification and statistical analysis of the ΔCa^{2+} and slope 50 s after the addition of Thap in the presence or absence of ACA in parental and *DTgTRPPL-2* mutants. Asterisk indicate p value for significant difference, *p< 0.01, **p< 0.003 ***p< 0.0003. **G.** Stimulation of Ca^{2+} influx by pre-addition of Thap in the presence or absence of 1 µM ACA. Green box shows the area used for the quantifications presented in H. **H.** Quantification of change of cytosolic Ca^{2+} 20 s after the addition of 1.8 mM Ca^{2+} following the addition of Thap under different conditions. Asterisk indicate p value for significant difference. **p<0.001,

****p<0.00001. The statistical analysis for all experiments were done from at least three independent trials using student's t-test.

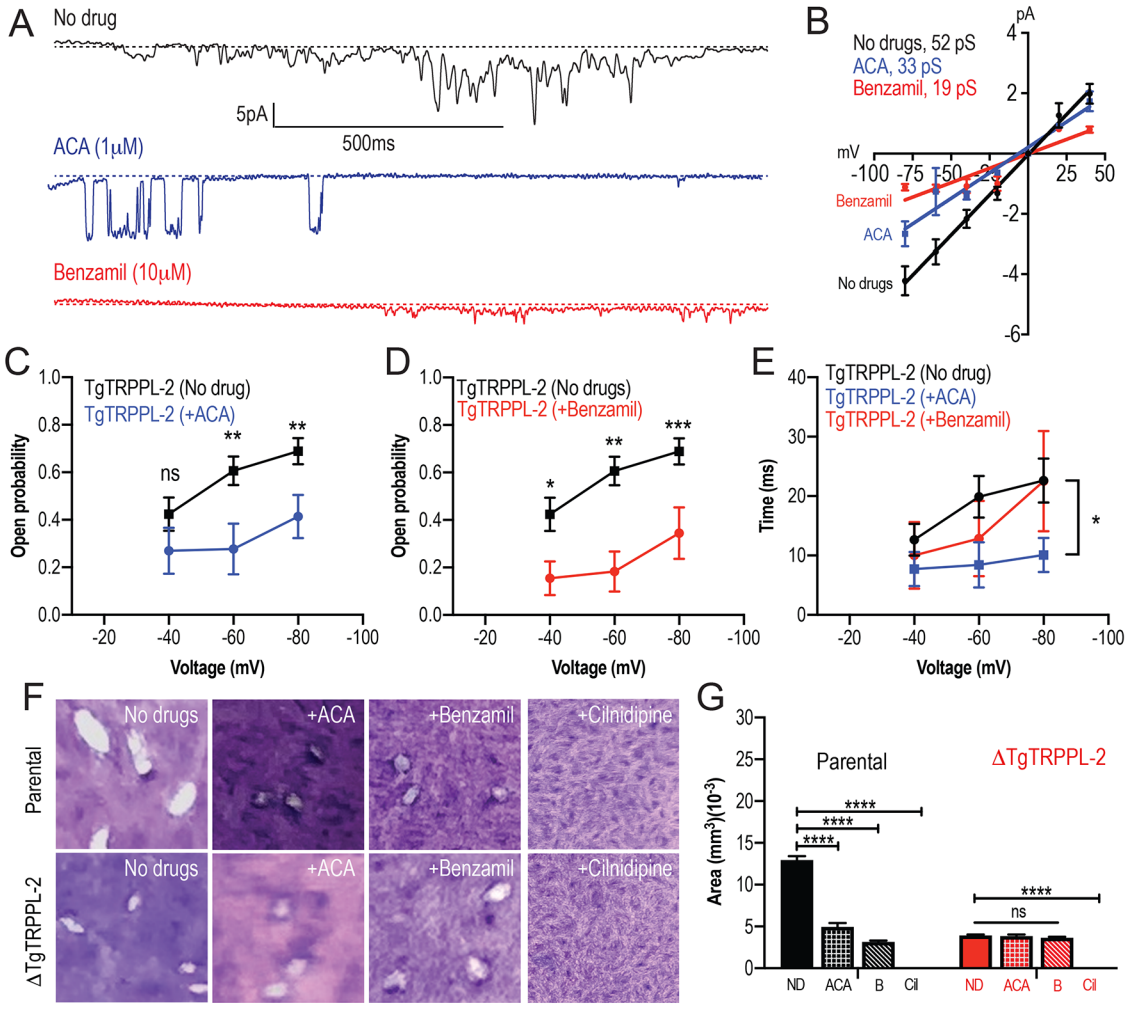

Figure 2.7. TRP Inhibitors decreased the activity of TgTRPPL-2. A. Example of currents recorded of *TgTRPPL-2* expressing cells at –80 mV without drug (*Black trace*) versus in the presence of 1 mM of ACA (*Blue trace*) or 10 mM of benzamil (*Red trace*). **B.** Current-voltage relationship comparing single-channel conductance in the presence of ACA or benzamil. Analysis was done from three

independent biological trials. *Inset*, conductance of TgTRPPL-2 in the different conditions analyzed. **C.** Calculated open probability of TgTRPPL-2 expressing cells (*black*) or in the presence of ACA (*blue*). Asterisk indicate p value for significant difference. ** p< 0.006-0.007. **D.** Calculated open probability of TgTRPPL-2 expressing cells (*black*) or in the presence of Benzamil (*red*). Asterisk indicate p value for significant difference. * p< 0.02, ** p< 0.002, *** p< 0.0002. **E.** Average time of channel opening of TgTRPPL-2 expressing cells in the presence of TRP inhibitors. Asterisk indicate p value for significant difference. * p< 0.02 **F.** Plaque assay of *DTgTRPPL-2* mutants and the parental strain in the presence of ACA (1 mM), benzamil (10 mM) (B) and cilnidipine (40 mM) (Cil) after 7 days of growth. ND means no drug. **G**. Quantification and statistical analysis of plaque sizes from three independent biological replicates using student's *t*-test. *ND, no drug, B, Benzamyl, Cil: Cilnedipine.* Asterisk indicate p value for significant difference. ****p< 0.0001.

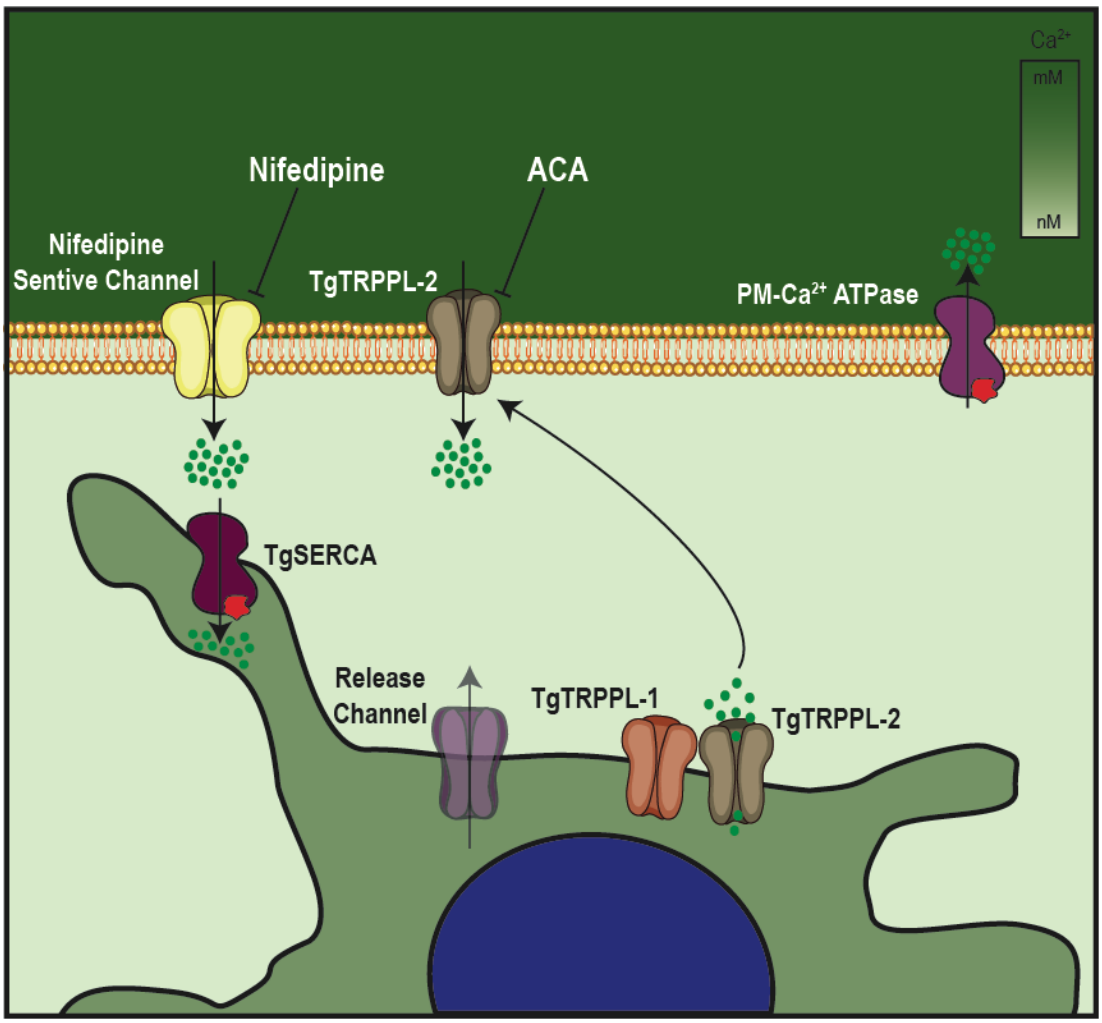

Figure 2.8. The role of TgTRPPL-2 in Ca^{2+} influx into the cytosol of *T. gondii.*

Schematic representation of the Ca^{2+} influx pathways of *T. gondii*. Ca^{2+} influx is mediated by two independent Ca^{2+} channels, a nifedipine-sensitive channel and TgTRPPL-2. TgTRPPL-2 localizes to the plasma membrane as well as the ER. TgTRPPL-2 at the plasma membrane is a cation permeable channel that mediates Ca^{2+} influx by a pathway that is activated by high [Ca^{2+}] and can be inhibited by broad TRP inhibitors like ACA and benzamil. The presence of the channel at the ER suggest that it may function as a Ca^{2+} efflux channel. Increase in cytosolic

[Ca^{2+}] can modulate TgTRPPL-2 by allowing the channel to open for longer time thus allowing more Ca^{2+} to enter the cell.

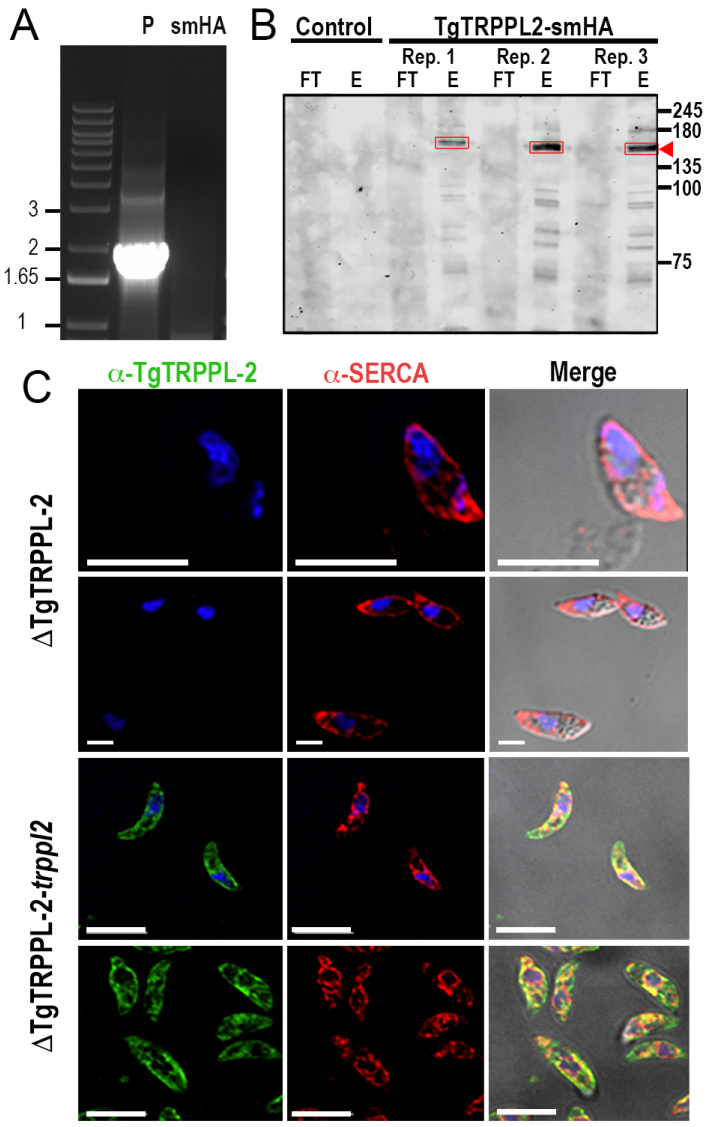

Figure S2.1. Validation of C-terminal tagging of TgTRPPL-2-smHA. A. Amplification of ~2 kB in the TgTRPPL-2-smHA cell line validating the correct integration of TgTRPPL-2-smHA. **B.** Western blot of three biological replicates of immunoprecipitated TgTRPPL-2-smHA using aHA antibody (1:1,000) shows a band of ~150kDa (highlighted by *red boxes* and *arrow*). No band is present in the

control cell line. **C.** IFAs of extracellular tachyzoites with aTgTRPPL-2 (1:1,000) co-localized with aSERCA (1:1,000) in DTgTRPPL-2 and DTgTRPPL-2-*trppl2*. Images were taken with equivalent time and laser power.

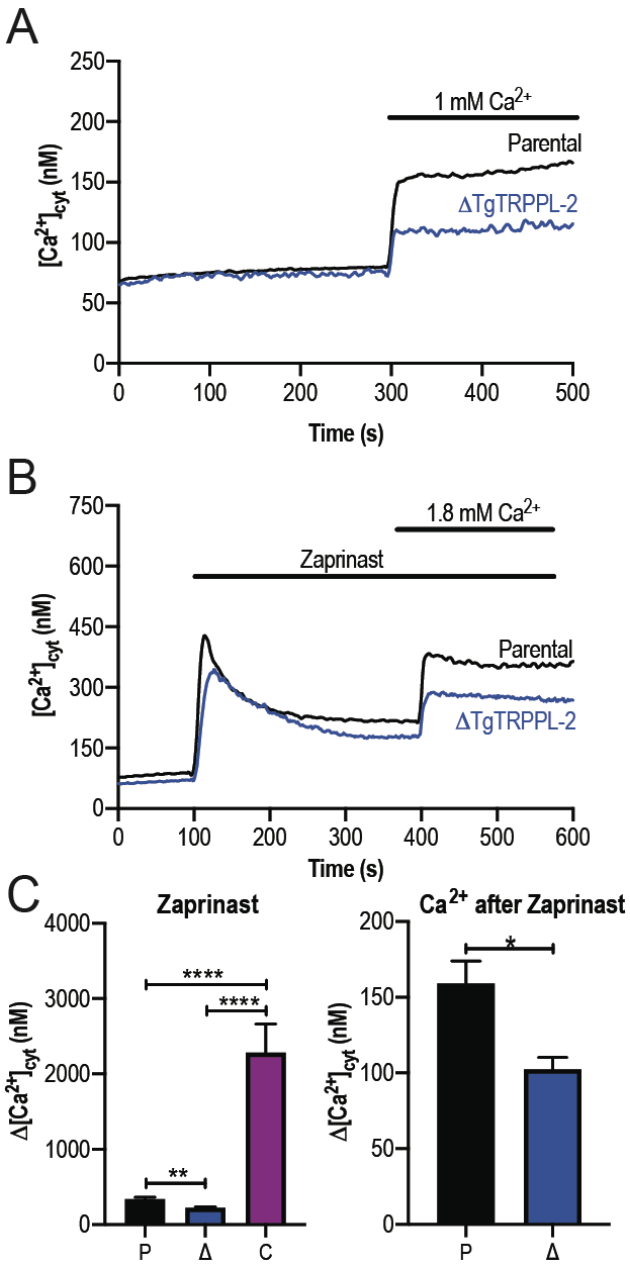

Figure S2.2. TgTRPPL-2 regulates Ca^{2+} in *T. gondii*. **A.** Cytosolic Ca^{2+} measurements of Fura-2 loaded tachyzoites of the parental and *ΔTgTRPPL-2* cell lines after addition of 1 mM extracellular Ca^{2+} at 300 s. **B.** Cytosolic Ca^{2+} measurement after the addition of Zaprinast (100 µM) at 100 s and Ca^{2+} influx was stimulated by the addition of 1.8 mM extracellular Ca^{2+} at 400s. **C.** Change in cytosolic Ca^{2+} 15 s after the addition of Zaprinast *(Labeled Zaprinast)* and 20 s after the addition of 1.8 mM of extracellular Ca^{2+} *(Labeled Ca^{2+} after Zaprinast)*. Asterisk indicate p value for significant difference. **p< 0.007, ****p< 0.0001.

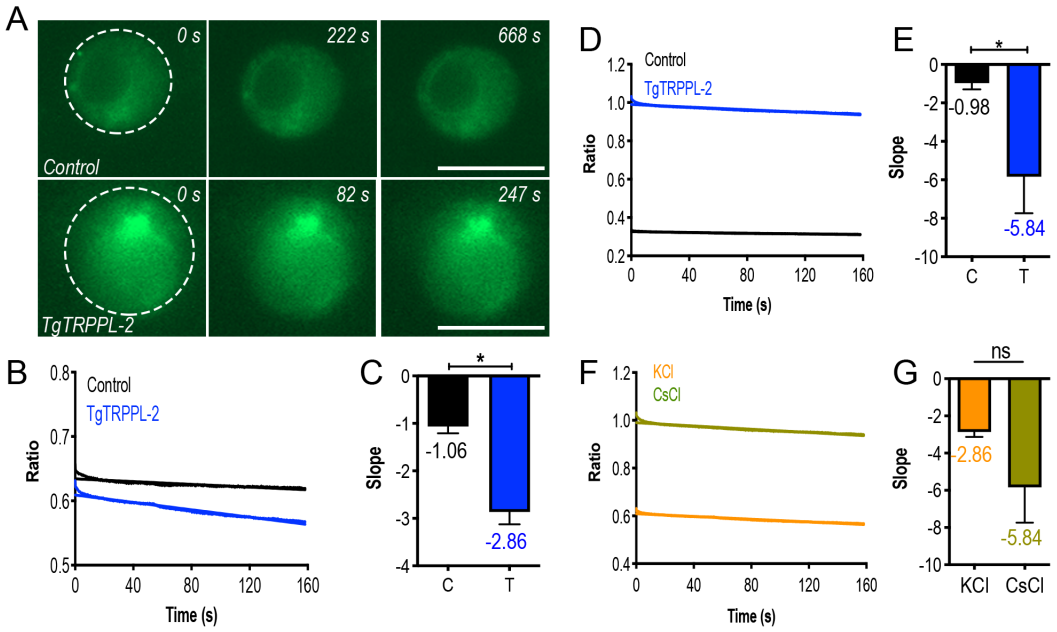

Figure S2.3. Measurement of ER Calcium of DT40-3KO cells expressing TgTRPPL-2. A. Fluorescence of ER calcium in ER-RFP-DT40 (*Control*) vs. TgTRPPL-2-DT40 (*TgTRPPL-2*) in a high calcium-potassium solution of patched nuclear membranes while the membrane is depolarized. **B.** Quantification of fluorescence of patched cells while the membrane is depolarized from -80 to +20 mV in a high calcium-potassium solution. **C.** Quantification of the slope of fluorescence in *B* comparing TgTRPPL-2-DT40-3KO cells versus the control cells. Slope of the fluorescence was quantified based on the 5 technical replicates of the

artificial membrane depolarization in each cell analyzed. Asterisk indicate p value for significant difference. Values represent the mean of the slope shown in *B*. * p< 0.01. **D.** Quantification of fluorescence of patched cells while the membrane is depolarized from -80 to +20 mV in a High calcium-cesium solution. **E.** Quantification of the slope of fluorescence in *D* comparing TgTRPPL-2-DT40-3KO cells versus control cells. The slope was quantified for the five technical replicates of patched membranes. Asterisk indicate p value for significant difference. Values represent the mean of the slope shown in *D*. * p< 0.03. **F.** Comparison of the fluorescence of patched nuclear extract of TgTRPPL-2-DT40 cells while the membrane was artificially depolarized. **G.** Quantification of the slope of fluorescence of patched TgTRPPL-2-DT40-3KO nuclear extracts in different experimental conditions. Slope of the fluorescence was quantified based on the 5 technical replicates of the artificial membrane depolarization in each cell analyzed.

Table S2.1. Top 10 hits of HHPRED analysis of TgTRPPL-2.

Name	***Probability***	***E-value***	***Target Length***	***PDB Reference Number***
Polycystic kidney disease 2-like 1	99.45	7.10 E^{-11}	805	6DU8_A
Polycystin-2; PKD2	99.44	1.10 E^{-10}	756	6WB8_D
Polycystic kidney disease 2-like 1	99.39	2.10 E^{-10}	566	5Z1W_C
Polycystin-2, Polycystin-1	99.38	2.40 E^{-10}	577	6A70_A
Polycystin-2	99.35	2.40 E^{-10}	968	5MKE_A
Polycystin-2, Polycystin-1	99.3	2.80 E^{-10}	1153	6A70_B
Polycystin-2; TRP channel, PKD2	99.22	3.30 E^{-09}	510	5T4D_A
TRPV2; Transport protein, TRP channel	98.52	6.6 E^{-05}	613	5AN8_B
Mucolipin-3; TRP channel, lysosomal	98.31	0.00031	558	6AYF_C
Transient receptor potential cation channel	98.28	0.00015	639	6LGP_D

Table S2.2. List of Mass spectrometry hits by TgTRPPL-2 Immunoprecipitation.

Gne ID	***Product description***	***Phenotype***	***MW (kDa)***	***Average Counts***
TGME49_280560	selenide, water dikinase	0.07	137.8	6
TgME49_201680	putative eukaryotic initiation factor-3 subunit 10	-4.55	118.8	6
TGME49_359490	elongation factor 1-alpha	-4.26	31.1	5.5
TgME49_228170	inner membrane complex protein IMC2A	-3.28	182.2	5.5
TgME49_209030	actin ACT1	-4.5	41.9	4
TGME49_310560	**hypothetical protein (TgTRPPL-2)**	**-2.49**	**237.3**	**3**
TGME49_212300	hypothetical protein	0.69	75.64	3
TGME49_214300	hypothetical protein (TgTRPPL-1)	-0.36	259.14	3
TGME49_229180	HEAT repeat-containing protein	-5.05	136	3
TGME49_247370	hypothetical protein	-1.42	140.9	2
TGME49_321440	SWI2/SNF2 ISWI-like SANT	-4.6	140.1	2
TGME49_226960	phosphofructokinase PFKII	-5.19	131.3	2
TGME49_263060	Proteasome/cyclosome repeat-containing protein	-4.45	107.1	2
TGME49_205540	DEAD/DEAH box helicase domain-containing protein	-5.86	116.58	2
TGME49_280600	putative histidyl-tRNA synthetase (HisRS)	-4.23	134.8	2
TgME49_226250	DEAD (Asp-Glu-Ala-Asp) box polypeptide DDX3X	-4.25	78.5	2
TgME49_209600	hypothetical protein	1.9	50.2	2
TgME49_308920	splicing factor U2AF protein	-4.57	83.1	2

Table S2.3. List of primers used in the study.

Endogenous Tagging of TgTRPPL2		
T1	TgTRPPL2_pLic_F	TACTTCCAATCCAATTTAATGCGAGAAGCGCATTGAGGAATGG
T2	TgTRPPL2_pLic_F	TCCTCCACTTCCAATTTTAGCCTCTTCTCCCAGGATGTTGACGC
T3	TgTRPPL2_Validation_Tag_F	TATGTGTGCCTGCCTGCGCAT
Disruption of TgTRPPL2		
K1	TgTRPPL2_Cas9_gRNA_F	TATGTCACATGTCTTTTCTCGTTTTAGAGCTAGAAATAGCAAG
K2	TgTRPPL2_DHFR_F	CTTTGGTTTCCCTCTCTCGTCCATGAAGCTTCGCCAGGCTGTAAATCC
K3	TgTRPPL2_DHFR_R	TGGACGCCCAGCTCGACATGTCATCCTGCAAGTGCATAGAAGGA
K4	TgTRPPL2_Validation R	CGATGAGGTGGATGTAGCTGAATG
RT-PCR of TgTRPPL2		
Q1	TgTRPPL2_qPCR_F	GAGCTCCGACGCAGGCCAGCAG
Q2	TgTRPPL2_qPCR_R	CCCGGGCGATGAGGTGGATGTAGCTGAATG
Cloning for Heterologous expression in DT-40-3KO cells		
C1	pCDNA3_TgTRPPL2_F	cagatatccatcacactggcATGCATGCATTCGACGAC
C2	tdTomato_TgTRPPL2_R	tgctcaccatCTCTTCTCCCAGGATGTTG
C3	TgTRPPL2_tdTomato_F	gggagaagagATGGTGAGCAAGGGCGAG
C4	pCDNA3_TgTRPPL2_tdTomato_R	acactatagaatagggccctCTACTTGTACAGCTCGTCCATG
C5	TgTRPPL2_Validation_F	GCAAGAAGAAGAAACGACGCAAG
C6	TgTRPPL2_Validation_R	CTTTGAGGTCCTAGTTCACCTCCGA

CHAPTER 3

Calcium Binding Proteins of the Endoplasmic Reticulum and Golgi *of Toxoplasma* and their role in signaling[2]

[2] Karla M. Márquez-Nogueras, Omar Salas, Breanna Marshalls, Abigail Calixto and Silvia NJ Moreno. To be submitted to the *Journal of Biological Chemistry*.

3.1 ABSTRACT

Calcium binding proteins (CaBP) are essential for the transduction of calcium signals and participate in a number of of cellular responses. CaBPs contain specific motifs that bind calcium. Binding of [Ca^{2+}] results in a change in the conformation of the CBP and exposes domains that interact with target proteins located in the cell cytosol or organelles. Calnuc is the major CaBP of the mammalian Golgi and is involved in the maintenance of Golgi Ca^{2+}. In this study we identified a *T. gondii* Golgi/ER CBP, TgGT1_255660, which we termed TgCalnuc. Deletion of TgCalnuc impairs the ability of the parasite to invade host cells. Ca^{2+} measurements demonstrate defects in the Ca^{2+} storage of both ER and Golgi. We also characterized the function of another CBP, CaM2, which was localized to the ER of the tachyzoite and to the conoid. *CaM2* mutant parasites have a deficiency in the release of Ca^{2+} from the ER. We present data supporting a role of CaM2 as a potential regulator of the mechanisms of calcium release from the ER.

3.2 INTRODUCTION

Toxoplasma gondii, the causative agent of Toxoplasmosis, is an obligate intracellular parasite that currently affects one third of the world's population [1]. Infection of immunocompromised patients can cause diseases like myocarditis, encephalitis and ocular diseases. Currently available drugs to treat toxoplasmosis in immunocompromised patients are not ideal because of toxicity [19, 20]. In order to develop new drugs against this parasite it is important to understand the biology of the parasite.

Once inside the host the parasite will undergo a lytic cycle where it will invade and replicate within the host cell [37]. Environmental cues will trigger parasite egress from the host cell to invade another where it will repeat this cycle. Calcium has been shown to be essential for the ability of the parasite to complete this lytic cycle [64-67]. Calcium signaling is the activation of essential processes within the cells that are regulated by Ca^{2+} ions [143]. Calcium signaling is tightly regulated by increasing and decreasing cytosolic [Ca^{2+}] [144]. These complex signals are stimulated by an increase of cytosolic Ca^{2+} that occurs from the release of intracellular store or influx from the intracellular environment [145]. In the majority of eukaryotic cells, the main intracellular stores that regulate the calcium release within the cells are the ER and Golgi [146].

The Golgi is an essential organelle involved in post-translational modification and protein trafficking [147]. It has been described that the Golgi is able to store high concentrations of Ca^{2+}, comparable to the levels in the ER [148].

Calcium within these stores is regulated by calcium-binding proteins (CaBP) that function as calcium sensors, which can sense changes in the [Ca^{2+}] [149]. The Golgi contains three calcium binding proteins that control luminal Ca^{2+}. Calnuc is the major CaBP present in the Golgi. It contains a DNA binding motif, a leucine zipper motif and two EF-hand motifs [150].

In *T. gondii* there are CaBPs, that regulate myosin chains like MyoA and MyoH [75, 77, 78]. However, in most eukaryotic cells, CaBPs have been described to regulate and activate a variety of essential proteins like kinases, phosphatases, transcription factors and ion channels [59, 151]. Most of the CaBP described in *T. gondii* are not essential and functionally redundant, so we hypothesize that these proteins have multiple targets within the calcium signaling pathway. Additionally, there is no information on how the ER and Golgi Ca^{2+} concentration (storage capacity) is regulated.

In mammalian cells, Calnuc regulates the storage capacity of the Golgi. In this study we characterized the role of TgCalnuc in Toxoplasma which sense changes of [Ca^{2+}] in the Golgi and ER. Regulation of the Ca^{2+} storage capacity of intracellular organelles is essential for the activation signaling. Decreased Ca^{2+} within the store will impact the ability to release the ion to the cytosol in response to specific signals, which will impact cellular responses. We also described the role a CaBP, CAM2, in the regulation of calcium release from the ER. This study provide insight into how CBPs regulate multiple effectors in the Ca^{2+} signaling pathway of *T. gondii*. Additionally, we characterize the role of the Golgi as an essential Ca^{2+} store within the parasite.

3.3 EXPERIMENTAL PROCEDURES

Parasite culture All parasite strains were continuously maintained *in vitro* by serial passage in Dulbecco's modified minimal essential media (DMEM) with 1% FBS, 2.5 µg/ml amphotericin B, 100 µg/ml streptomycin in the human telomerase reverse transcriptase immortalized foreskin fibroblasts (hTERT) [91] .

C-Terminal Tagging The smHA-LIC-CAT plasmid was used for in situ C-terminal tagging of TgCalnuc. Carboxy-terminus tagging was done in the parental line RHTatiΔku80 (TatiΔku80) [92] which contains the tetracyclin-regulated transactivator system that allows conditional expression of genes [93] and also in which the *ku80* gene was deleted increasing efficiency of homologous recombination [94]. Briefly, a homology region of 767 bp covering the 3' region of the gene of interest excluding the STOP codon was amplified by PCR using *T. gondii* RH genomic DNA as template and cloned into the smHA-LIC-CAT plasmid. Plasmids correctly built were selected by restriction digest and confirmed by sequencing. The oligonucleotides primers used for PCR and for creating the gene-tagging plasmids and for PCR validations are listed in Table S1 (Primers T1-T3). Prior to transfection all plasmids were linearized within the region of homology. Approximately 20 µg of plasmid DNA was transfected into $1x10^7$ *T. gondii* strain RHTatiΔKu80 using a Gene Pulser X Cell electroporator (BioRad). Selection for integration of the plasmid was performed with 20 µM chloramphenicol, and clones were isolated by limiting dilution. DNA of selected clones were isolated and

screened by PCR using primers located upstream of the homology region (forward) and downstream into the plasmids (reverse).

Gene disruption and complementation of TgCalnuc In order to disrupt the *TgCalnuc* (TgGT1_255660) gene a single guide RNA against *TgCalnuc* was constructed as previously described [95]. The single guide RNA was mutagenized with the desired sequence in a plasmid that contains the Cas9 using the Q5 Mutagenesis Kit following manufacturer's instructions. The pyrimethamine-resistant DHFR cassette was amplified by PCR with primers containing 50 bp homology arms of the region upstream and downstream of the start and stop codon of the *TgCalnuc* gene (Table S1 Primers K2-K3). The *sgTgCalnuc* CRISPR plasmid was co-transfected with the DHFR cassette (3:1 respectively) into RH tachyzoites. Selection followed with pyrimethamine for 7 days. Parasites were sub-cloned by limiting dilution and screening for clones was done by PCR. TgCalnuc cDNA was amplified using primers described in Table S1 (Primers K5-K6) from RH cDNA. Using the T4 ligase *TgCalnuc* cDNA was cloned into pCTH3 plasmid which was previously digested with AvrII and BglI. Approximately 20 µg of plasmid DNA was transfected into $1x10^7$ ΔTgCalnuc tachyzoites using a Gene Pulser X Cell electroporator (BioRad). Selection for integration of the targeting plasmid was performed with 20 µM chloramphenicol, and clones were isolated by limiting dilution. DNA of selected clones were isolated and screened by qRT-PCR, western blot and IFA. Gene disruption and complementation of CaM2 was performed following the same protocol as previously described for TgCalnuc.

Quantitative PCR Total RNAs from parental, ΔTgCalnuc and ΔTgCalnuc-*tgcalnuc* lines was extracted and reversed-transcribed into cDNA. The qPCR reaction was done using the iQ^{TM}SYBR Green master mix (BioRad), plus primers, and the reversed-transcribed cDNA (Primers are shown in Table S1 Primers Q1-Q2). The qRT-PCR was carried out on a CFX96^{TM} PCR Real-Time detection system (C1000Touch^{TM} Thermal cycler, BioRad). Relative quantification software (CFX Maestro^{TM} software) was used for the analysis and relative expression levels were calculated as the fold change using the formula $2^{\Delta\Delta}$CT [152]. Normalization was done using Actin and Tubulin primers as reference. Experiments were repeated three times using three biological replicates with triplicate samples.

Immunofluorescence microscopy Extracellular parasites were collected and purified as previously described [97]. Parasites were washed in buffer A with glucose (BAG, 116 mM NaCl, 5.4 mM KCl, 0.8 mM $MgSO_4$, 5.5 mM glucose and 50 mM HEPES, pH 7.4) and 2 x 10^4 parasites were overlaid on a coverslip previously treated with poly-L-Lysine. Intracellular tachyzoites were grown on hTERT cells on coverslips previously infected with freshly lysed parasites. Both extracellular and intracellular parasites were fixed with 3% paraformaldehyde for 20 min at room temperature (RT), permeabilized with 0.3% Triton X-100, blocked with 3% bovine serum albumin (BSA), and exposed to primary antibodies (Ratα-HA 1:100). The secondary antibodies used were goat-αrat Alexa-Fluor488 (Life Technologies) at 1:1,000. For co-localization studies Grasp55-RFP plasmids were transiently transfected and analyzed using goat-antiRFP Alexa-Fluor 546 as Golgi Marker. For ER co-localization α-TgSERCA (1:1,000) was used. Slides were

examined using an Olympus IX-71 inverted fluorescence microscope with a photometric CoolSNAP HQ charge-coupled device (CCD) camera driven by DeltaVision software (Applied Precision, Seattle, WA).

Western blot analysis SDS-polyacrylamide gel electrophoresis (SDS-PAGE) followed established protocols [96]. Lysates were prepared by resuspending a pellet of 1 x 10^8 tachyzoites in 50 µL of Cell Lytic^M lysis buffer containing 12.5 U benzonase and 1 X protease cocktail inhibitor (P8340 Sigma). The reaction was stopped with one volume of 2% SDS and 1 mM EDTA. Total lysates were boiled in Laemmli sample buffer (BioRad). Immunoblotting followed established protocols using mouse anti-HA monoclonal antibody (1:1,000) (Roche). Detection was done using the Odyssey Clx LICOR system using goat anti-mouse IRDye800WC (1:10,00). Loading control for westerns were done with primary mouse-anti-tubulin antibodies at a 1:15,000 dilution and goat anti-mouse IRDDye800WC as secondary.

Growth and Invasion Assays Plaque growth was done as previously described, with slight modifications [99]. Briefly, 200 egressed tachyzoites per well were allowed to infect confluent hTERT cells for 7 days. After seven days cells were fixed in ethanol and stained with crystal violet. Plaque sizes were analyzed using FIJI [98]. Growth assay at different [Ca^{2+}] were done using Dulbecco's modified essential media (DMEM) without calcium and extracellular calcium was titrated to the desired concentration with 100 µM EGTA. Invasion assay were performed as previously described with slight modifications [99]. A subconfluent monolayer of HFF cells were infected with 2x10^7 tachyzoites in the presence of 1.8 mM or 1 mM

Ca^{2+} and placed for 20 min on ice and subsequently transferred for 5 min to a 37°C water bath for parasite invasion. Cells were immediately fixed with 3% paraformaldehyde for 20 min. Extracellular parasites (attached) were stained using RabbitαSag1 (1:1,000) before permeabilization while intracellular parasites (invaded) were stained with MouseαSag1 (1:200). Secondary antibodies were goat-αrabbit Alexa Fluor 546 (1:1,000) and goat-αmouse Alexa Fluor 488 (1:1,000). Images were taken with an Olympius IX-71 inverted fluorescence microscope with a Photometry CoolCNAP HQ CCD camera driven by DeltaVision software (Applied Precision, Seattle, WA). Quantification was made of ten-fields of views at a 1000 magnification from three independent biological replicates. Percentage of invaded vs attached was quantified by dividing the amount of parasite invaded or attached by the total parasites quantified in the field of view.

Egress experiments hTERT cells were infected with $5x10^5$ of the parental or ΔTgCalnuc tachyzoites. 24 hours after infection parasitophorous vacuoles were observed by microscopy after washing them with Ringer's buffer. Ringer's buffer was used as extracellular buffer in the presence or absence of 1.8 mM Ca^{2+}. Drugs were added in Ringer's buffer (155 mM NaCl, 3 mM KCl, 1 mM MgCl2, 3 mM NaH2PO4H2O, 10 mM HEPES, pH 7.3, and 5 mM glucose) 30 sec after imaging at the following concentrations: saponin (0.02%) or Zaprinast (100 µM). Images were acquired in a time-lapse mode with an acquisition rate of 3 sec for 20 min. For statistical analysis, egress time was quantified as the first parasite to egress out of the parasitophorous vacuole. Statistical analysis was done for 3 independent biological replicates and at least 5 PVs per experiment.

Cytosolic calcium measurements of mutants Parasites loading with Fura-2-AM were performed as described in [100]. Briefly, fresh lysed parasites were washed twice at 1,800 rpm for 10 min at room temperature in buffer A (BAG) (116 mM NaCl, 5.4 mM KCl, 0.8 mM $MgSO_4$, 5.5 mM d-glucose and 50 mM Hepes, pH 7.4). Parasites were resuspended to a final density of $1x10^9$ parasites/mL in loading buffer (Ringer's plus 1.5% sucrose, and 5 uM Fura2-AM). The suspension was incubated for 26 min in a 26 °C with mild agitation. Subsequently, the parasites were washed twice with Ringer's buffer (155 mM NaCl, 3 mM KCl, 1 mM $MgCl_2$, 3 mM $NaH_2PO_4H_2O$ 10 mM HEPES, pH 7.3, and 5 mM glucose) to remove extracellular dye. Parasites were resuspended to a final density of $1x10^9$ parasites/mL in Ringer's buffer and kept in ice. Parasites are viable for a few hours under these conditions. For fluorescence measurements, $2x10^7$ parasites/mL were placed in a cuvette with 2.5 mL of Ringer's buffer. The cuvette was placed in a thermostatically controlled Hitachi F-7000 fluorescence spectrophotometer for Ca^{2+} measurements. Excitation was at 340 and 380 nm, and emission was at 510 nm. The Fura2-AM fluorescence relationship to intracellular Ca^{2+} concentration ($[Ca^{2+}]_i$) was calibrated from the ratio of 340/380 nm fluorescence values after subtraction of the background fluorescence of the cells at 340 and 380 nm as previously described [102]. Changes in $[Ca^{2+}]_i$ (□F $[Ca^{2+}]$) were measured by subtracting the highest peak of Ca^{2+} in the first 20 s after addition of calcium or 100 s after the addition of drugs minus the baseline.

3.4 RESULTS

3.4.1. TgGT1_255660 localizes to the Golgi and ER of T. gondii

We characterize the gene *TgGT1_255660*, annotated as an EF-Hand Domain Containing Protein in ToxoDB. The structure of the putative protein encoded by the gene TgGT1_255660 is predicted to possess a signal peptide and three canonical and one degenerate EF-Hand Motif (Fig. 3.1A).

To identify the localization of this protein we inserted a high affinity tag at the C-terminus region of the protein (Fig. 3.1A). C-terminal tagging was done in the RHTatiΔku80 (*TatiΔku80*) and clonal population of cells expressing the tagged gene were isolated. Validation of the tag was done by western blots, where a band of ~56 kDa was observed only in the tagged cell line (Fig. 3.1B).

Localization of TgGT1_255660 in both extracellular and intracellular tachyzoites was identified by immunofluorescence assay where it appeared to localize both to the Golgi and ER. Using known ER marker like the sarco-endoplasmic reticulum Ca^{2+}-ATPase (SERCA) and a Golgi marker like GRASP55, showed co-localization in both compartments (Fig. 3.1C).

3.4.2 Comparison of the structure of TgCalnuc and HsCalnuc

In mammalian cells there are only three calcium-binding proteins that localize to the Golgi: Calnuc, Cab45 and p54/NEFA. Calnuc contains a signal peptide, an EF-hand domain and a leucine zipper motif. Analysis of the TgGT1_255660 sequence suggest functional similarity as Calnuc, so we named the gene TgCalnuc. Using BLAST to compare the amino acid sequence of Calnuc with TgCalnuc identified only low sequence identity (27%). Identity was mainly concentrated at the signal peptide and EF-Hand domains. The identity of the EF-

Hand domains can be observed by overlaying the crystalized calcium binding domain of *HsCalnuc* to the predicted model of TgCalnuc (Fig. 3.1D-E).

We performed a phylogenetic analysis of TgCalnuc and its orthologs from a variety of organisms using PhyML. Alignment of TgCalnuc demonstrated high conservation between Apicomplexan homologs. They were divergent from the mammalian sequences, as most of the identity was concentrated at the EF Hand Motifs (Fig. 3.1F). Conservation between Apicomplexan homologs could point to a specific role in these parasites.

2.4.3. Disruption of TgCalnuc affects growth of T. gondii

To characterize the role of TgCalnuc in the lytic cycle of *T. gondii* we generated TgCalnuc mutants using the CRISPR-Cas9 system. We disrupted the transcription of TgCalnuc by inserting a Dihydrofolate reductase-thymidylate synthase (DHFR) cassette (Fig. 3.2A). Using primers upstream and downstream of the insertion site, we validated the incorporation of the drug cassette. An amplification of ~3 kb is seen in the *TgCalnuc* mutant in comparison to the parental cell line which showed the intact genomic locus (Fig. 3.2B).

Validation of TgCalnuc expression was performed by RT-PCR of the mutant cell line. Quantitative PCR of the *TgCalnuc* mutant showed the absence of transcripts compared to the parental and complemented cell line (Fig. 3.2C). *TgCalnuc* in the complemented cell line is highly over expressed (Fig. 3.2C). Immunofluorescence assay shows that complementation of TgCalnuc restores localization to the Golgi and ER (Fig. 3.2D). Western blot analysis of ΔTgCalnuc-*calnuc* lysates using anti-HA shows complementation of TgCalnuc (Fig. 3.2E).

We next investigated the role of TgCalnuc in growth of the parasite through plaque assays. Disruption of TgCalnuc lead to a defect in parasite growth, as plaques are significantly smaller in comparison to the parental cell line (Fig. 3.3A). Defect was partially restored in the complemented cell line (Fig. 3.3A, *bar graph*). Partial complementation can be due to the overexpression of Calnuc as seen in the RT-PCR. Overexpression of CaBP can be detrimental to the cell as it may reduce the concentration of luminal Ca^{2+}.

To determine which step of the lytic cycle was affected in the TgCalnuc mutant we performed invasion and egress assays. Invasion in the presence of high Ca^{2+} concentrations showed that there is a significant reduction in the ability of the parasite to invade (Fig. 3.3B). Egress of *T. gondii* can be stimulated by permeabilizing the cells in the presence of high [Ca^{2+}]. Contrary to invasion, stimulation of egress in TgCalnuc mutants showed no defect (Fig. 3.3C-D). This data suggests that deletion of TgCalnuc affects invasion of *T. gondii* into a new host cell.

3.4.4. CaM2 has multiple locations and deletion impacts the growth of T. gondii

CaM2 is a CaBP, that localizes to the conoid, has been previously described to activate MyoH [78]. CBPs are known to activate a variety of target proteins downstream to Ca^{2+}. Using high affinity tags, we were able to identify that in addition to the conoid localization CaM2 also localizes to the ER as seen by co-localization with αSERCA (Fig. 3.4B). Previous work determined the role of CaM2 by creating double mutants of CaM1 and CaM2. Since CaM2 localized to multiple

places in the parasite we generated single gene knock outs of CaM2 by disrupting the transcription of the gene in RH tachyzoite. Using the previously described approach, we disrupted the transcription of CaM2 by inserting a DHFR cassette. We then complemented the gene by cloning the cDNA into a $pCTH_3$ plasmid and transfecting in the mutant cell line. To validate the deletion of the protein we generated polyclonal antibodies against recombinant CaM2. Western blot of total lysates of the parental, ΔCaM2 confirmed deletion and successful complementation. CaM2 was restored in the complemented cell lines as shown by western blot.

CaM2 mutant showed a significant growth defect as measured by plaque assays (Fig. 3.4D). Plaque assays show the ability of the parasite to complete its lytic cycle as it measures invasion, egress and replication of the tachyzoite. We also performed invasion and egress assays to determine which step was affected. Invasion of CaM2 mutant were significantly decreased in a high calcium environment (Fig. 3.4E). Additionally, stimulation of egress by saponin lead to a delayed egress of ΔCaM2 (Fig. 3.4F-G). In conclusion, CaM2 is essential for invasion and egress of *T. gondii*.

3.4.5. Regulation of calcium homeostasis by TgCalnuc and CaM2

CaBPs activate key molecules of the Ca^{2+} signaling pathway like phosphatases, kinases and channels. In order to understand the role of TgCalnuc in the Ca^{2+} signaling pathway, we analyze changes of cytosolic Ca^{2+} in Fura2 loaded tachyzoites (Fig. 3.5A). Resting cytosolic Ca^{2+} in both *TgCalnuc* and *CaM2* mutant remained within normal levels (~70-100 nM). Addition of 1.8 mM of

extracellular Ca^{2+} increases cytosolic calcium in wild type tachyzoites an indication of Ca^{2+} influx. In both *ΔTgCalnuc* and ΔCaM2, the increase of cytosolic Ca^{2+} due to influx is significantly enhanced (Fig. 3.5B-C). The change of cytosolic Ca^{2+} is approximately 2-3 times compared to the change observed with the parental strain (Fig. 3.5B-C, *insets*).

Since Ca^{2+} influx is already enhanced in both mutant cell lines, we next investigated whether cytosolic Ca^{2+} had an effect on Ca^{2+} influx (Ca^{2+}-activated Ca^{2+} Entry or CACE). We showed in the previous chapter that cytosolic Ca^{2+} can stimulates CACE through a Transient Receptor Potential-Like (TgTRPPL-2) Channel. We added thapsigargin (Thap) to Fura2 loaded tachyzoites and observed an increase in cytosolic Ca^{2+}. Thap inhibits the SERCA-Ca^{2+} ATPase in the ER, which causes leakage of Ca^{2+} into the cytosol. *ΔTgCalnuc* mutant showed approximately 50% less increase of cytosolic Ca^{2+} when stimulated by Thap (Fig. 3.5E). Interestingly, Ca^{2+} influx after the addition of Thap was comparable to the Ca^{2+} influx observed without the previous addition of Thap (Fig. 3.5G). In contrast, the ΔCaM2 tachyzoites did not show any defect in the leakage of Ca^{2+} stimulated by Thap (Fig. 3.5F-G). However, Ca^{2+} influx was not further enhanced and also remained comparable to the Ca^{2+} influx without previous stimulus (Fig. 3.5H). In conclusion, the mechanisms of CACE which is mediated by a TRPL Channel (TgTRPP2-L), appears to be constitutively activated in both of these mutant cell lines.

We then tested whether any other Ca^{2+} store was affected in these mutants. We proceeded to investigate the release of Ca^{2+} from acidic stores through glycyl-

L-phenylalanine 2-naphthylamide (GPN) a reagent utilized to release calcium from acidic stores like the lysosome. GPN is a dipeptide that is hydrolyzed by cathepsin C, which localizes to lysosomes, and causes swelling and consequent leakage of Ca^{2+} from the organelle. However, recent studies demonstrated that the mechanism of action of GPN is Cathepsin C-independent. GPN increases cytosolic pH stimulating an unknown channel in the ER which upon activation releases Ca^{2+} from the ER.

To determine the specific store from where Ca^{2+} is released by GPN we released Ca^{2+} from different compartments. In resting [Ca^{2+}] conditions, addition of GPN increases cytosolic calcium about 100 nM in the parental tachyzoites (Fig. 3.6B, *black trace*). Addition of GPN after the addition of 1.8 mM extracellular Ca^{2+} causes a cytosolic increase approximately 7-8 times higher compared to the increase observed under resting [Ca^{2+}] (Fig. 3.6B, *red trace*). Increased release suggests the presence of mechanisms in the membrane of the organelle that bring Ca^{2+} into the store. Addition of Thap prior to GPN also caused a larger release of Ca^{2+} into the cytosol. (Fig. 3.6C, *turquoise trace*). Stimulation by ammonium chloride, which neutralizes all the acidic compartments does not alter the amount of Ca^{2+} released by GPN (Fig. 3.6B, purple trace). Quantification of the increase by GPN are shown in Fig. 3.6C.

Based on the previous results, extracellular Ca^{2+} and Thap increase the amount of total Ca^{2+} of the intracellular store where GPN acts. Collection of tachyzoites and measurements of cytosolic Ca^{2+} were done under basal Ca^{2+} conditions (<100 nM), which resembles the conditions of the intracellular

environment where the parasites are surrounded by low [Ca^{2+}]. To determine the store at which GPN acts, we added 1.8 mM of extracellular Ca^{2+} to the Fura-2 loaded tachyzoites to keeps the intracellular stores filled. Release of Ca^{2+} by GPN after Ca^{2+} and Thap was significantly lower than the release of Ca^{2+} alone (Fig. 3.6E, *light purple bar vs. dark purple bar*). Using the Ca^{2+} release in a replete store, versus depleted or after stimulus with Thap we quantified where GPN is acting. Percentage of Ca^{2+} release by GPN in the different store is ~31% in the Golgi, ~28% from the ER (~28%) and ~40% from the PLV (Fig. 3.6F).

We looked at the effect of GPN in the Δ*TgCalnuc* and Δ*CaM2* mutants. Under resting Ca^{2+} conditions in ΔTgCalnuc, GPN caused a small and constant cytosolic Ca^{2+} increase (Fig. 3.7A). Addition of 1.8 mM Ca^{2+} intensified the rate of cytosolic Ca2+ increase, but the effect was significantly lower compared to the parental line (Fig. 3.7A). In ΔCaM2 tachyzoites, GPN released less Ca^{2+} than the parental strain but at a similar rate (Fig. 3.7B). However, release after the addition of Ca^{2+} is significantly reduced. Quantifications of Ca^{2+} released by GPN under basal vs. after Ca^{2+} are shown in Fig. 3.7C-D. In a similar manner, release of Ca^{2+} by GPN in ΔTgCalnuc and ΔCaM2 tachyzoites after stimulus by thap was significantly reduced (Fig. 3.7E-F). Ca^{2+} release stimulated by GPN after thap only releases about 30% of Ca^{2+} in both mutant cell lines (Fig. 7G). In summary, TgCalnuc and CaM2 play a role in the release of Ca^{2+} stimulated by GPN from the Golgi and ER.

3.4.6 TgCalnuc and CaM2 are recruited to the ER after stimulus of Ca^{2+} release

TgCalnuc and CaM2 localize to multiple organelles within the parasite and they share ER localization. We wondered if altering ER Ca^{2+} recruited these proteins to the organelle or modified their localization. TgCalnuc-smHA and CaM2-smHA were stimulated by either Thap or GPN and fixed at different time points and analyzed by IFAs for co-localization with anti-SERCA as ER marker. Co-localization of TgCalnuc and CaM2 with anti-SERCA was significantly increased after 5 min of pre-incubation with Thap as quantified by Pearson's coefficient (Fig. 3.8A-C). Similarly, stimulation with GPN in both tagged cell lines increased recruitment to the ER (Fig. 3.8D-F). In conclusion, decrease of ER and Golgi Ca^{2+} by GPN or Thap recruits TgCalnuc and CaM2 to the ER.

3.5. DISCUSSION

In *T. gondii* calcium signaling has been shown to activate key biological processes like invasion, egress and motility [70]. Initiation of the calcium signaling cascade commences by the release of calcium from intracellular stores, mainly the ER. The molecular components that are part of the intracellular signaling cascade is still under characterized. Important molecules like the IP_3 Receptor have not been identified in the parasite. However, *T. gondii* contains a variety of calcium-binding proteins. In this study we characterized the role of a novel calcium binding protein in the calcium storage within the ER and Golgi. We described the role of a previously characterize protein, CaM2, in the release of Ca^{2+} from the ER.

Calcium-binding proteins are key molecules within the calcium signaling pathway as they are the first molecules that are activated downstream to Ca^{2+}. The

CBPs present in *T. gondii* are Calmodulin-Like (CML) proteins due to their low homology to calmodulin. There are five calcium binding proteins that have been characterized as playing roles in the activation of myosins, which are necessary for the motility of tachyzoites [75, 77]. These CML have been localized to the conoid and to the periphery of the parasite [78]. In mammalian cells, both the ER and the Golgi contain important CBPs that regulate storage capacity and release from these stores. In *T. gondii* very little is known about the molecules that regulate or modulate Ca^{2+} homeostasis within the ER and especially the Golgi.

Organelles, like the ER and Golgi, are essential calcium storage that upon stimulus release calcium into the cytosol activating this important signaling pathway. In the ER and Golgi there are proteins that are specialized in binding calcium ions that can activate other molecules or maintain calcium homeostasis. In the ER there are proteins like Calsequestrin, which is found in high concentrations and regulate the activation of Ryanodine Receptors [157]. Calreticulin, is another CaBP in the ER which regulates the activity of the SERCA and $InsP_3R$ [158]. Cab45, is a CaBP localized to the Golgi that regulates protein trafficking and sorting [159]. CaBPs play an essential role in regulating Ca^{2+} signaling within the intracellular stores.

In the Golgi, sensing of luminal Ca^{2+} in the Golgi is regulated by Calnuc. It contains a signal peptide in the N-terminus, two EF-hand domains and a leucine zipper domain in the C-Terminus. In contrast, TgCalnuc is a significantly smaller protein than its mammalian homolog and localizes to the ER in addition to the Golgi. Deletion of TgCalnuc affected the ability of the parasite to invade host cells

which lead to a growth defect. A defect in the ability to invade can be due to the fact that calcium in the stores is significantly reduced. Release from the intracellular stores stimulates higher Ca^{2+} influx which replenishes the depleted stores. Reduced luminal [Ca^{2+}] within the store in *TgCalnuc* mutants maintains Ca^{2+} influx constantly stimulated.

It is known that the ER and Golgi share a number of proteins that can be transported between the two compartments. The shared localization between the compartments is known as the ER-Golgi Intermediate Compartment (ERGIC). The ERGIC has been identified to contain important molecules known to work on transporting cargo proteins. Based on the localization of TgCalnuc it is possible that this molecule can be transported between these two compartments to regulate the capacity of the storage of calcium in these two organelles. We propose that the mechanism of action of TgCalnuc is to sense the [Ca^{2+}] in both the ER and Golgi. The inability of the mutants to sense incorrectly the [Ca^{2+}], can lead to a decreased release of calcium from these organelles.

Glycyl-L-phenylalanine 2-naphthylamide (GPN) is a membrane permeable peptide that is cleaved by cathepsin C [153]. The breakdown of GPN causes release of Ca^{2+} from lysosomes into the cytosol in mammalian cells. Recent work proposed that the mechanism of action of GPN is cathepsin-C independent [154]. The release of calcium evoked by GPN, is a result from the stimulus of a channel in the ER that is affected by the change in cytosolic pH. More importantly, addition of Thap before GPN, abolishes the response from GPN, providing further evidence that the calcium release is from the ER [154].

Here we demonstrated that GPN does in fact release calcium from the ER as well as the Golgi and Plant-Like Vacuole (PLV). Depletion of TgCalnuc, leads to a deficiency in sensing luminal Ca^{2+} within the Golgi and the ER. Release of calcium from the intracellular organelles will be dependent on the state of the storage in that compartment. A store that is slightly depleted will release less calcium than a store that is filled. In the case of the *ΔTgCalnuc* mutant, the storage capacity of the Golgi and the ER are at a semi-depleted state, as evidence by the efflux stimulated by Thap and GPN.

CaM2 was previously described to interact with MyoH, which control invasion and motility in *T. gondii* [78]. Although CaBP may sometimes overlap in their potential interactors, these proteins are known to activate a variety of targets within the Ca^{2+} signaling pathway. Localization of CaM2 in the conoid as well as the ER, indicates that MyoH may not be the only target in the parasite. Deletion of CaM2, leads to an invasion and egress defect which resulted in a growth defect.

ΔCaM2 and ΔTgCalnuc mutants share some phenotypic characteristics, however there are some significant differences between the two. CaM2 does not show any defect in the storage capacity of intracellular stores. Defect of Ca^{2+} release stimulated by GPN in CaM2 mutants is only observed when the stores is first depleted. This phenotype provides evidence that the mechanism of release from the ER, stimulated by GPN, is affected and comes from the ER.

In mammalian cells, calcium release from the ER can be stimulated by IP_3 through the opening of an IP_3Receptor or by Ca^{2+} by activation of ryanodine receptors. It has been shown that regulation of these channels through a number

of CaBPs localized to the cytosolic side of the ER [155, 156]. Previous work has demonstrated that *T. gondii* is able to release Ca^{2+} when stimulated by IP_3 [122]. The channels responsible for this release have yet to be identified. Decrease of ER Ca^{2+} appeared to stimulate recruitment of CaM2. We then propose that CaM2, in addition to its interaction with MyoH, is able to regulate Ca^{2+} release from the ER.

The Ca^{2+} signaling pathway regulates essential biological processes in *T. gondii*. The identification of the proteins that comprises this signaling pathway is severely under characterized. The regulation of this pathway relies on key molecules like calcium binding proteins. Understanding the role of these proteins in the parasite will unveil key processes that are still not understood. Since the ER is one of the master regulators of the signaling pathway in *T. gondii*, characterizing the molecules that regulate calcium within the organelle is essential.

In this study we provide evidence of how the ER and the Golgi are able to maintain storage capacity by a calcium-binding protein like TgCalnuc. TgCalnuc becomes the first Ca^{2+} regulated protein described to be present in the Golgi. Additionally, we described the potential regulation of Ca^{2+} release in the ER through a CaBP. The data presented confirms that CaBP regulate a variety of targets within the Ca^{2+} signaling pathway of *T. gondii*. Further studies of the possible interactors of these proteins may unveil essential molecules that for a long time have remained undiscovered in *T. gondii*.

3.6 REFERENCES

1. Dubey, J.P., *Toxoplasmosis - a waterborne zoonosis.* Vet Parasitol, 2004. **126**(1-2): p. 57-72.
19. Lapinskas, P.J. and R.R. Ben-Harari, *Perspective on current and emerging drugs in the treatment of acute and chronic toxoplasmosis.* Postgrad Med, 2019. **131**(8): p. 589-596.
20. Konstantinovic, N., et al., *Treatment of toxoplasmosis: Current options and future perspectives.* Food Waterborne Parasitol, 2019. **15**: p. e00036.
37. Black, M.W. and J.C. Boothroyd, *Lytic cycle of Toxoplasma gondii.* Microbiol Mol Biol Rev, 2000. **64**(3): p. 607-23.
59. Berchtold, M.W. and A. Villalobo, *The many faces of calmodulin in cell proliferation, programmed cell death, autophagy, and cancer.* Biochim Biophys Acta, 2014. **1843**(2): p. 398-435.
64. Carruthers, V.B., S.N. Moreno, and L.D. Sibley, *Ethanol and acetaldehyde elevate intracellular [Ca2+] and stimulate microneme discharge in Toxoplasma gondii.* Biochem J, 1999. **342 (Pt 2)**: p. 379-86.
65. Borges-Pereira, L., et al., *Calcium Signaling throughout the Toxoplasma gondii Lytic Cycle: A STUDY USING GENETICALLY ENCODED CALCIUM INDICATORS.* J Biol Chem, 2015. **290**(45): p. 26914-26.
66. Mondragon, R. and E. Frixione, *Ca(2+)-dependence of conoid extrusion in Toxoplasma gondii tachyzoites.* The Journal of eukaryotic microbiology, 1996. **43**(2): p. 120-7.
67. LaFavers, K.A., et al., *A novel dense granule protein, GRA41, regulates timing of egress and calcium sensitivity in Toxoplasma gondii.* Cell Microbiol, 2017. **19**(9).
70. Hortua Triana, M.A., et al., *Calcium signaling and the lytic cycle of the Apicomplexan parasite Toxoplasma gondii.* Biochim Biophys Acta Mol Cell Res, 2018. **1865**(11 Pt B): p. 1846-1856.
75. Williams, M.J., et al., *Two Essential Light Chains Regulate the MyoA Lever Arm To Promote Toxoplasma Gliding Motility.* mBio. **6**(5).
77. Nebl, T., et al., *Quantitative in vivo analyses reveal calcium-dependent phosphorylation sites and identifies a novel component of the Toxoplasma invasion motor complex.* PLoS Pathog, 2011. **7**(9): p. e1002222.
78. Long, S., et al., *Calmodulin-like proteins localized to the conoid regulate motility and cell invasion by Toxoplasma gondii.* PLoS Pathog, 2017. **13**(5): p. e1006379.
91. Farwell, D.G., et al., *Genetic and epigenetic changes in human epithelial cells immortalized by telomerase.* Am J Pathol, 2000. **156**(5): p. 1537-47.
92. Sheiner, L., et al., *A systematic screen to discover and analyze apicoplast proteins identifies a conserved and essential protein import factor.* PLoS Pathog, 2011. **7**(12): p. e1002392.
93. Meissner, M., et al., *Modulation of myosin A expression by a newly established tetracycline repressor-based inducible system in Toxoplasma gondii.* Nucleic Acids Res, 2001. **29**(22): p. E115.
94. Fox, B.A., et al., *Efficient gene replacements in Toxoplasma gondii strains deficient for nonhomologous end joining.* Eukaryot Cell, 2009. **8**(4): p. 520-9.
95. Shen, B., et al., *Development of CRISPR/Cas9 for Efficient Genome Editing in Toxoplasma gondii.* Methods Mol Biol, 2017. **1498**: p. 79-103.

96. Laemmli, U.K., *Cleavage of structural proteins during the assembly of the head of bacteriophage T4.* Nature, 1970. **227**(5259): p. 680-5.
97. Liu, J., et al., *A vacuolar-H(+) -pyrophosphatase (TgVP1) is required for microneme secretion, host cell invasion, and extracellular survival of Toxoplasma gondii.* Mol Microbiol, 2014. **93**(4): p. 698-712.
98. Schindelin, J., et al., *Fiji: an open-source platform for biological-image analysis.* Nat Methods, 2012. **9**(7): p. 676-82.
99. Kafsack, B.F., C. Beckers, and V.B. Carruthers, *Synchronous invasion of host cells by Toxoplasma gondii.* Mol Biochem Parasitol, 2004. **136**(2): p. 309-11.
100. Moreno, S.N. and L. Zhong, *Acidocalcisomes in Toxoplasma gondii tachyzoites.* Biochem J, 1996. **313 (Pt 2)**: p. 655-9.
102. Grynkiewicz, G., M. Poenie, and R.Y. Tsien, *A new generation of Ca2+ indicators with greatly improved fluorescence properties.* J Biol Chem, 1985. **260**(6): p. 3440-50.
109. Omasits, U., et al., *Protter: interactive protein feature visualization and integration with experimental proteomic data.* Bioinformatics, 2014. **30**(6): p. 884-6.
122. Lovett, J.L., et al., *Toxoplasma gondii microneme secretion involves intracellular Ca(2+) release from inositol 1,4,5-triphosphate (IP(3))/ryanodine-sensitive stores.* J Biol Chem, 2002. **277**(29): p. 25870-6.
143. Carafoli, E., *Calcium signaling: a tale for all seasons.* Proc Natl Acad Sci U S A, 2002. **99**(3): p. 1115-22.
144. Batistic, O. and J. Kudla, *Analysis of calcium signaling pathways in plants.* Biochim Biophys Acta, 2012. **1820**(8): p. 1283-93.
145. Clapham, D.E., *Calcium signaling.* Cell, 1995. **80**(2): p. 259-68.
146. Brini, M., et al., *Intracellular calcium homeostasis and signaling.* Met Ions Life Sci, 2013. **12**: p. 119-68.
147. Yang, Z., et al., *The Golgi apparatus is a functionally distinct Ca2+ store regulated by the PKA and Epac branches of the beta1-adrenergic signaling pathway.* Sci Signal, 2015. **8**(398): p. ra101.
148. Pizzo, P., et al., *Ca(2+) signalling in the Golgi apparatus.* Cell Calcium, 2011. **50**(2): p. 184-92.
149. Dodd, A.N., J. Kudla, and D. Sanders, *The language of calcium signaling.* Annu Rev Plant Biol, 2010. **61**: p. 593-620.
150. Aradhyam, G.K., et al., *Calnuc: Emerging roles in calcium signaling and human diseases.* IUBMB Life, 2010. **62**(6): p. 436-46.
151. Zeng, H., et al., *Involvement of calmodulin and calmodulin-like proteins in plant responses to abiotic stresses.* Front Plant Sci, 2015. **6**: p. 600.
152. Livak, K.J., et al., *Oligonucleotides with fluorescent dyes at opposite ends provide a quenched probe system useful for detecting PCR product and nucleic acid hybridization.* PCR Methods Appl, 1995. **4**(6): p. 357-62.
153. Haller, T., et al., *The lysosomal compartment as intracellular calcium store in MDCK cells: a possible involvement in InsP3-mediated Ca2+ release.* Cell Calcium, 1996. **19**(2): p. 157-65.

154. Atakpa, P., et al., *GPN does not release lysosomal Ca(2+) but evokes Ca(2+) release from the ER by increasing the cytosolic pH independently of cathepsin C.* J Cell Sci, 2019. **132**(3).
155. Heiny, J.A., *S100A1: a physiological modulator of RYR1, Ca2+ release, and contractility in skeletal muscle. Focus on "S100A1 promotes action potential-initiated calcium release flux and force production in skeletal muscle".* Am J Physiol Cell Physiol, 2010. **299**(5): p. C882-4.
156. Prosser, B.L., E.O. Hernandez-Ochoa, and M.F. Schneider, *S100A1 and calmodulin regulation of ryanodine receptor in striated muscle.* Cell Calcium, 2011. **50**(4): p. 323-31.
157. Beard, N.A., D.R. Laver, and A.F. Dulhunty, *Calsequestrin and the calcium release channel of skeletal and cardiac muscle.* Prog Biophys Mol Biol, 2004. **85**(1): p. 33-69.
158. Bononi, A., et al., *Mitochondria-associated membranes (MAMs) as hotspot Ca(2+) signaling units.* Adv Exp Med Biol, 2012. **740**: p. 411-37.
159. Blank, B. and J. von Blume, *Cab45-Unraveling key features of a novel secretory cargo sorter at the trans-Golgi network.* Eur J Cell Biol, 2017. **96**(5): p. 383-390.

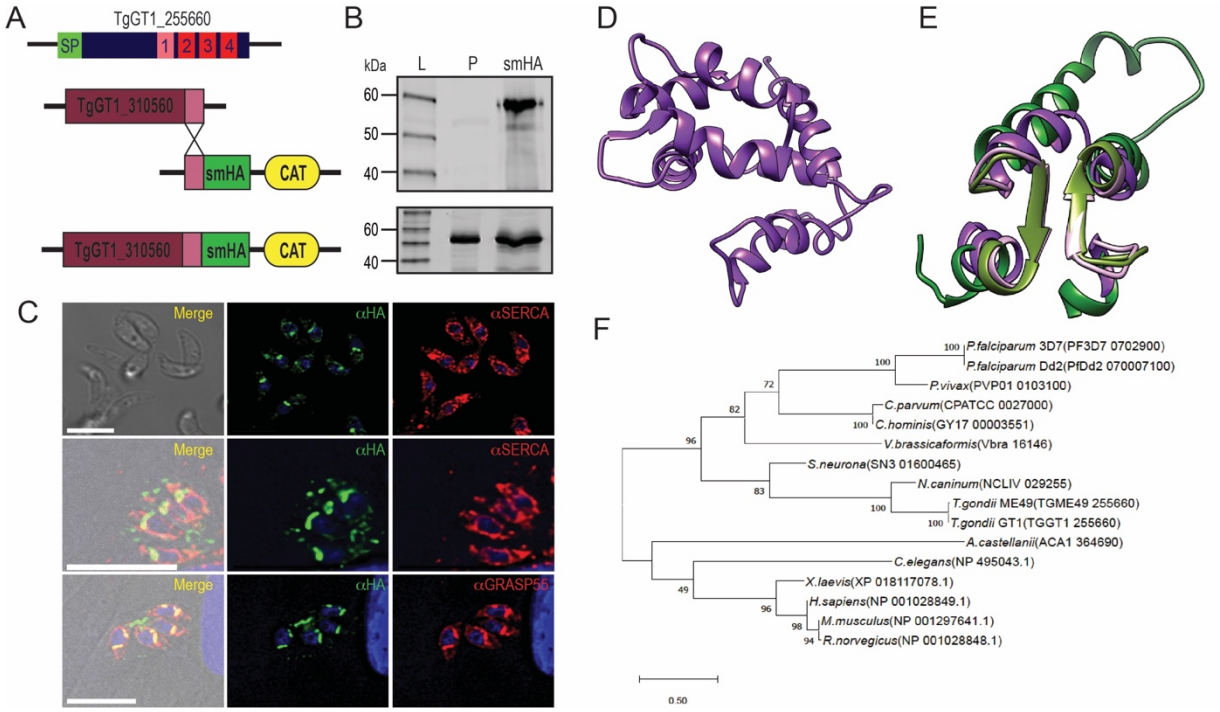

Figure 3.1. TgGT1_255660 localizes to the golgi and Endoplasmic reticulum of *T. gondii*. A. Schematic representation of TgGT1_255660 with the identified Signal Peptide (*SP, green*) and EF-hand domains (*Degenerate-pink, Canonical-red*). Schematic representation of C-Terminal tagging using smHA-pLic in Tati□Ku80 cell line. **B.** Western blot of total lysates from TgGT1_255660-smHA and parental cell line. *Top panel*, a band around ~56 kDa is seen only in the tagged cell line. *Bottom panel*, anti-tubulin is used as loading control for both samples. **C.** Immunofluorescence assay of both extracellular and intracellular tachyzoites of TgGT1_255660-smHA. *Top panel*, staining with αHA (1:100) shows labeling in the Golgi with partial co-localization with αSERCA (1:1,000). *Middle panel*, intracellular localization shows labeling in the Golgi with some co-localization with αSERCA (1:1,000). *Bottom panel*, transiently transfected TgGT1_255660-smHA tachyzoites

with GRASP55-RFP shows both Golgi and ER localization. **D.** Modeling of the predicted sequence of TgCalnuc generated using I-Tasser. **E.** Overlay of TgCalnuc predicted model with the crystal structure of the calcium binding domain HsCalnuc. **F.** Phylogenetic tree alignment of Calnuc in different organisms. Tree was generate using PhyML.

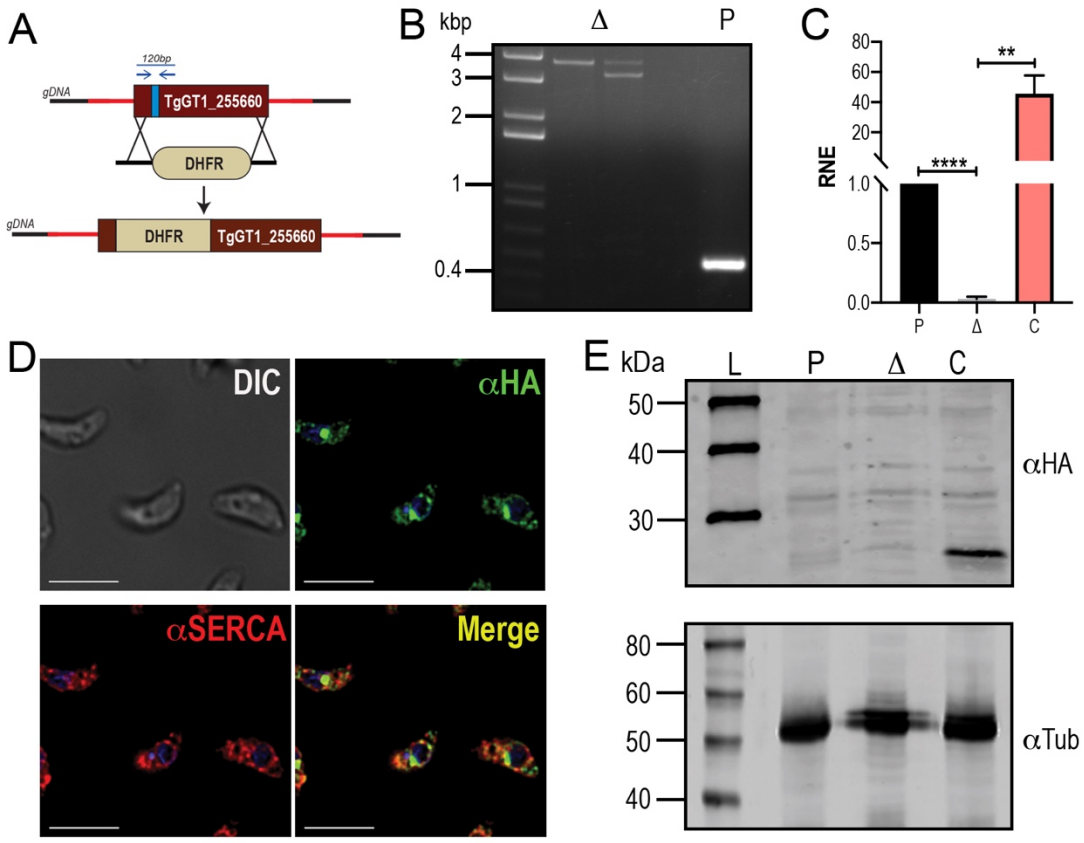

Figure 3.2. Disruption of TgCalnuc in *T. gondii* tachyzoites. A. Schematics showing the genomic disruption of Tgcalnuc using CRISPR-Cas9 in RH tachyzoites. **B.** Genomic validation showing insertion of the drug cassette in locus of TgCalnuc. Primers used are indicated with arrows in A and they are complementary to sequences upstream and downstream the drug cassette. **C.** qPCR from total RNA isolated from ΔTgCalnuc, ΔTgCalnuc-*Calnuc* and parental cell lines. Primers are upstream and downstream of the insertion site. **D.** IFAs of extracellular tachyzoites of ΔTgCalnuc-*Calnuc* using αHA (1:100) co-localizes with αSERCA (1:1,000). **E.** Western blot analysis of total lysate of the ΔTgCalnuc, ΔTgCalnuc-*Calnuc* and parental cell lines using aHA (1:1,000). *Bottom panel*, α-tubulin (1:15,000) is used as a loading control for all samples.

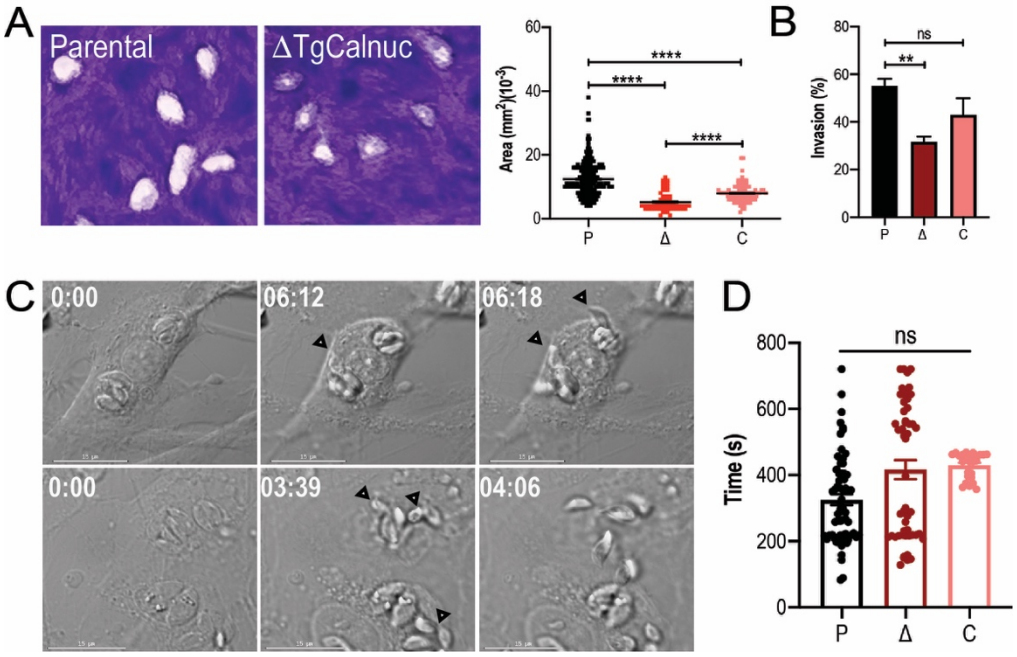

Figure 3.3. TgCalnuc is necessary for the invasion of *T. gondii*. A. Plaque assay of ΔTgCalnuc, ΔTgCalnuc-*Calnuc* and parental cell lines. Quantification of plaque sizes from three independent biological experiments using student's t-test. **** p< 0.0001. **B.** Red-green assay of the different cell lines quantifying percentage of invaded tachzoites. Measurements were done from three independent biological replicate using student's t-test. ** p< 0.0001. **C.** Egress stimulated by saponin comparing parental (*top panels*) and ΔTgCalnuc (*bottom panel*) at 1.8 mM of extracellular Ca^{2+}. **D.** Quantification of egress average time at 1.8mM Ca^{2+} using saponin as a stimulant. Measurements were done from three independent biological replicate using student's t-test.

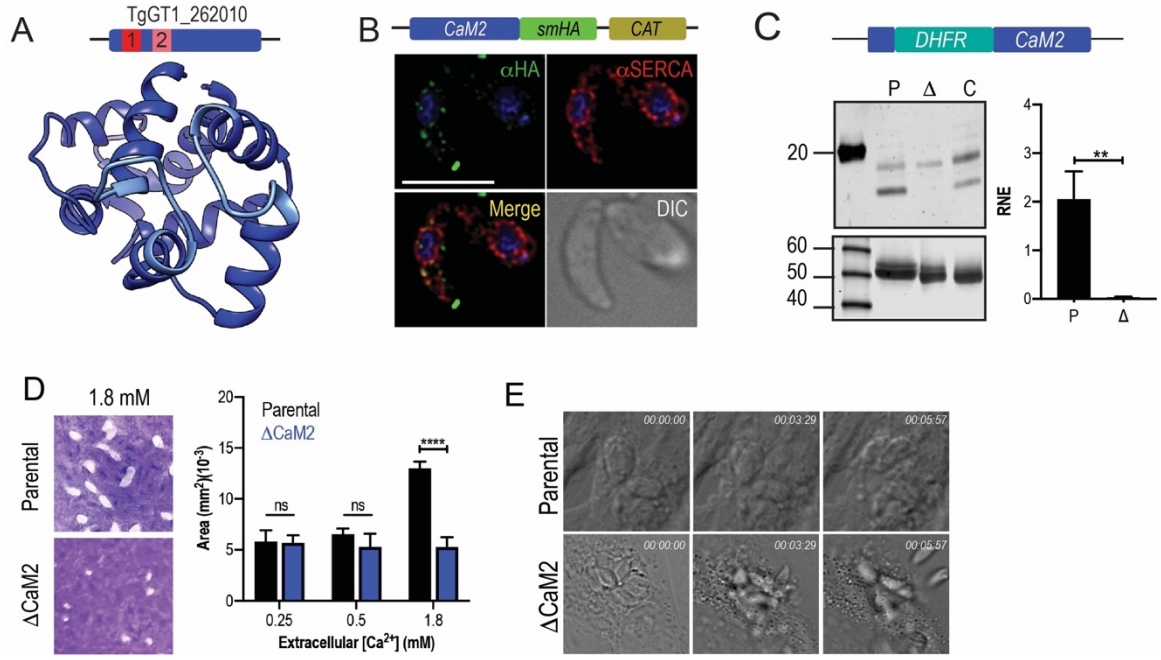

Figure 3.4. CaM2 localizes to the ER and is necessary for invasion and egress of *T. gondii*. A. Schematics of the *CaM2* gene model with the identified EF hand motifs. *Red*, canonical EF Hand, *Pink,* degenerate EF hand. Predicted protein modeling of CaM2 using I-Tasser. **B.** Schematic representation of C-terminal tagging of CaM2. Extracellular IFA using αHA (1:100) co-localized with αSERCA (1:1,000), a known ER marker. **C.** Schematic representation of the generation of ΔCaM2 in *T. gondii* RH strain. *Bottom left*, Western blot using αCAM2 (1:1,000) in ΔCaM2, ΔCaM2-*CaM2* and parental strain lysates. αTubulin (1:10,000) was used as loading control. *Bottom right*, qPCR of total RNA of ΔCaM2 and ΔCaM2-*CaM2* and parental strain using primers upstream and downstream of the insertion site

of the DHFR cassette. **D.** Plaque assay of ΔCaM2, ΔCaM2-*CaM2* and parental strain lysates. Quantification of plaque sizes from three independent biological experiments using student's t-test. ****p<0.0001. **E.** Egress stimulated by saponin at high [Ca^{2+}] lead to slower egress in DCaM2 tachyzoites. **F**. Statistical analysis of average egress time stimulated by saponin at high [Ca^{2+}]. Analysis was performed by student's t-test using three independent biological replicates. **** p< 0.0001.

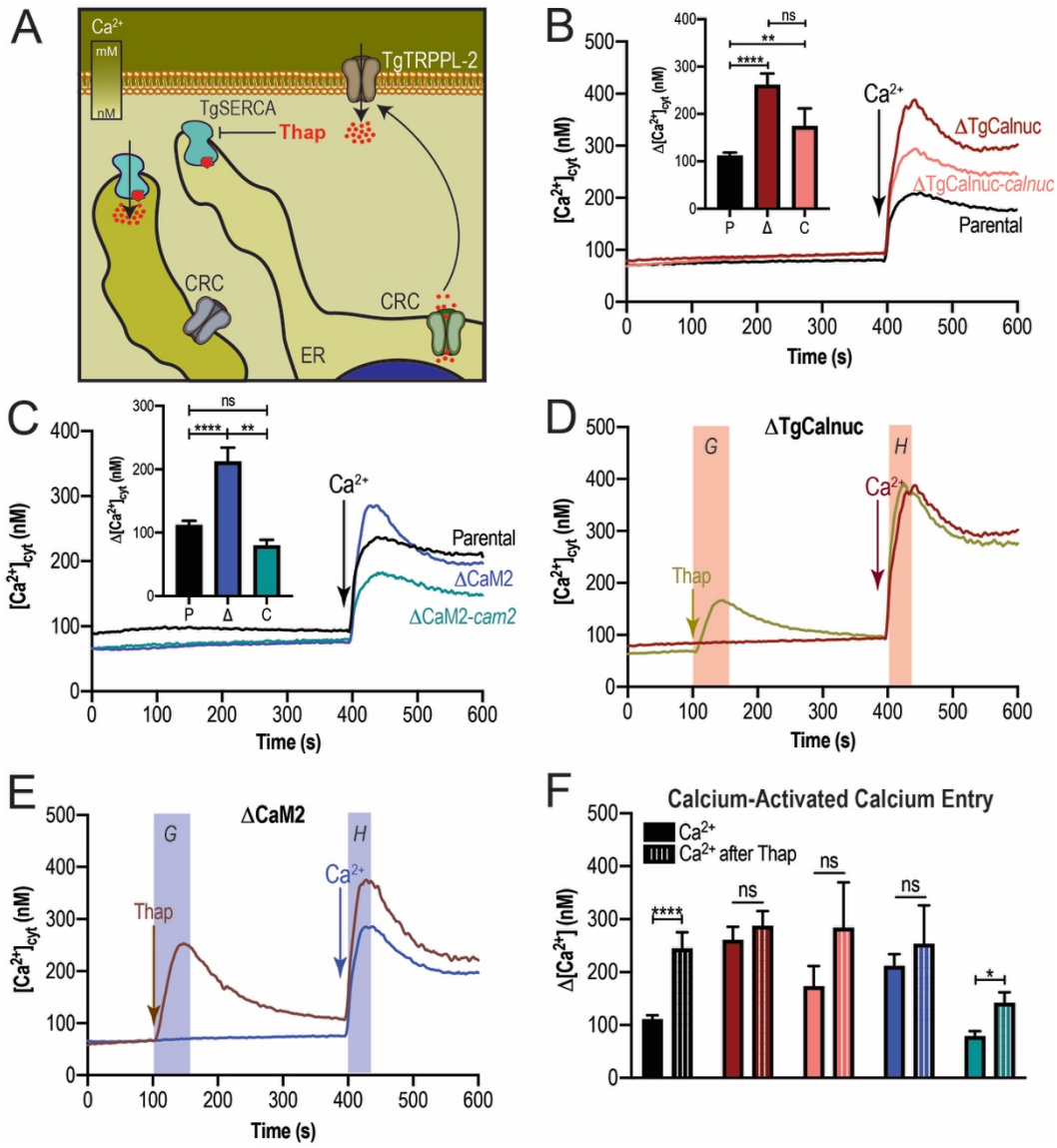

Figure 3.5. Calcium-Activated Calcium Entry (CACE) is constitutively activated in TgCalnuc and CaM2 mutants. A. Cartoon representing CACE in *T. gondii* activated by increase of cytosolic Ca^{2+}. *Thap, thapsigargin; CRC, Calcium Release Channel; LC, leakage channel.* **B.** Cytosolic Ca^{2+} measurements of Fura-2 loaded tachyzoites of ΔTgCalnuc. The solution contained 100 μM EGTA and 1.8 mM of Ca^{2+} was added at 400s. *Inset,* quantification of the change in cytosolic Ca^{2+} the first 20 s after the addition of Ca^{2+}. Statistical analysis was done from three

independent biological replicates using student's t-test. **** p< 0.0001, ** p< 0.001. **C.** Cytosolic Ca^{2+} measurements after the addition of 1.8mM Ca^{2+} in the ΔCaM2 tachyzoites. *Inset*, quantification of the change in cytosolic calcium the first 20 s after the addition of Ca^{2+}. Statistical analysis was done from three independent biological replicates using student's t-test. **** p< 0.0001, ** p< 0.001. **D.** Calcium efflux caused by the addition of 1 μM Thap (*purple*) followed by 1.8 mM extracellular Ca^{2+} in ΔTgCalnuc and ΔCaM2 (**E**) cell lines. Compared to the addition of 1.8 mM extracellular Ca^{2+} alone (*black*). Colored boxes in each graph highlight the quantification of the change in cytosolic calcium. **F.** Quantification of Ca^{2+} increased after the addition of 1.8 mM extracellular Ca^{2+} with or without Thap stimulus highlighted in the colored boxes labeled *F*. Analysis was performed by three independent biological replicates using student's t-test. * p< 0.01, **** p< 0.0001. *Black bar*, parental; *Maroon bar*, ΔTgCalnuc; *Pink bar*, ΔTgCalnuc-*Calnuc*; *Blue*, ΔCaM2; *Turquoise*, ΔCaM2-*CaM2*.

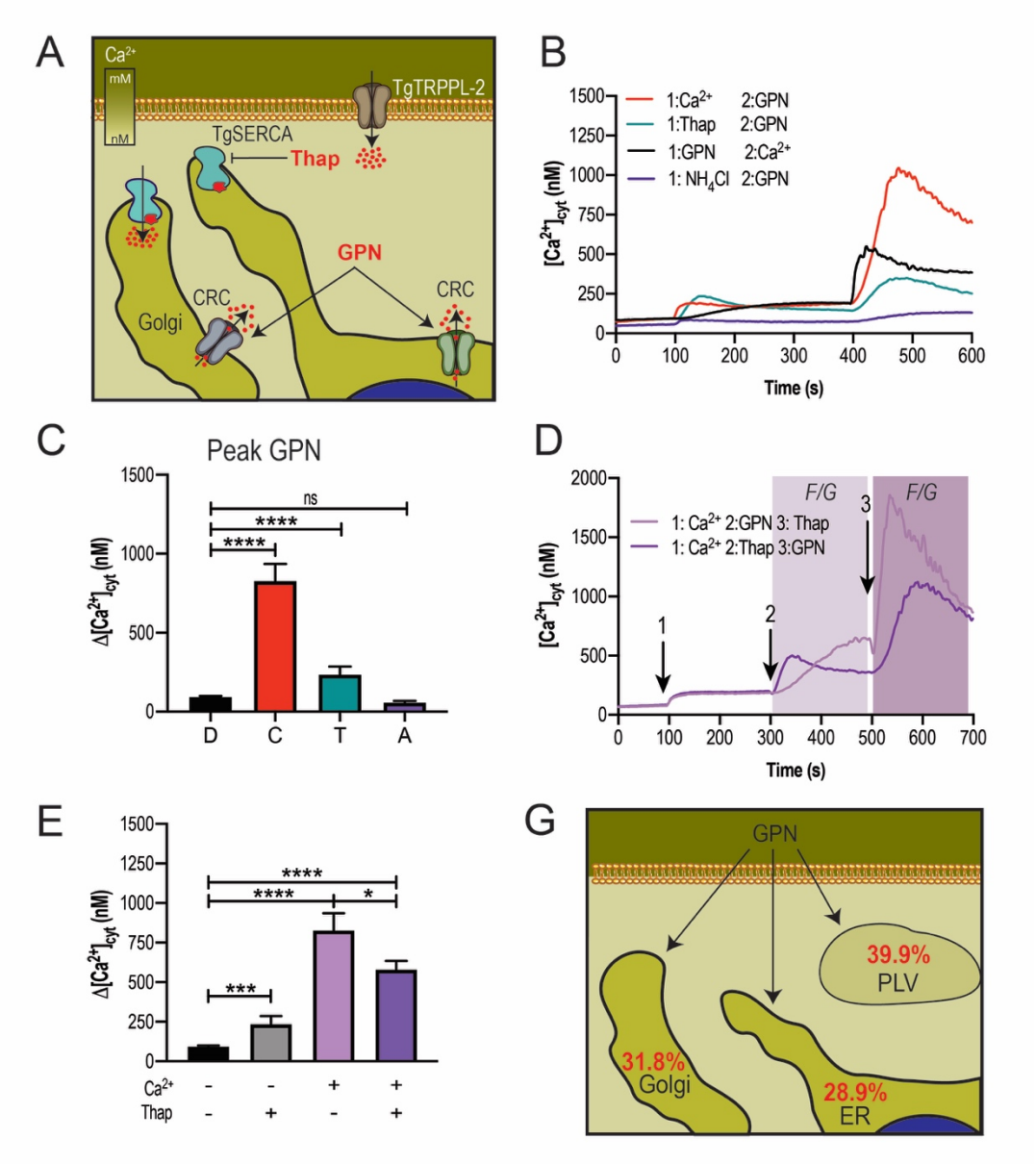

Figure 3.6. GPN releases calcium from the Endoplasmic Reticulum, Golgi and Plant-Like Vacuole. A. Schematic representation of the intracellular signaling stimulation by GPN in *T. gondii*. *Thap, thapsigargin; CRC, Calcium Release Channel; LC, leakage channel.* **B.** Release of calcium stimulated by 20 μM GPN after the addition of 1.8 mM extracellular Ca^{2+} (*red*), 1 μM Thap (*turquoise*) and 20 mM NH_4Cl (*purple*). Colored boxes highlight the quantification in *C*. **C.** Quantification of calcium release by GPN after different conditions. Analysis was

performed by three independent biological replicates using student's t-test. **** p< 0.0001. *D, depleted; C, after Ca^{2+}; T, after thapsigargin; A, after ammonium chloride*. **D.** Release of calcium by 20 mM GPN after 1.8 mM extracellular Ca^{2+} before (*light purple*) or after (*dark purple*) the addition of 1 mM Thap. Colored boxes represent the quantification in *F* and *G*. **E.** Quantification of cytosolic increase highlighted in *B*. Analysis was performed by three independent biological replicates using student's t-test. **** p< 0.0001. **G.** Schematic representation of the release of Ca^{2+} by GPN in the different intracellular stores.

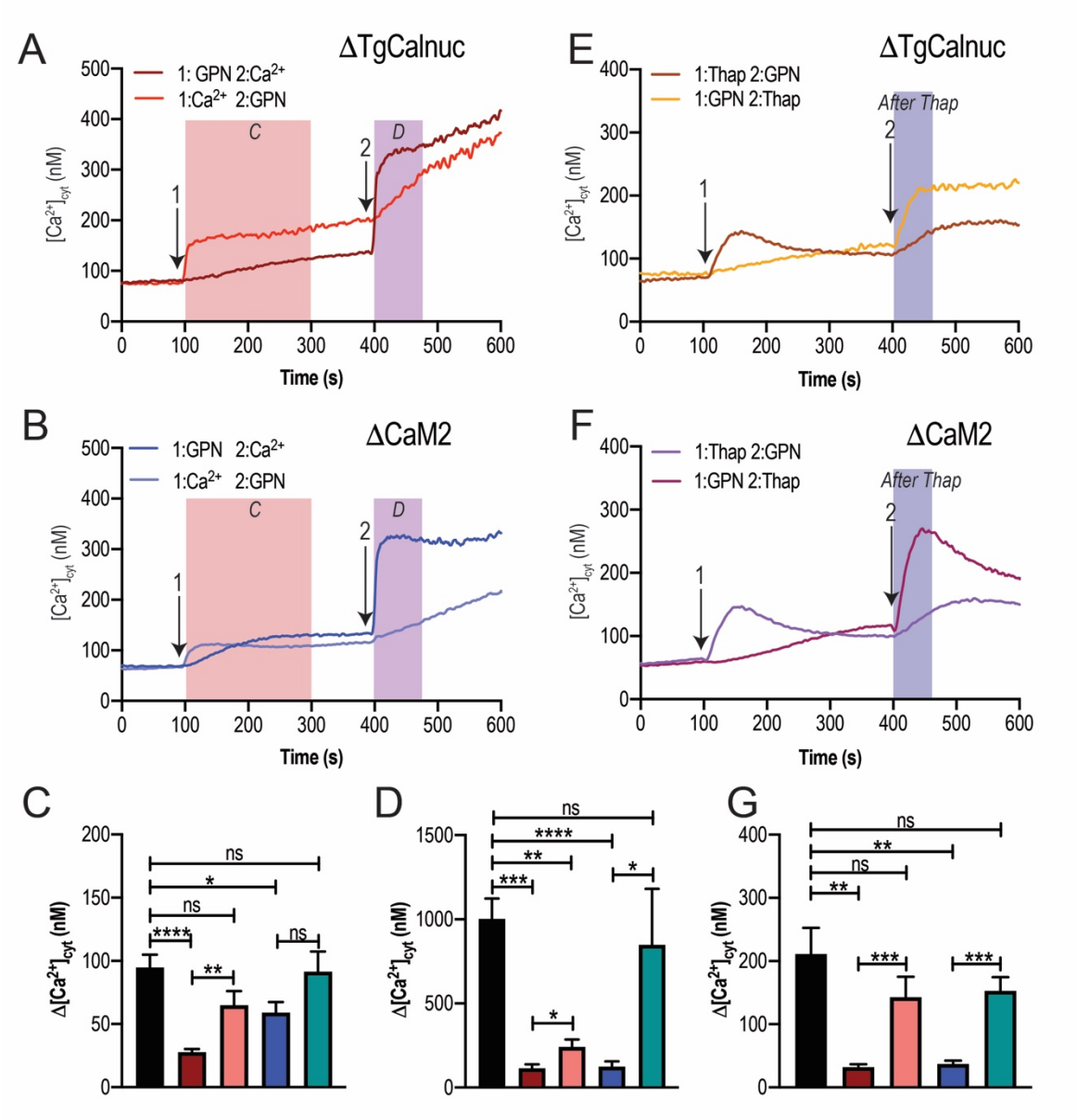

Figure 3.7. TgCalnuc and CaM2 are necessary for calcium homeostasis and release from the ER and Golgi. A. Release of calcium stimulated by 20 μM GPN before (*wine*) or after (*red*) the addition of 1.8 mM extracellular Ca^{2+} in the ΔTgCalnuc and ΔCaM2 ***(C)***. Colored box highlights the quantification of Ca^{2+} release quantified in *C* and *D*. **C.** Quantification of cytosolic increase stimulated by GPN in basal Ca^{2+} conditions. Analysis was performed of three independent biological replicates using student's t-test. * p< 0.04, ** p< 0.002, ****p<0.0001. D.

Quantification of cytosolic increase stimulated by GPN after 1.8 mM of Ca^{2+}. Analysis was performed of three independent biological replicates using student's t-test. * p< 0.02, ** p< 0.004, *** p< 0.0002 **** p<0.0001. **E.** Release of calcium stimulated by 20 μM GPN before (*yellow*) or after (*maroon*) the addition of 1 μM of Thap in ΔTgCalnuc and DCaM2 ***(F)***. Colored box highlights the quantification of calcium release quantified in *G*. **G.** Quantification of the rate of Ca^{2+} release stimulated by GPN after Thap. Analysis was performed of three independent biological replicates using student's t-test. ** p< 0.002, *** p< 0.0003.

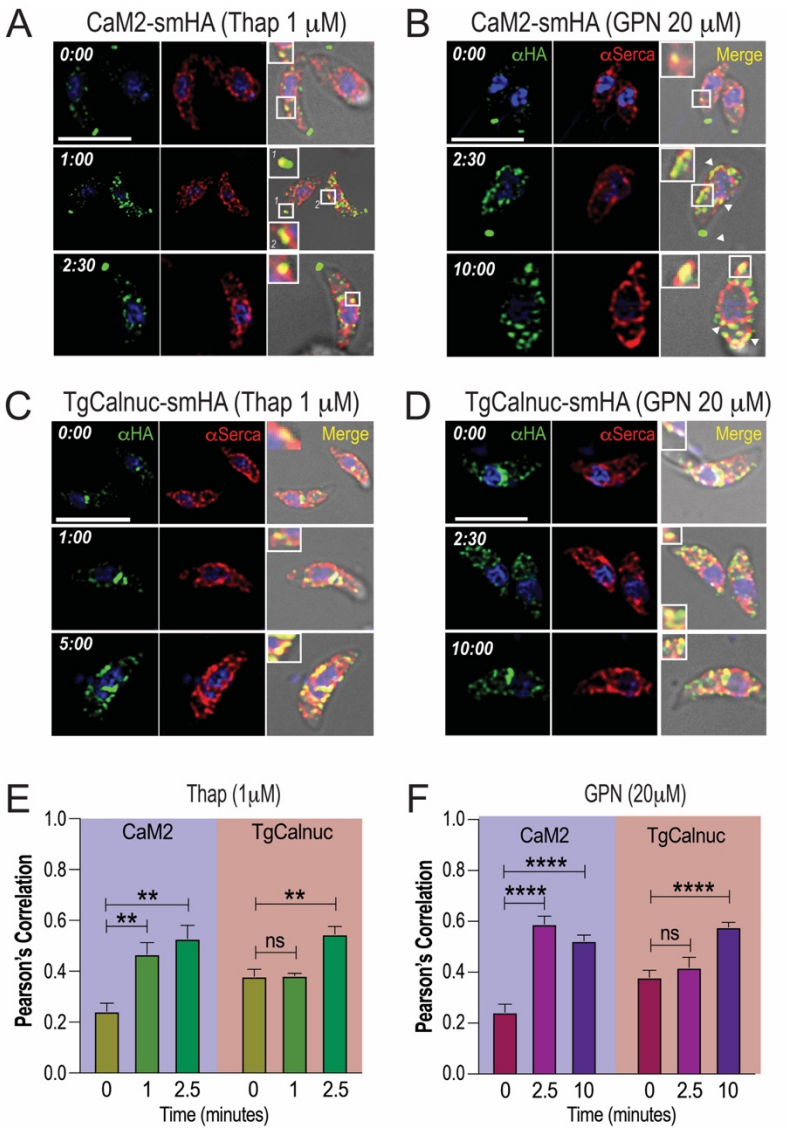

Figure 3.8. CaM2 and Calnuc are recruited to the ER and Golgi when stimulated by Thapsigargin and GPN. A. IFA of CaM2-smHA after the addition of 1 mM of Thap using αHA (1:100) co-localized with αSERCA (1:1,000). White boxes in the Merge panel highlight the co-localized vesicles by CaM2-smHA and αSERCA. **B.** IFA of CaM2-smHA after the addition of 20 μM of GPN using αHA co-localized with αSERCA. **C.** IFA of TgCalnuc-smHA after the addition of 1 μM of

Thap using αHA (1:100) co-localized with αSERCA (1:1,000). White boxes in the Merge panel highlight the co-localized vesicles by TgCalnuc-smHA and αSERCA. **D.** IFA of CaM2-smHA after the addition of 20 mM of GPN using αHA co-localized with αSERCA. **E.** Quantification of Pearson's Correlation between αHA and αSERCA after stimulation by Thap. Analysis was performed by two independent biological replicates using student's t-test. ** $p < 0.001$. **F.** Quantification of Pearson's Correlation between αHA and αSERCA after stimulation by GPN. Analysis was performed by two independent biological replicates using student's t-test. **** $p < 0.0001$.

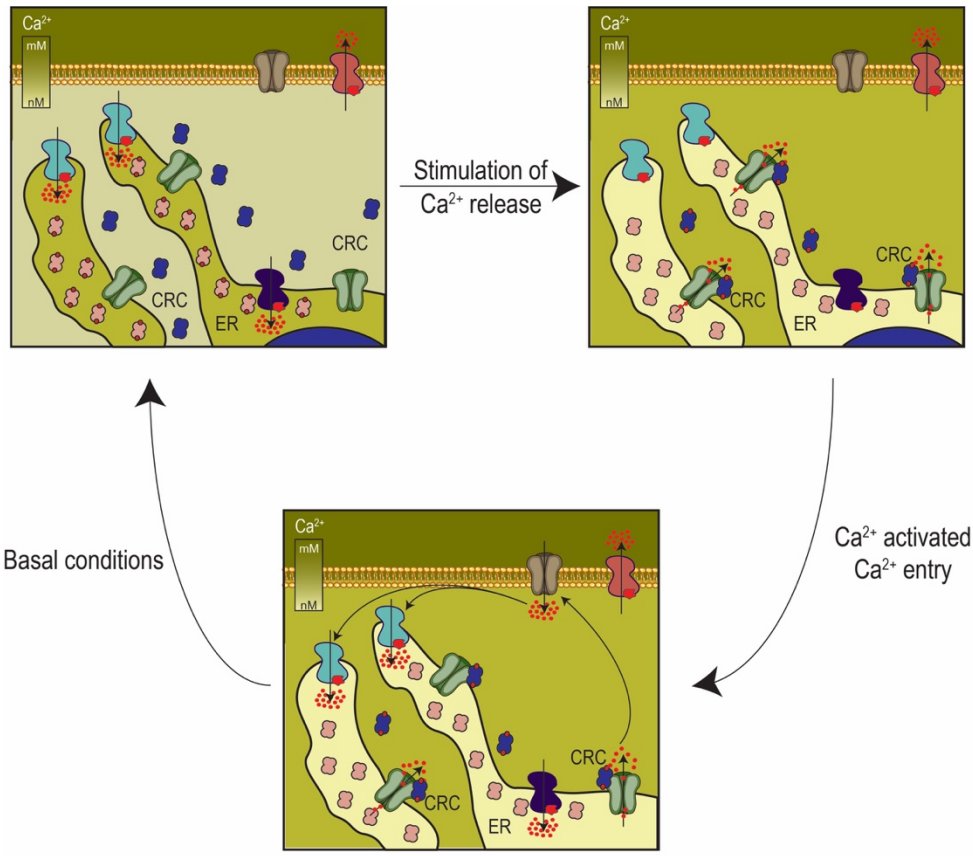

Figure 3.9. Model of the regulation of calcium storage and release in the ER and Golgi of TgCalnuc and CaM2. ER and Golgi have the capacity to hold high concentrations of calcium levels (~mM). TgSERCA which localizes both to the ER and Golgi, constitutively pumps Ca^{2+} into the stores, which upon entry binds to TgCalnuc. TgCalnuc is able to sense changes to the luminal [Ca^{2+}] based on the binding of Ca^{2+} to its EF-hand motifs. Ca^{2+} increase in the ER and Golgi stimulates Ca^{2+} release through a channel in the ER and Golgi membrane. CaM2 is recruited to these channels which enhances the release of calcium. Increase of cytosolic calcium due to the release of the stores, stimulates calcium influx which refill the depleted store and returns the stores to basal conditions. CaM2 disassociates from the ER and Golgi release channels.

Table S1- List of primers used in this study

#	Primer name	Sequence
1	Calnuccompl-F	CCTAGGTACCCGTACGACGTCCCG
2	Calnuccompl-R	CGTCGTACGGGTACCTAGGaatagctgatgatacatactcgcg
3	Calnuc-SM-Val-F	AAGAGCCTCTGCTCTCAACCT
4	Calnuc-KO-Val-F	ATGCAAGTCTCTCCTGGTGCTC
5	Calnuc-KO-Val-1-R	ACTCCATGAATTCCTCGCGGA
6	Calnuc-KO-Val-2-R	ACTCCATGAATTCCTCGCGGA
7	Calnuc-Tag-F	TACTTCCAATCCAATTTAATGCAATGCAAGTCTCTCCTGGTGCTC
8	Calnuc-Tag-R	TCCTCCACTTCCAATTTTAGCAATAGCTGATGATACATACTCGCGATA TTCT

CHAPTER 4

The Multiple Roles of Calcium Binding Proteins in the Calcium Signaling Pathway of *Toxoplasma gondii*[3]

[3] Karla M. Márquez-Nogueras and Silvia N.J. Moreno. *To be submitted to mSphere*.

4.1 ABSTRACT

Toxoplasma gondii is an Apicomplexan parasite that infects one third of the world's population. Calcium signaling in *Toxoplasma* regulates the activation of effectors that decode into biological functions involved in the lytic cycle. An important source of Ca^{2+} that triggers signaling is by influx from the extracellular environment, as it enhances the steps of the lytic cycle. Calcium-binding proteins, like calmodulins or calmodulin-like play an important role in activating other effectors within the Ca^{2+} signaling pathway. Essential Light Chain (ELC) 1 has been shown to localize to the glideosome, a protein complex involved in motility. In this study we characterize the role of ELC1 in the regulation of plasma membrane Ca^{2+} channels. Growth of the parasite is impaired by the deletion of ELC1. Mutant parasites have a significant defect in Ca^{2+} influx and the activation of the Ca^{2+}-activated Ca^{2+} entry mechanism in *T. gondii*. Calcium binding protein activate a variety of targets, and in this study, we propose A new role for ELC1.

4.2. INTRODUCTION

Toxoplasma gondii (*T. gondii)* is an Apicomplexan parasite that infects one third of the world's population [23, 24]. The disease caused by this obligate intracellular parasite, toxoplasmosis, is clinically relevant for immunocompromised patients and for the unborn fetus [4]. The pathology of toxoplasmosis is the result of *T. gondii* engagement in a lytic cycle which consists in invasion of host cells, replication inside a parasitophorous vacuole followed by egress and finding another host cell to invade [37].

Calcium signaling in *T. gondii* regulates biological traits like invasion, motility and egress [69, 70]. Increase of cytosolic Ca^{2+} activates a signaling cascade in which CBPs are involved in the transduction of the signals. CBPs are small acidic proteins that contain specific motifs that allow them to bind calcium ions [52]. EF-Hand Motifs are helix-loop-helix motifs that can bind one calcium ion [54]. CaBPs will predominantly exist in an open conformation in resting conditions. Binding of Ca^{2+} will collapse the protein to a close conformation [58] and this structural change allow the protein to activate its targets.

T. gondii contains a variety of CBPs that were described to be essential in the activation of Myosin Light Chains [75, 77, 78]. Essential Light Chain (ELC) 1 is a Ca^{2+} binding protein that activates Myosin A (Myo A) [76]. MyoA localizes to the glideosome, a complex that allows for motility in the parasite [160]. MyoA belongs to the Class XIV of the myosin family. MyoA is the smallest known isoform for myosins which is highly conserved in Apicomplexan [76]. ELC1 is not essential for the parasite and works in a mutually exclusive manner with another Ca^{2+} binding

protein, ELC2 [75]. ELC2, is a calcium binding protein that contains 4 EF-hand motifs.

In this work we characterized the Ca^{2+} phenotype of the ELC1 mutants. Previous work characterized the role of this protein in a double knock out strain with ELC2 [75]. To determine other potential targets of ELC1 we study Ca^{2+} changes in Fura-2 loaded tachyzoites. We provide an alternative role for ELC1 in the regulation of plasma membrane Ca^{2+} channels.

4.3. EXPERIMENTAL PROCEDURES

Parasite culture All parasite strains were continuously maintained in vitro by serial passage in Dulbecco's modified minimal essential media (DMEM) with 1% FBS, 2.5 µg/ml amphotericin B, 100 µg/ml streptomycin in the human telomerase reverse transcriptase immortalized foreskin fibroblasts (hTERT) [91].

Gene disruption In order to disrupt the *ELC1* gene a single guide RNA against ELC1 was constructed as previously described [161]. To obtain the desired sgRNA against ELC1 we used the Q5 Mutagenesis Kit following manufacturer's instructions. The pyrimethamine-resistant DHFR cassette was amplified by PCR with primers containing 50 bp homology arms of the region upstream and downstream of the start and stop codon of the *ELC1* gene (Table S1 Primers X-Y). The sgELC1 CRISPR plasmid was co-transfected with the DHFR cassette (3:1 respectively) into RH tachyzoites. Selection followed with pyrimethamine for 7 days. Parasites were sub-cloned by limiting dilution and screening for clones was done by PCR and western blot.

Quantitative PCR Total RNAs from parental and ΔELC1 lines were extracted and reversed-transcribed into cDNA. The qPCR reaction was done using the

iQ™SYBR Green master mix (BioRad), plus primers, and the reversed-transcribed cDNA (Primers are shown in Table S1 Primers Q1-Q2). The qRT-PCR was carried out on a CFX96™ PCR Real-Time detection system (C1000Touch™ Thermal cycler, BioRad). Relative quantification software (CFX Maestro™ software) was used for the analysis and relative expression levels were calculated as the fold change using the formula $2^{\Delta\Delta}$CT (Livak et al. 1995). Normalization was done using Actin and Tubulin primers as reference. Experiments were repeated three times using three biological replicates with triplicate samples.

Immunofluorescence microscopy Extracellular parasites were collected and purified as previously described [97]. Parasites were washed once with buffer A with glucose (BAG, 116 mM NaCl, 5.4 mM KCl, 0.8 mM $MgSO_4$, 5.5 mM glucose and 50 mM HEPES, pH 7.4) and an aliquot with 2 x 10^4 parasites was overlaid on a coverslip previously treated with poly-L-Lysine. Extracellular tachyziotes were fixed with 3% paraformaldehyde for 20 min at room temperature (RT), permeabilized with 0.3% Triton X-100, blocked with 3% bovine serum albumin (BSA), and exposed to the primary antibodies α-ELC1 (1:1,000) (Kindly provided by Cristopher Tonkin). The secondary antibodies used were goat-αrat Alexa-Fluor488 (Life Technologies) at 1:1,000. Slides were examined using an Olympus IX-71 inverted fluorescence microscope with a photometric CoolSNAP HQ charge-coupled device (CCD) camera driven by DeltaVision software (Applied Precision, Seattle, WA).

Immunoprecipitation assays Freshly lysed tachyzoites expressing TgTRPPL2-smHA were collected and filtered through an 8 µm membrane (Whatman).

Tachyzoites were washed twice in BAG and resuspended in a lysis buffer (50mM Tris-HCl, pH 7.4, 150 mM KCl, 1mM EDTA, 0.4% NP-40) to a final concentration of 2 x 10^9 total cells. Lysis was allowed to proceed for thirty minutes at 4^{o}C and cells were centrifuged at 15,000 x g for 20 minutes. Immunoprecipitation of TRPL2-smHA protein was performed using the Pierce Ha Tag/Co-IP Kit (Thermo Fisher Scientific, Waltham, MA) according to the manufacturer's instructions. Briefly, HA magnetic beads were washed twice in lysis buffer and mixed with the parasite lysate by vortexing for 1 hour at RT. Beads were collected and the flow-through fraction was saved for further analysis. Beads were washed twice in wash buffer (50mM Tris-HCl, pH 7.4, 150mM KCl, 1mM EDTA, 0.1% NP-40) and once in ddH_2O by gentle mixing. The tagged protein was recovered by mixing the beads with 1x Laemmli buffer and heated at 65^{o}C for 10 minutes. The supernatant was collected and used for electrophoresis gel and western blot analysis.

Western blot analysis SDS-polyacrylamide gel electrophoresis (SDS-PAGE) followed established protocols [96]. Lysates were prepared by resuspending a pellet of 1 x 10^8 tachyzoites in 50 µL of Cell Lytic^M lysis buffer containing 12.5 U benzonase and 1 X protease cocktail inhibitor (P8340 Sigma). The reaction was stopped with one volume of 2% SDS and 1 mM EDTA. Total lysates were boiled in Laemmli sample buffer (BioRad). Immunoblotting followed established protocols using mouse anti-HA monoclonal antibody (1:1,000) (Roche) or anti-ELC1 (1:1,000) (Kindly provided by Cristopher Tonkin). Detection was done using the Odyssey Clx LICOR system using goat anti-mouse IRDye800WC (1:10,000).

Loading control for westerns were done with primary mouse-anti-tubulin antibodies at a 1:15,000 dilution and goat anti-mouse IRDDye800WC as secondary.

Growth and Invasion Assays Plaque growth was done as previously described, with slight modifications. Briefly, 200 parasites per well were allowed to infect confluent hTERT cells for 7 days. Cells were then fixed with ethanol and stained with crystal violet. Plaque sizes were analyzed using FIJI [98]. Growth assay at different [Ca^{2+}] were done using Dulbecco's modified essential media (DMEM) without calcium and extracellular calcium was titrated to the desired concentration using 100 mM of EGTA. Invasion assay were performed as previously described with slight modifications [99]. A subconfluent monolayer of HFF cells were infected with $2x10^7$ tachyzoites in the presence of 0.25, 0.5 or 1.8 mM Ca^{2+} and placed for 20 minutes on ice and subsequently transferred for 5 minutes to a 37^{o}C water bath for parasite invasion. Cells were immediately fixed with 3% paraformaldehyde for 20 minutes. Extracellular parasites (attached) were stained using rabbit-αSag1 (1:1,000) before permeabilization while intracellular parasites (invaded) were stained with mouse-αSag1 (1:200). Secondary antibodies were goat-αrabbit Alexa Fluor 546 (1:1,000) and goat-αmouse Alexa Fluor 488 (1:1,000). Images were taken with an Olympius IX-71 inverted fluorescence microscope with a Photometru CoolCNAP HQ CCD camera driven by DeltaVision software (Applied Precision, Seattle, WA). Quantification was made of ten-fields of views at a 1000 magnification from three independent biological replicates. Percentage of invaded vs attached was quantified by dividing the amount of parasite invaded or attached by the total parasites quantified in the field of view.

Egress experiments hTERT cells were infected with $5x10^5$ of the parental or ΔELC1 cell line. 24 hours after infection parasitophorous vacuoles were observed by microscopy after washing them with Ringer's buffer. Ringer's buffer was used as extracellular buffer in the presence or absence of 1.8 mM Ca^{2+}. Drugs were added in Ringer's buffer (155 mM NaCl, 3 mM KCl, 1 mM MgCl2, 3 mM NaH2PO4H2O, 10 mM HEPES, pH 7.3, and 5 mM glucose) 30 seconds after imaging at the following concentrations: saponin (0.02%) and Zaprinast (100 μM). Images were acquired in a time-lapse mode with an acquisition rate of 3 seconds for 20 minutes. For statistical analysis, egress time was quantified as the first parasite to egress out of the parasitophorous vacuole. Statistical analysis was done for 3 independent biological replicates and at least 5 PVs per experiment.

Cytosolic calcium measurements of mutants Parasites loading with Fura-2-AM were performed as described in (Moreno, 1996 #215). Briefly, fresh lysed parasites were washed twice at 1,800 rpm for 10 min at room temperature in buffer A (BAG) (116 mM NaCl, 5.4 mM KCl, 0.8 mM $MgSO_4$, 5.5 mM d-glucose and 50 mM Hepes, pH 7.4). Parasites were resuspended to a final density of $1x10^9$ parasites/mL in loading buffer (Ringer's plus 1.5% sucrose, and 5 uM Fura2-AM). The suspension was incubated for 26 min in a 26 °C with mild agitation. Subsequently, the parasites were washed twice with Ringer's buffer (155 mM NaCl, 3 mM KCl, 1 mM $MgCl_2$, 3 mM $NaH_2PO_4H2_O$, 10 mM HEPES, pH 7.3, and 5 mM glucose) to remove extracellular dye. Parasites were resuspended to a final density of $1x10^9$ parasites/mL in Ringer's buffer and kept in ice. Parasites are viable for a few hours under these conditions. For fluorescence measurements, $2x10^7$ parasites/mL were

placed in a cuvette with 2.5mL of Ringer's buffer. The cuvette was placed in a thermostatically controlled Hitachi F-7000 fluorescence spectrophotometer for Ca^{2+} measurements. Excitation was at 340 and 380 nm, and emission was at 510 nm. The Fura2-AM fluorescence relationship to intracellular Ca^{2+} concentration ($[Ca^{2+}]_i$) was calibrated from the ratio of 340/380 nm fluorescence values after subtraction of the background fluorescence of the cells at 340 and 380 nm as previously described [102]. Changes in $[Ca^{2+}]_i$ (ΔF $[Ca^{2+}]$) were measured by subtracting the highest peak of calcium in the first 20 s after addition of calcium or 100 s after the addition of drugs minus the baseline.

4.4. RESULTS

4.4.1 Calcium binding proteins regulate biological traits of T. gondii

ELC1 is a Ca^{2+} binding protein that was previously described to activate MyoA within the glideosome [76, 77, 162]. A previous study analyzed the phenotype of a double knock out mutants for ELC1 and ELC2 creating a synthetic lethality phenotype [75]. To uncover new roles within the Ca^{2+} signaling pathway of ELC1, we generated single knockouts. Generation of ΔELC1 was performed through the CRISPR-Cas9 approach to disrupt the transcription of ELC1 by inserting a Dihydrofolate reductase-thymidylate synthase (DHFR) cassette in the *ELC1* locus (Fig. 4.1A). Protein validation of the insertion was confirmed by western blots using ELC1 antibodies (Fig. 4.1B). We further confirm the absence of ELC1 by immunofluorescence assay using ELC1 antibodies, where there is no labeling of ELC1 in the mutant cell line (Fig. 4.1C).

4.4.2. ELC1 is necessary for T. gondii invasion and egress

Activation of Ca^{2+} binding proteins are dependent of the increase in cytosolic calcium. Ca^{2+} entry directly impacts the ability of the parasite to complete its lytic cycle. We tested growth of ΔELC1 mutants in the presence of different extracellular Ca^{2+} concentrations in plaque assays (Fig. 4.2A). Growth of the parental strain is significantly decreased as the Ca^{2+} concentration is decreased (Fig. 4.2B, *black bars*). Growth of the *ELC1* mutants was not impacted by variations in the concentration of extracellular Ca^{2+} (Fig. 4.2A). Plaque sizes were significantly bigger in the mutants in comparison to the parental strain (Fig. 4.2B, *black bars vs green bars*).

Lowering the concentration of extracellular [Ca^{2+}] decreased the percentage of invading tachyzoites in the wild type strain (Fig. 4.2C, *black bars*). ΔELC1 invasion is significantly decreased in comparison to the parental strain (Fig. 4.2C, *green bars*). Contrary to growth, change of extracellular Ca^{2+} lead to a significant decrease in the ability of the parasite to invade the host cell.

Lastly, we tested the role of ELC1 in egress. Egress of *T. gondii* can be stimulated by the permeabilization of the host cell or the release of calcium by intracellular stores. Addition of saponin at high calcium concentration stimulated egress at a similar rate as the parental strain (Fig. 4.2D-E). Increasing cytosolic Ca^{2+} through Zaprinast in the absence of extracellular Ca^{2+} does not affect the rate of egress in ΔELC1 mutants. However, egress stimulated by Zaprinast in the presence of 1.8 mM Ca^{2+} lead to a slower egress by the mutants (Fig. 4.2E). Modulation of extracellular Ca^{2+} impacts the ability of the parasite to successfully

complete its lytic cycle. Taken together these results supports a role for ELC1 in transducing Ca^{2+} signals that lead to invasion and egress of *T. gondii*.

4.4.3. ELC1 regulates plasma membrane Ca^{2+} *influx in T. gondii*

Activation of invasion, egress and motility is stimulated by the release from intracellular stores as well as influx from the extracellular environment [81]. Based on the localization of ELC1 at the periphery of the parasite, we studied whether there is any defect in Ca^{2+} influx. We loaded ΔELC1 tachyzoites with Fura-2AM to study changes of cytosolic calcium. The levels of resting cytosolic Ca^{2+} between the mutants and the parental strain remained at similar levels (~70nM) (Fig. 4.3A). Addition of 1.8 mM Ca^{2+} caused an increase of cytosolic calcium in both mutants and parental, however increased was 50% lower in the mutant parasites (Fig. 4.3B). Addition of different [Ca^{2+}] showed similar defect in ΔELC1 mutants, where influx was reduced around 50% (Fig. 4.3B).

We hypothesize that Ca^{2+} influx in *T. gondii* is likely mediated by two independent channels with different calcium affinities. Incubation with Nifedipine, which targets Voltage Gated Calcium Channels (VGCC), or Anthranilic Acid, which targets Transient Receptor Potential Like Channel (TRPPL), are able to decrease calcium influx in tachyzoites. We next investigated if Nifedipine inhibited Ca^{2+} influx in ΔELC1. Pre-incubation of Nifedipine significantly increased the resting cytosolic calcium 3x more in the mutants. Addition of 1.8 mM Ca^{2+} in the presence of Nifedipine, resulted in a slow and passive leakage of calcium (Fig. 4.3C, *brown line*). Increased cytosolic calcium can be due to the dysregulation in the maintenance of cytosolic calcium due to the inhibition of Ca^{2+} influx.

We also tested the effect of ACA in the mutants. Incubation of ACA in the wild type strain leads to a 40-50% decrease of calcium influx (Fig. 4.3D, *gold bar in parental group*). In ΔELC1, pre-incubation of ACA had no effect on the inhibition of Ca^{2+} influx. (Fig. 4.3D, *black bar vs gold bar in mutant group*). In summary, these results suggest the role of ELC1 regulating a mechanism of calcium influx in *T. gondii.*

4.4.4. ELC1 activates a Transient Receptor Potential Like Channel in T. gondii

We have previously shown that increase of cytosolic Ca^{2+} enhances Ca^{2+} influx through a TRPPL Channel by a mechanism that we termed Calcium Activated Calcium Entry (CACE) (Fig. 4.4A). In Fura-2 loaded tachyzoites we added thapsigargin (Thap) that inhibits the Sarco-Endoplasmic Reticulum Ca^{2+} ATPase (SERCA) which results in calcium leaking from the ER. In ΔELC1 tazhyoites, leakage stimulated by Thap showed no significant difference when compared to the parental strain (Fig. 4.4B). Stimulation of CACE by the addition of high extracellular Ca^{2+} after Thap appears to be absent in ΔELC1 (Fig. 4.4C).

We also tested the stimulation of CACE by the addition of Zaprinast. Zaprinast is a phosphodiesterase inhibitor which increases the levels of cGMP, resulting in Ca^{2+} release from an unidentified store [117]. In ΔELC1 mutants, addition of Zaprinast showed no difference of Ca^{2+} release. Ca^{2+} influx stimulated by the addition of high [Ca^{2+}] after Zaprinast was significantly decreased in the mutants. Release or efflux of Ca^{2+} by Zaprinast or Thap is not affected in the ΔELC1 mutants. In conclusion, deletion of ELC1 prevents the activation of Ca^{2+} influx through the TRPP-L channel in the plasma membrane of *T. gondii*.

4.4.5. Interaction between ELC1 and TgTRRPL2

We identified TgTRPPL2, as a calcium permeable channel that is involved in Ca^{2+} influx in *T. gondii*. Although not essential, deletion of this protein in the parasites has serious impact in the biological traits of the tachyzoites. The observed phenotype of the ΔELC1 mutants resembled key defects observed in the ΔTgTRPPL2 line. In Fura-2 loaded tachyzoites, addition of 1.8 mM extracellular Ca^{2+} lead to a significant decreased Ca^{2+} influx (Fig. 4.5A). Calcium influx was not inhibited by preincubation with ACA in either mutant cell line (Fig. 4.5B). The change of cytosolic Ca^{2+} in the presence of ACA in the parental tachyzoites is similar to the change in the mutant cell lines. In comparison to the ΔTgTRPPL2 parasites, ELC1 does not have any effect in the intracellular stores but its role its limited to the regulation of Ca^{2+} influx (Fig. 4.5C). Stimulation of CACE through Zaprinast with high Ca^{2+}, is absent in both mutant cell lines (Fig. 4.5D).

Based on the similarities of the phenotypes in ΔTgTRPPL2 and ΔELC1 we investigated whether there is direct regulation of TgTRPPL2 by ELC1 (Fig. 4.5E). Using a lysate from TgTRPPL2-smHA parasite we performed immunoprecipitations with anti-HA magnetic beads. The eluted samples were run in an SDS-Page gel using αELC1. ELC1 was not present in the eluted sample of TgTRPPL2 (Fig. 4.5F). These results indicated that there are no direct interactions between ELC1 and TgTRPPL2.

4.5 DISCUSSION

Ca^{2+} signaling is universal and regulates a variety of cellular functions [43]. Ca^{2+} increase in the cytosol of *T. gondii*, resulting from influx or release from intracellular stores, will start a signaling cascade that can activate vital cellular functions like the ones that are part of the lytic cycle [70]. Due to the diffusion rate of processes like Ca^{2+} influx or release through calcium channels, the surrounding areas of these channel have higher concentrations of Ca^{2+} [163]. Concentrations within these areas can reach up to μM levels in comparison to nM levels within the cytosol.

The concentration gradient around these channels contain a number of proteins that have calcium-binding motifs, like EF-hands. Calcium-binding proteins are among the first proteins to become activated in the calcium signaling cascade. *T. gondii* contains a high number of proteins in its genome with EF-Hand motifs [164]. A small number of proteins have been characterized, where the proposed role is the activation of Myosin light chains, which are essential for both invasion and motility. ELC1 and ELC2, which are CaBPs, have been previously characterized to function in a redundant manner by activating MyoA within the glideosome [75]. In this study, we characterize an alternative role for ELC1 in the regulation of calcium influx channels.

When the parasite egresses from its host cell, it goes from a low [Ca^{2+}] environment into a high [Ca^{2+}]. Tachyzoites utilize the extracellular Ca^{2+} in order to successfully complete its lytic cycle. Changes in extracellular Ca^{2+} can lead to reduction in parasite growth, suggesting the presence of a mechanism in the

parasite to sense changes in extracellular [Ca^{2+}]. Deletion of ELC1 alters the ability of the parasite to sense those changes, as growth is not reduced when Ca^{2+} is modified.

Invasion of the parasite into a new host cell is predominantly governed by the influx of Ca^{2+}. Contrary to growth, invasion in the mutants was significantly decreased in the different concentrations of Ca^{2+}. This reduction in invasion can be correlated to a defect in Ca^{2+} influx in these mutants. Interestingly when egress was stimulated through the activation of Ca^{2+} influx through the TRPPL channel, the mutants showed a delay in egress. Defect in the biological traits that are mainly governed by Ca^{2+} influx showed the possibility that ELC1 could regulate a plasma membrane channel.

Calcium-binding proteins are known to activate a variety of targets within the cell [53]. The activation of MyoA through ELC1 and ELC2 occurs in a mutually exclusive manner, meaning that ELC1 will not exist in the same complex as ELC2 when bound to MyoA. The localization of ELC1 to the periphery of parasite, in addition to the existing redundancy with ELC2, opens the possibility that it activates other molecules within the periphery of the parasite.

Ca^{2+} channels are known to be regulated by CaBPs [55]. When Ca^{2+} influx was stimulated in ELC1 deficient tachyzoites there was a decrease in the amount of Ca^{2+} that entered the cytosol. Stimulation of the Ca^{2+}-Activated Calcium Entry Mechanism was absent in the mutant cell line. The release of calcium from the intracellular stores was not affected, but the phenotype observed was specific to the regulation of the mechanism of calcium influx into the tachyzoite.

We previously described the role of TgTRPPL2 as a cation permeable channel in *T. gondii*. This channel mediates the Ca^{2+} Activated Calcium Entry mechanism of *Toxoplasma* and is sensitive to TRP channel inhibitors like ACA. Ca^{2+} influx deficiency of ELC1 mutants resembles the phenotype observed when TgTRRPL2 was deleted for the tachyzoites. The main difference observed between these cell lines is that TgTRPPL2 has a defect in the efflux of Ca^{2+} from the ER which is not observed in ELC1 mutants. Meaning that the regulation of TgTRPPL2 by ELC1 is localized only in the plasma membrane. Although immunoprecipitation assays did not show a direct regulation of TgTRPPL2 by ELC1 this possibility need to be explored further.

STRING (Search tool for recurring stances of neighbor genes) is a database that utilizes the information from five different databases to predict direct or indirect protein-protein interactions [165]. Although previous experimental data was obtained to confirm the interaction between ELC1 and MyoA, other potential interactors have not been described. Predictions obtained through the bioinformatic analysis through STRING, shows the potential interaction of ELC1 with a variety of phosphatases like Calcineurin (Fig. 4.6A). We hypothesize that the activation of TgTRPPL2 is mediated by an ELC1-Phosphatase Complex (Fig. 4.6B), which is activated by the increase of cytosolic Ca^{2+}.

Ca^{2+} signaling and homeostasis is important for *Toxoplasma* survival and success [69, 70]. CBPs play key roles in the activation and regulation of these signaling pathways [166]. These proteins localize to strategic locations where other signaling molecules like kinases, phosphatases and channels localize [151]. In this

study, we provide an alternative role to a previously characterize CaBP, ELC1. The potential regulation of Ca^{2+} channels by these CaBPs increase our knowledge of the Ca^{2+} signaling pathway in *T. gondii*. The presence of multiple CaBP in the parasite indicate that these proteins are able to regulate a variety of molecules within the parasite which are translated in the activation of the lytic cycle. Understanding the multiple targets of these proteins may aid in the discovery of new signaling molecules which will produce important information about this complex signaling network.

4.6 REFERENCES

4. Hill, D. and J.P. Dubey, *Toxoplasma gondii: transmission, diagnosis and prevention.* Clin Microbiol Infect, 2002. **8**(10): p. 634-40.
23. Djurkovic-Djakovic, O., et al., *Toxoplasmosis: Overview from a One Health perspective.* Food Waterborne Parasitol, 2019. **15**: p. e00054.
24. Pinto-Ferreira, F., et al., *Patterns of Transmission and Sources of Infection in Outbreaks of Human Toxoplasmosis.* Emerg Infect Dis, 2019. **25**(12): p. 2177-2182.
37. Black, M.W. and J.C. Boothroyd, *Lytic cycle of Toxoplasma gondii.* Microbiol Mol Biol Rev, 2000. **64**(3): p. 607-23.
52. Pepke, S., et al., *A dynamic model of interactions of Ca2+, calmodulin, and catalytic subunits of Ca2+/calmodulin-dependent protein kinase II.* PLoS Comput Biol, 2010. **6**(2): p. e1000675.
54. Zhou, Y., et al., *Prediction of EF-hand calcium-binding proteins and analysis of bacterial EF-hand proteins.* Proteins, 2006. **65**(3): p. 643-55.
58. Kursula, P., *The many structural faces of calmodulin: a multitasking molecular jackknife.* Amino Acids, 2014. **46**(10): p. 2295-304.
69. Lourido, S. and S.N. Moreno, *The calcium signaling toolkit of the Apicomplexan parasites Toxoplasma gondii and Plasmodium spp.* Cell Calcium, 2015. **57**(3): p. 186-93.
70. Hortua Triana, M.A., et al., *Calcium signaling and the lytic cycle of the Apicomplexan parasite Toxoplasma gondii.* Biochim Biophys Acta Mol Cell Res, 2018. **1865**(11 Pt B): p. 1846-1856.
75. Williams, M.J., et al., *Two Essential Light Chains Regulate the MyoA Lever Arm To Promote Toxoplasma Gliding Motility.* mBio. **6**(5).
76. Powell, C.J., et al., *Dissecting the molecular assembly of the Toxoplasma gondii MyoA motility complex.* J Biol Chem, 2017. **292**(47): p. 19469-19477.

77. Nebl, T., et al., *Quantitative in vivo analyses reveal calcium-dependent phosphorylation sites and identifies a novel component of the Toxoplasma invasion motor complex.* PLoS Pathog, 2011. **7**(9): p. e1002222.
78. Long, S., et al., *Calmodulin-like proteins localized to the conoid regulate motility and cell invasion by Toxoplasma gondii.* PLoS Pathog, 2017. **13**(5): p. e1006379.
81. Vella, S.A., et al., *The Role of Potassium and Host Calcium Signaling in Toxoplasma gondii egress.* bioRxiv, 2020: p. 2020.03.06.980508.
91. Farwell, D.G., et al., *Genetic and epigenetic changes in human epithelial cells immortalized by telomerase.* Am J Pathol, 2000. **156**(5): p. 1537-47.
96. Laemmli, U.K., *Cleavage of structural proteins during the assembly of the head of bacteriophage T4.* Nature, 1970. **227**(5259): p. 680-5.
97. Liu, J., et al., *A vacuolar-H(+) -pyrophosphatase (TgVP1) is required for microneme secretion, host cell invasion, and extracellular survival of Toxoplasma gondii.* Mol Microbiol, 2014. **93**(4): p. 698-712.
98. Schindelin, J., et al., *Fiji: an open-source platform for biological-image analysis.* Nat Methods, 2012. **9**(7): p. 676-82.
99. Kafsack, B.F., C. Beckers, and V.B. Carruthers, *Synchronous invasion of host cells by Toxoplasma gondii.* Mol Biochem Parasitol, 2004. **136**(2): p. 309-11.
102. Grynkiewicz, G., M. Poenie, and R.Y. Tsien, *A new generation of Ca2+ indicators with greatly improved fluorescence properties.* J Biol Chem, 1985. **260**(6): p. 3440-50.
117. Sidik, S.M., et al., *Using a Genetically Encoded Sensor to Identify Inhibitors of Toxoplasma gondii Ca2+ Signaling.* J Biol Chem, 2016. **291**(18): p. 9566-80.
160. Meissner, M., D. Schlüter, and D. Soldati, *Role of Toxoplasma gondii myosin A in powering parasite gliding and host cell invasion.* Science (New York, N.Y.), 2002. **298**(5594): p. 837-840.
161. Shen, B., et al., *Efficient gene disruption in diverse strains of Toxoplasma gondii using CRISPR/CAS9.* MBio, 2014. **5**(3): p. e01114-14.
162. Williams, L.E., et al., *Multimodality depiction of findings in branchio-oto-renal syndrome: two case reports.* Acta Radiol Open, 2019. **8**(7): p. 2058460119861606.
41. Clapham, D.E., *Calcium signaling.* Cell, 2007. **131**(6): p. 1047-58.
46. Lourido, S. and S.N. Moreno, *The calcium signaling toolkit of the Apicomplexan parasites Toxoplasma gondii and Plasmodium spp.* Cell Calcium, 2015. **57**(3): p. 186-93.
47. Hortua Triana, M.A., et al., *Calcium signaling and the lytic cycle of the Apicomplexan parasite Toxoplasma gondii.* Biochim Biophys Acta Mol Cell Res, 2018. **1865**(11 Pt B): p. 1846-1856.
81. Elies, J., et al., *An Update to Calcium Binding Proteins.* Adv Exp Med Biol, 2020. **1131**: p. 183-213.
83. Villalobo, A., M. Gonzalez-Munoz, and M.W. Berchtold, *Proteins with calmodulin-like domains: structures and functional roles.* Cell Mol Life Sci, 2019. **76**(12): p. 2299-2328.
93. Williams, M.J., et al., *Two Essential Light Chains Regulate the MyoA Lever Arm To Promote Toxoplasma Gliding Motility.* mBio. **6**(5).

99. Zeng, H., et al., *Involvement of calmodulin and calmodulin-like proteins in plant responses to abiotic stresses.* Front Plant Sci, 2015. **6**: p. 600.
157. Wolf, I.M.A. and A.H. Guse, *Ca(2+) Microdomains in T-Lymphocytes.* Front Oncol, 2017. **7**: p. 73.
158. Chang, L., et al., *Characterization of Two EF-hand Domain-containing Proteins from Toxoplasma gondii.* J Eukaryot Microbiol, 2019. **66**(2): p. 343-353.
159. Snel, B., et al., *STRING: a web-server to retrieve and display the repeatedly occurring neighbourhood of a gene.* Nucleic Acids Res, 2000. **28**(18): p. 3442-4.
160. Ranty, B., D. Aldon, and J.P. Galaud, *Plant calmodulins and calmodulin-related proteins: multifaceted relays to decode calcium signals.* Plant Signal Behav, 2006. **1**(3): p. 96-104.

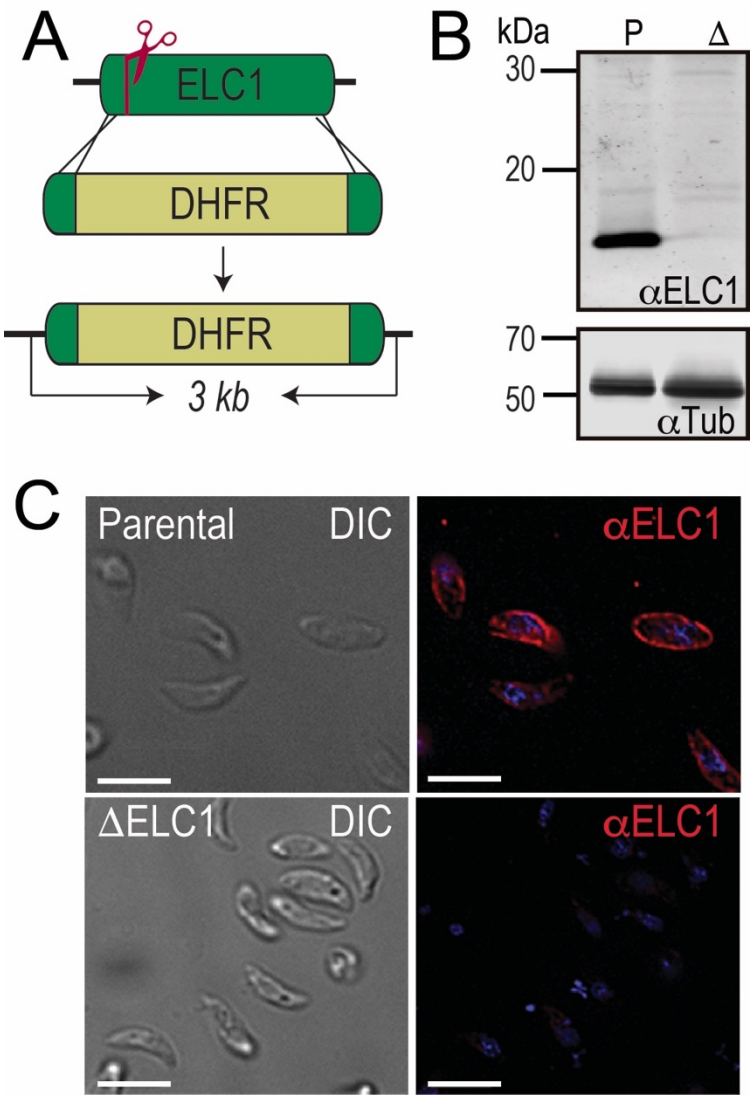

Figure 4.1. Disruption of ELC1 in RH tachyzoites. A. Schematic representation of the ΔELC1 knock-out strategy using CRISPR-Cas9 in the RH strain. **B.** Western blot analysis for total lysates of both ΔELC1 and parental using αELC1 (1:1,000). *Bottom panel*, α-Tubulin (1:10,000) was used as a loading control. **C.** Immunofluorescence assay of extracellular tachyzoites in the ΔELC1 and parental strain using αELC1 (1:1,000) which confirms the deletion of ΔELC1.

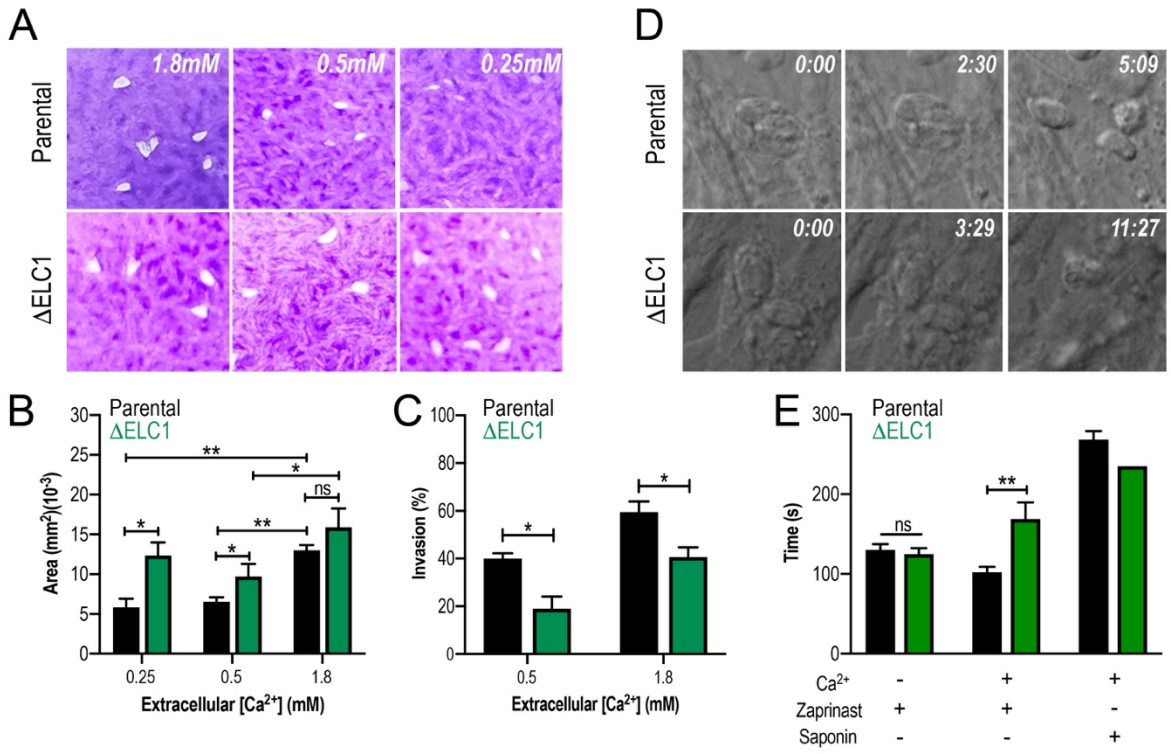

Figure 4.2. ELC1 is required for the invasion and egress of *T. gondii*. A. Plaque assay of *ELC1* mutants in comparison to the parental strain using different $[Ca^{2+}]_E$. **B.** Quantification of plaque size of ELC1 mutants at different $[Ca^{2+}]_E$. Analysis was done using Student's T-test of three independent biological replicates. Asterisk indicate p value for significant difference. *p< 0.04, **p< 0.003. **C.** Invasion assay of *ELC1* mutants at different $[Ca^{2+}]_E$. Analysis was done using student's t-test of three independent biological replicates. *p<0.02. **D.** Egress stimulated by Zaprinast in the presence of 1.8mM extracellular Ca^{2+}. **E.** Statistical analysis of the average egressed time of *ELC1* mutants in comparison to the parental strain in different conditions. Analysis was performed from three biological

replicates using student's t-test. Asterisk indicate p value for significant difference. **p<0.004.

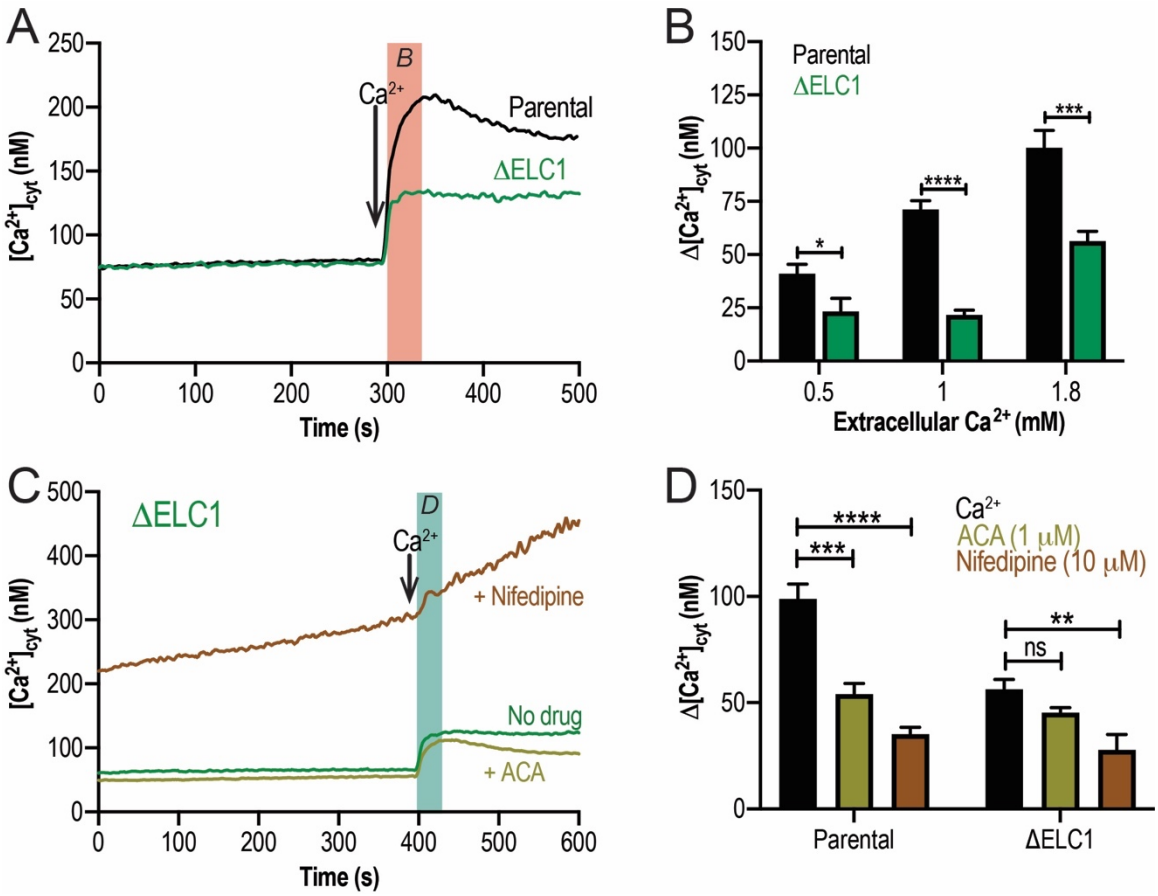

Figure 4.3. ELC1 regulates calcium influx in *T. gondii*. A. Average of calcium influx after the addition of 1.8mM extracellular Ca^{2+} of *ELC1* mutants versus parental strain. **B.** Quantification of Ca^{2+} influx 20 s after the addition of different [Ca^{2+}]. Statistical analysis was done using Student's T-test of three independent biological replicates. Asterisk indicate p value for significant difference. *p< 0.04, ***p<0.0006, ****p<0.0001. **C.** Pre-incubation with Nifedipine (10 μM) or ACA (1 μM) for 3 minutes in ΔELC1 tachyzoites before the addition of 1.8 mM Ca^{2+}. **D.** Quantification of the change in cytosolic Ca^{2+} in the presence or absence of

different inhibitors. Statistical analysis was performed from three biological replicates using Student's T-test. Asterisk indicate p value for significant difference. **p< 0.004, ***p<0.0002, ****p<0.0001.

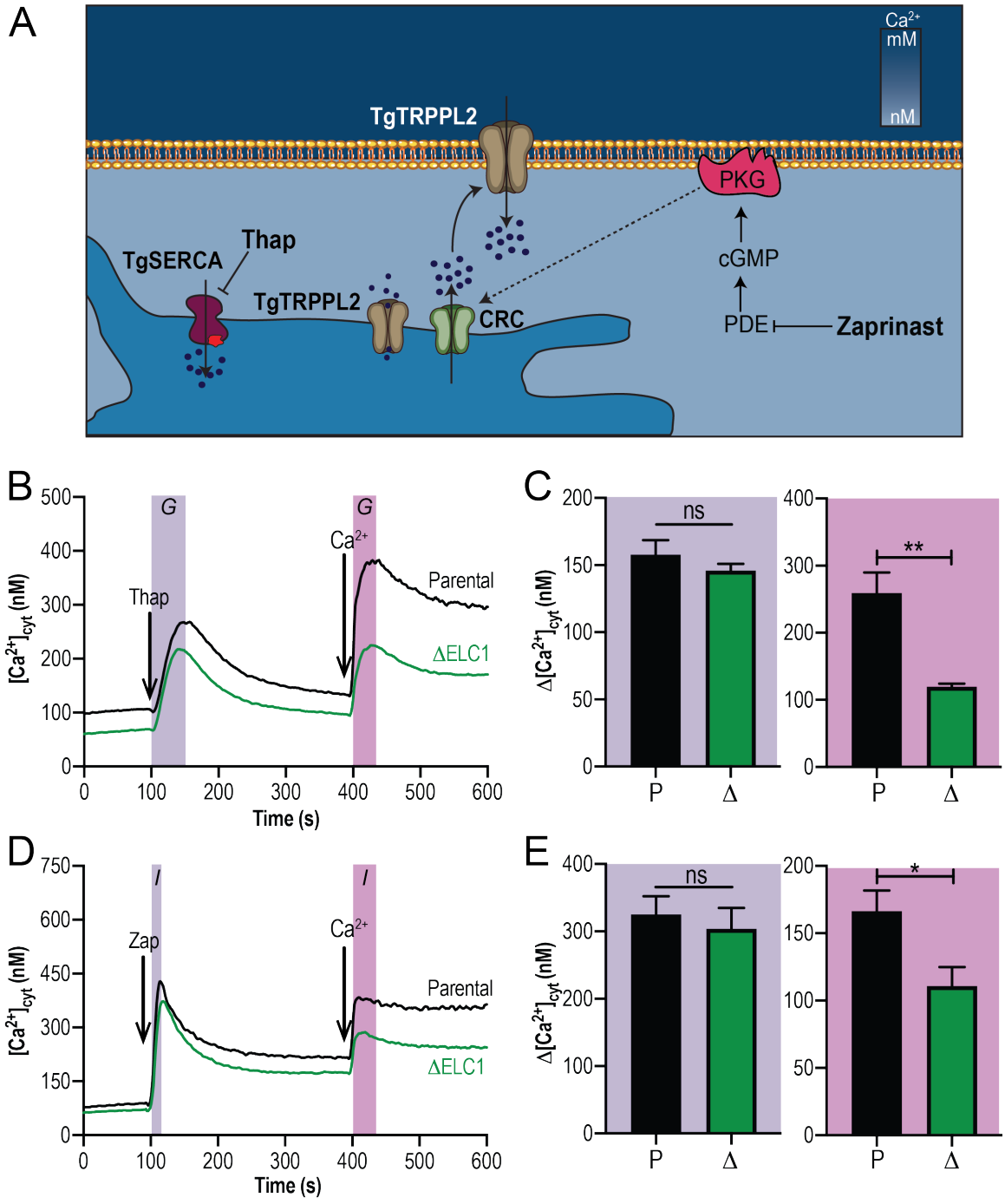

Figure 4.4. ELC1 is not involved in Ca^{2+} homeostasis of intracellular stores. **A.** Cartoon of the stimulation of intracellular calcium signaling by Thapsigargin (Thap) and Zaprinast (Zap). **B.** Ca^{2+} efflux stimulated by Thap (1μM) at 100s followed by 1.8 mM Ca^{2+}. **H.** Quantification of the change of cytosolic calcium after the addition of Thapsigargin (*Left bar graph*) or after extracellular Ca^{2+} (*Right bar graph*). Statistical analysis was done using Student's T-test of three independent biological replicates. Asterisk indicate p value for significant difference. **p< 0.006. **I.** Cytosolic Ca^{2+} measurement after the addition of Zap (100 μM) followed by 1.8 mM Ca^{2+} at 400 s. **E.** Quantification of the change of cytosolic Ca^{2+} after the addition of Zaprinast (*Left bar graph*) or after 1.8 mM Ca^{2+} (*Right bar graph*). Statistical analysis was done using Student's T-test of three independent biological replicates. Asterisk indicate p value for significant difference. *p< 0.03.

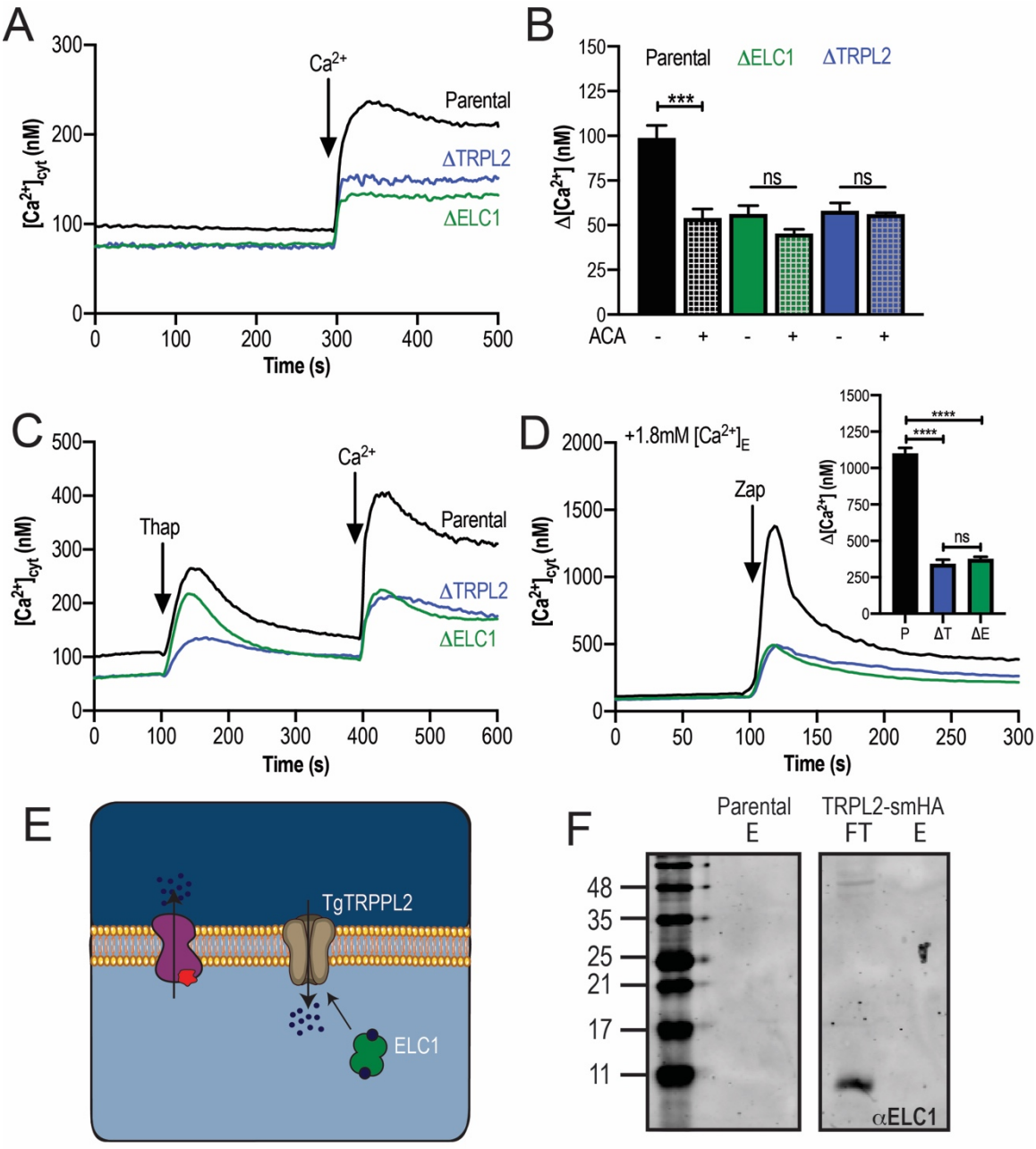

Figure 4.5. Regulation of Calcium Entry Channels by ELC1. A. Comparison of Ca^{2+} influx after the addition of 1.8mM of extracellular calcium of *TgTRPPL-2* and *ELC1* mutants. **C.** Quantification of the change in cytosolic calcium 20s after the addition of 1.8mM of extracellular calcium in the presence or absence of ACA (1 μM) in the both mutant cell lines. Statistical analysis was performed using

Student's T-test from three biological replicates. ***p<0.0002. **D.** Leakage of calcium stimulated by Thap in *TgTRPPL2* and *ELC1* mutants. Measurement of Ca^{2+} influx was done by adding 1.8 mM Ca^{2+} 300s after Thap. **E.** Stimulation of CACE by Zap in the presence of high extracellular Ca^{2+} in both cell lines. *Inset*, quantification of the change in cytosolic calcium 15s after the addition of Zaprinast. Statistical analysis was perfomed from three independent biological replicates using Student's T-test. Asterisk indicate p value for significant difference. ****p<0.0001. **E.** Schematic representation of the putative regulation of TRPL2 by ELC1. **F.** Western blot from the Immunoprecipitation of TgTRPPL2-smHA using αELC1 (1:1,000).

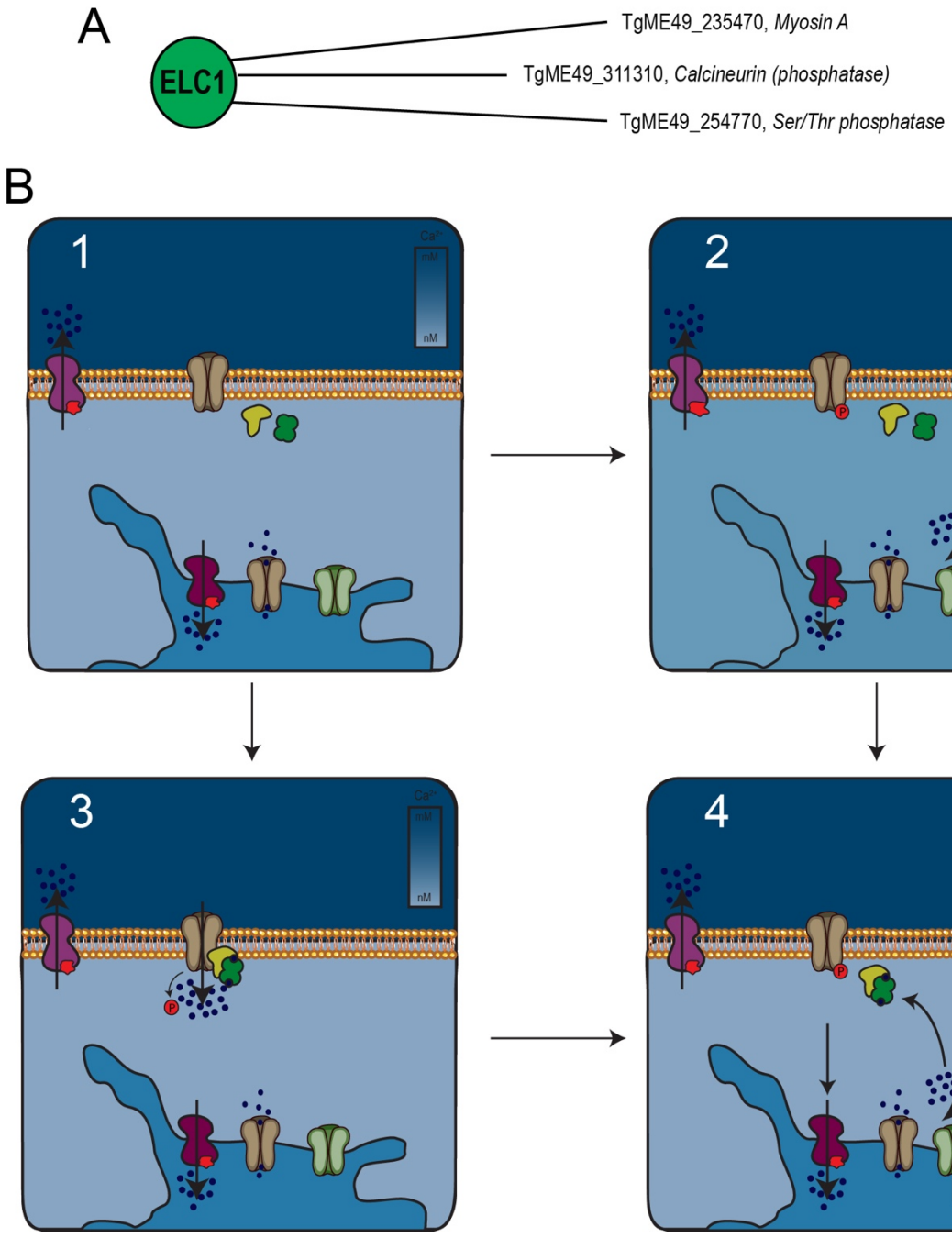
A
ELC1
TgME49_235470, Myosin A
TgME49_311310, Calcineurin (phosphatase)
TgME49_254770, Ser/Thr phosphatase
B
1
2
3
4
Ca2+
mM
nM
P

Figure 4.6. Proposed model of Regulation of TRPL2 by ELC1. A. Predicted interactions of ELC1 with different phosphatases using the web predictor: STRING. **B.** Schematic representation of the interaction of ELC1 and a phosphatase regulating the opening and closing of TgTRPPL2. Cytosolic Ca^{2+} increase by the release of intracellular stores binds to ELC1 (1) which causes a structural change in the protein. The activation of ELC1 (2) leads to the formation of a phosphatase/ELC1 complex (3) that can dephosphorylate the channel (4) leading to the activation of the channel.

Chapter 5

Conclusion and Future Work

Calcium signaling is essential for the completion of the lytic cycle of *Toxoplasma gondii*. Very few proteins that regulate and activate Ca^{2+} signaling in *Toxoplasma* have been characterized. There is no previous information on Ca^{2+} channels in *T. gondii*. In the research presented through this dissertation we provide new information about the function of one channel involved in Calcium signaling and its potential regulation by Calcium binding Proteins.

The characterization of TgTRPPL-2 provides the first channel described in mediating Ca^{2+} influx in *T. gondii*. We have established new protocols for future studies of new proteins that may mediate Ca^{2+} release or influx. Since TgTRPPL-2 is a cation permeable channel, future studies should be performed to determine ion selectivity, and the pore of the channel. Studies can also address the identification of potential calcium binding site.

In mammalian cells it is known that PC2, the mammalian ortholog, works in complex with PC1. PC1 is not a pore forming channel meaning it does not

permeate ions. Although TgTRPPL-1 has been localized to the ER of the parasite there is no characterization of this molecule. Additional studies can be performed to determine if TgTRPPL-1 works in a similar manner as the mammalian ortholog, where it may function as activator of TgTRPPL-2.

Intracellular stores like the ER and Golgi play an essential role in the activation of the calcium signaling. In this study we provide key evidence that the Golgi plays an important role as a calcium store. Calnuc becomes the first characterized calcium binding protein to localize to the Golgi and ER. Calnuc is able to sense changes in Ca^{2+} concentration within these two organelles. HsCalnuc has also been described in regulating other proteins within the Golgi. Future studies can be directed to understand potential interactors of Calnuc.

Calcium-binding proteins are known to regulate many protein targets in cells. Many of the CaBPs described in *Toxoplasma* are proposed to be redundant in their function. Studying single knock outs of these CaBPs provided us with understanding of the additional targets of one of these proteins. Immunoprecipitation of these proteins are needed to discover its potential targets.

The discovery of new molecules within the Calcium-Signaling pathway is essential for our understanding of how this pathway is both regulated and activated in the T. gondii. Through the use of immunoprecipitation techniques we will be able to uncover the missing links of this signaling pathway.